GEOLOGICAL SURVEY OF CANADA

OPEN FILE 3442

Geological and geophysical investigations of massive ground ice in glaciofluvial deposits, Slave Geological Province, Northwest Territories

S.A. Wolfe, M.M. Burgess, M. Douma,
C. Hyde, S. Robinson

1997

Natural Resources Canada Ressources naturelles Canada

Canada

GEOLOGICAL SURVEY OF CANADA

OPEN FILE 3442

Geological and geophysical investigations of massive ground ice in glaciofluvial deposits, Slave Geological Province, Northwest Territories

S.A. Wolfe, M.M. Burgess, M. Douma, C. Hyde
Geological Survey of Canada
Terrain Sciences Division
Ottawa, ON K1A 0E8

S. Robinson
Department of Geography
McGill University
Montreal, PQ H3A 2K6

1997

TABLE OF CONTENTS

FIGURES (Located at the end of each section)

TABLES (Located at the end of document)

1. INTRODUCTION (S. Wolfe)

1.1 PURPOSE OF GROUND ICE INVESTIGATIONS

Massive ice, defined as ice greater than 1 m thick with a gravimetric water content exceeding 250% (Permafrost Subcommittee, 1988), is well documented in circumpolar regions. In the Slave Geological Province (Figure 1.1), laterally extensive bodies of massive ground ice ranging from 5 to 10 m thick have been identified within esker deposits and beneath till in the Lac de Gras region (EBA Engineering Consultants Ltd., 1995; BHP Diamonds Inc., 1995). Similar occurrences have also been encountered in esker and outwash deposits west of Contwoyto Lake near Ham Lake (EBA Engineering Consultants, 1993) and Carat Lake (this report). Massive ice may be common beneath surficial sediments within the Slave, possibly limiting the volume of material available for extraction and posing potential hazards to ground stability and water quality upon disturbance.

The two major types of massive ice in permafrost are buried ice and intrasedimental ice. Buried ice includes glacier ice, snowbank ice, aufeis (river icings) and other forms of ground ice subsequently buried by sediment. Buried Pleistocene glacier ice has been identified in the Northwest Territories in the Mackenzie Delta-Beaufort region, and on Banks Island, Victoria Island, and west of the Coronation Gulf coast (Lorrain and Demeur, 1985; Dallimore and Wolfe, 1988; French and Harry, 1988; St-Onge and McMartin, 1995). By comparison, intrasedimental ice is formed by the in-situ freezing of water within sediments, and includes segregation and intrusive ice (Mackay, 1971; Mackay and Dallimore, 1992). Massive intrasedimental ice is common in the Mackenzie Delta-Beaufort region and is believed to have formed during the downward aggradation of permafrost (Mackay and Dallimore, 1992) into surficial sediments. Other forms of intrasedimental ice includes wedge ice and pingo ice.

The occurrence of massive ground ice in surficial deposits in the Slave Geologic Province poses a number of issues of engineering and scientific significance. Continued development of the region will require an understanding of ground ice in surficial deposits in order that development

proceeds without excessive disturbance of potentially ice-rich terrain. The purpose of geological and geophysical ground ice investigations conducted by the Geological Survey of Canada are to:

1) Determine the thickness, lateral extent and stratigraphic relationships of massive ground ice and enclosing sediments utilizing boreholes for geologic control and surface and downhole geophyiscal methods for interpolation and extrapolation.

2) Provide geotechnical data on ground ice and associated surficial deposits in permafrost terrain in order to assess the potential hazards or associated constraints to development caused by massive ice occurrences.

3) Determine the origin of massive ground ice bodies utilizing detailed isotopic and geochemical analysis of the ground ice and enclosing sediments.

4) Attempt to determine the regional extent of massive ground ice (ground ice potential) utilizing information collected from these investigations, coupled with an understanding of the regional surficial geology and permafrost distribution in the Slave Geological Province.

1.2 SUMMARY

1.2.1 Airstrip and Misery Lake Eskers

Eight geotechnical boreholes were drilled by Indian and Northern Affairs Canada in the vicinity of the BHP Koala Camp in March, 1996 (Figure 1.1). The Geological Survey of Canada carried out ground ice sampling for geochemical water analysis, to determine the origin of various ice-types within the sediments. Downhole geophysics, including electrical conductivity, magnetic susceptibility and natural gamma was also performed on all boreholes at Airstrip, and one hole at Misery to aid in stratigraphic characterization. Due to time constraints, other boreholes at Misery

were preserved with plastic casing in the event that downhole geophysics could be conducted on these holes at a later date.

Approximately 1.2 line kilometres of ground penetrating radar (GPR) were run at the Airstrip esker in order to determine the lateral extent of ground ice and the stratigraphic relationship with enclosing sediments. This was further supplemented with approximately 5.0 line kilometres of resistivity profiles with the Ohm Mapper (2.0 km at Airstrip and 3.0 km at Misery), providing information pertaining to overburden thickness and the bedrock surface profile.

In addition to these activities the GSC conducted snow, lake ice and water sampling for comparison to ground ice and a sounding program of Airstrip Lake. Several resistivity and GPR calibration experiments were also conducted across the Airstrip esker.

The geophysical techniques identified massive ground ice, sedimentological structure and bedrock contacts. The presence of massive ground ice identified by the GPR was confirmed during the drilling program. Resistivity profiles obtained from the Ohm Mapper appeared to produce good correlation to overburden thickness, and were useful in confirming depth to bedrock. While the Airstrip esker was found to contain discrete bodies of massive ground ice up to 5 m thick, very little ice was encountered at Misery (with the exception of one borehole at the north end of the INAC transect). A till-like diamicton was encountered at a depth of about 5 m in most boreholes drilled at Misery.

The geoscience program conducted in March, 1996 complemented the ground ice sampling program conducted by the GSC in August, 1995. Oxygen isotope values in the range of -26‰ to -30‰ for the ice in the Airstrip esker indicates a cold-water source of glacial or glaciofluvial origin for the massive ground ice encountered in the Airstrip esker. Therefore, it is suggested that the massive ground ice identified in borehole logs and the GPR profiles represents buried ice that was likely deposited as part of the esker system, contemporaneous with deposition of the esker sediments (as water in the sub-glacial channel froze), and has since been preserved by the presence of

permafrost. More enriched isotopic values for ground ice encountered near the surface of the esker suggest a modern water source such as rain or snow. Elemental, cation and anion analysis further suggest separate water sources for the two ground ice types and indicate that the upper ice is more similar to the lake and surface waters in the area, perhaps having percolated through sediments within the active layer. The geochemistry of the lower ice is strongly dissimilar to the upper ice and to modern surface waters, further suggesting a separate (glacial or glaciofluvial) water source for this ice.

1.2.2 Carat Outwash Terrace

One borehole was drilled in the Canamera Carat Camp outwash terrace, in co-operation with Indian and Northern Affairs Canada in March, 1996 (Figure 1.1). The GSC carried out sampling for water analysis to determine the origin of various ice-types encountered, including a 3 m thick body of massive ice. Surface geophysical surveys included approximately 4.5 line kilometres of resistivity profiles with the Ohm Mapper; 1.0 line kilometres of EM-34 surveys and 3.5 line kilometres of GPR. Snow, lake ice and water samples were also collected for comparison to the ground ice encountered in the borehole.

The GPR unit was particularly useful in identifying massive ground ice, subsurface stratigraphy and bedrock contacts at the Carat outwash terrace. As with the BHP investigation, resistivity profiles obtained from the Ohm Mapper appear to produce good correlation to overburden thickness. While parts of the outwash terrace appear to contain discrete bodies of massive ground ice in excess of 10 m thick, the ice occurs sporadically and much of the terrace sediments appear devoid of massive ground ice.

Results from the present geoscience program are inconclusive. The ice encountered in the borehole represents either buried glacial ice, or ice that grew in-situ during permafrost aggradation into the surficial sediments. In either case it has since been preserved by the continued presence of

permafrost. Additional information from a drilling program conducted in the summer of 1996 in conjunction with Canamera Geological Ltd. should provide more conclusive results.

1.3 REFERENCES

BHP Diamonds Inc. 1995. NWT Diamonds Project Environmental Impact Statement, IV Volumes.

Dallimore, S.R. and Wolfe, S.A. 1988. Massive ground ice associated with glaciofluvial sediments, Richards Island, N.W.T., Canada. *In* Proceedings, 5th International Conference on Permafrost. *Edited by* K Senneset. Tapir Publishers, Tondheim, v. 1, p. 132-137.

EBA Engineering Consultants. 1993. Metall Mining Corporation Izok Project, Mine Site Geotechnical Investigation. EBA Report 0101-11157

EBA Engineering Consultants Ltd. 1995. Koala Mine Airport Esker Evaluation. Submitted to BHP Diamonds Inc. EBA Report 0101-94-11439.3.

French, H.M. and Harry, D.G. 1988. Nature and origin of ground ice, Sandhills Moraine, southwest Banks Island, western Canadian Arctic. Journal of Quaternary Science. v.3, p. 19-30.

Lorrain, R.D. and Demeur, P. 1985. Isotopic evidence for relic Pleistocene glacier ice on Victoria Island, Canadian Arctic Archipelago. Arctic and Alpine Research, v. 17, p.89-98.

Mackay, J.R. 1971. The origin of massive icy beds, western Arctic coast, Canada. Canadian Journal of Earth Sciences, v. 8, p. 397-422.

Mackay, J.R. and Dallimore, S.R. 1992. Massive ice of the Tuktoyaktuk area, western Arctic coast, Canada. Canadian Journal of Earth Sciences, v. 29, p. 1235-1249.

Permafrost Subcommittee. Associate Committee on Geotechnical Research. **1988**. Glossary of permafrost and related ground-ice terms. National Research Council of Canada, Technical Memorandum 142.

St-Onge, D.A. and McMartin, I. 1995. Quaternary Geology of the Inman River Area, Northwest Territories. Geological Survey of Canada, Bulletin 446, pp. 59.

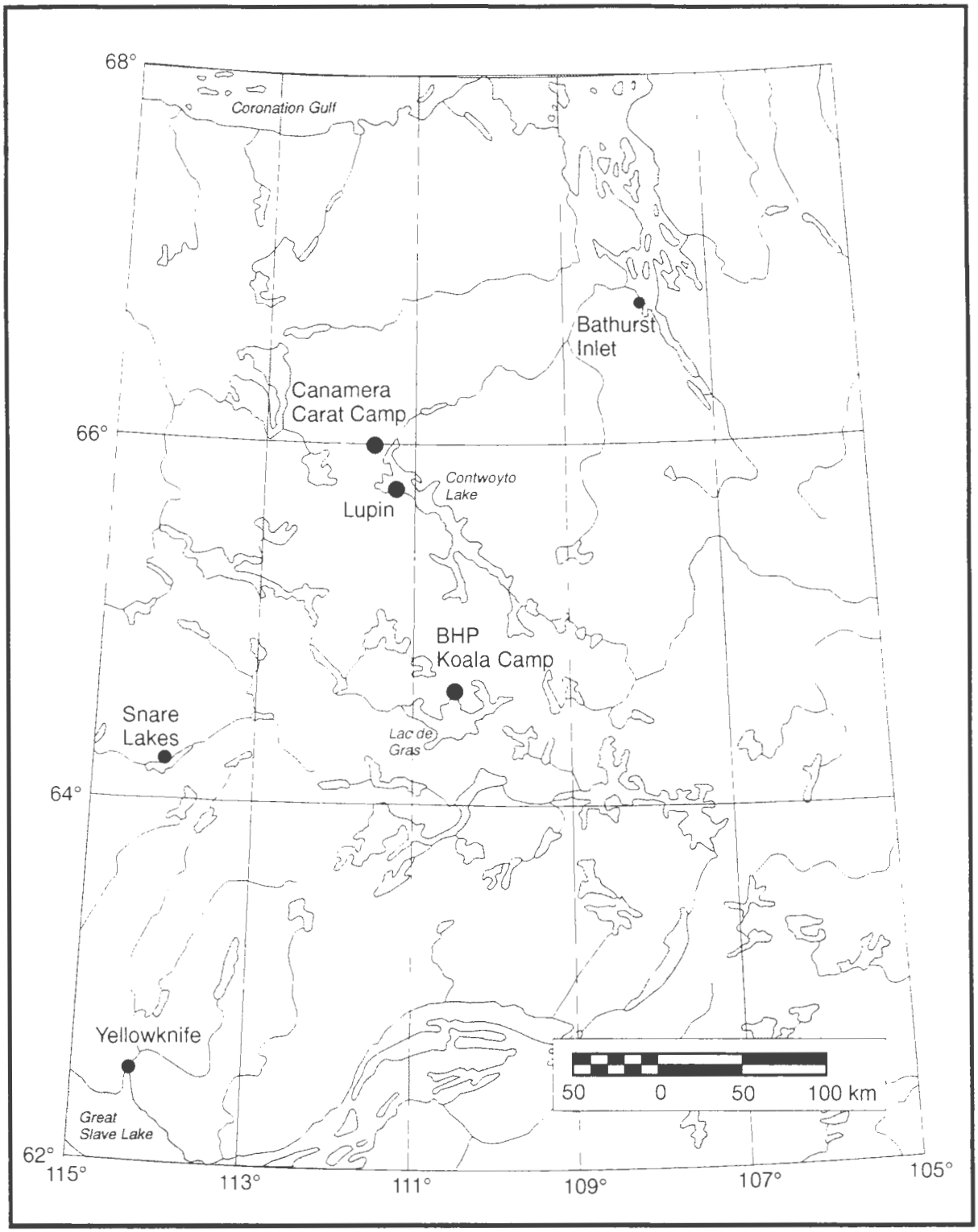

Fig. 1.1 Location of BHP Diamonds Inc. Koala Camp and Canamera Geological Ltd. Carat Camp in the Slave Geological Province.

2. SURFICIAL GEOLOGY AND SUBSURFACE CONDITIONS (S. Wolfe)

2.1 SURFICIAL GEOLOGY AND PERMAFROST

2.1.1 Lac de Gras Region

The BHP Diamond Inc. Koala Camp is located north of Lac de Gras, within the Slave Geological Province of the N.W.T. (Figure 1.1). The surficial geology of this area was mapped by Ward et al. (1995) and a description of the nature and distribution of the local surficial sediments may be found therein. The eskers, other glaciofluvial deposits, and the surficial tills were deposit during the most recent advance of the Late Wisconsinan Laurentide Ice Sheet. Esker deposits are geographically widespread but limited in extent. Associated with the esker systems are small kames and boulder-rich washed zones surrounding the deposits (Dredge et al., 1994).

The Lac de Gras area resides just inside the southerly limit of continuous permafrost (Brown, 1967). Permafrost is estimated to extend to depths of up to 280 m (Brown, 1967). As a result of geotechnical investigations by BHP Diamonds Inc., ground temperature data in the area has been systematically collected since 1993. A number of thermistor cables in drill holes exist in the vicinity of Koala Camp. Temperature data confirm the presence of permafrost in most areas other than beneath lakes. Mean annual ground temperatures at 15 m depth are reported to range from 0°C to -6°C, depending upon the proximity to water bodies (EBA Engineering Consultants Ltd., 1995a, 1995b).

The presence of permafrost in the area often results in the formation of ice wedge polygons on eskers and glaciofluvial sediments. Ice wedge polygons are typically well developed on flat-topped outwash deposits despite often thin organic cover. Ice wedge polygons are seldomly visible on sinuous eskers in most areas, perhaps due to the narrow and steep-sided nature of these features. In addition to wedge-ice, laterally extensive massive ground ice bodies have been identified in esker deposits and in till in the Lac de Gras region (EBA Engineering Consultants Ltd., 1995b; BHP

Diamonds Inc., 1995), and to the north in the Contwoyto Lake region. It appears that massive ice may be common in surficial sediments in the Slave Geological Province, possibly limiting the volume of material available for extraction and posing potential hazards to ground stability and water quality upon disturbance. Presently, however, the origin and extent of massive ground ice in the region is not known.

Both the BHP Airstrip esker and the Misery esker reside on till mantled terrain, and are northwest trending deposits connected to a larger east-west trending esker system north of Lac de Gras. The eskers in this region commonly run through and alongside lakes, and occasionally act as natural dams or partial barriers to surface water drainage. In addition, small perched lakes or ponds may be found on top of larger eskers and outwash deposits.

2.1.2 Northern Contwoyto Lake Region

The Canamera Geological Ltd. Carat Lake exploration site is located northwest of Contwoyto Lake, in the District of Mackenzie, NWT (Figure 1.1). The surficial geology of the region is being systematically mapped by the GSC. The surrounding areas of 86I, 86H and parts of the 76E map sheet have been mapped by Kerr et al. (1995) while the area encompassing Carat Lake was recently mapped in the summer of 1996. The eskers, other glaciofluvial deposits, and surficial tills are all related to the most recent advance of the Late Wisconsinan Laurentide Ice Sheet which remained in the region until about 9000 years BP.

The Carat Lake site resides within the region of continuous permafrost (Brown, 1967). Permafrost is estimated to extend to depths of approximately 460 m (Canamera Geological Ltd. 1996b). Although ground temperature data in the region is extremely limited, thermistor cables have been installed in drill holes in the Jericho (Carat) kimberlite pipe and, more recently, on the outwash terrace. Unpublished data confirms the presence of permafrost to a depth of more than 200 m in bedrock, as well as a mean annual ground temperature of approximately -5.8°C at a depth of 25 m

on the outwash terrace.

2.2 SITE INVESTIGATIONS

2.2.1 Airstrip Esker

Airstrip esker is approximately two kilometres long and is part of a northerly trending complex of eskers, connecting to a larger east-west trending esker system approximately 8 km north of Koala Camp. The Airstrip esker acts as a natural dam impounding a significant sized lake on the east side (Figure 2.1). Locally, the esker reaches a maximum elevation of 18 m above the adjacent terrain to the west, although the elevation difference between the top of the esker and Airstrip Lake on the east side is approximately 5 m. Depth soundings conducted on Airstrip Lake in March 1996 indicate a lake depth in excess of 7 m.

EBA Investigations, July 1994

In July 1994, EBA Engineering Consultants Ltd. were retained by BHP Diamonds Inc. to evaluate the esker for potential granular material and to provide development guidelines that would ensure the integrity of the esker and prevent the natural dam from being breached (EBA Engineering Consultants Ltd., 1995b). At that time, three geotechnical boreholes were drilled through the esker for the purpose of granular investigations and to install temperature cables in the esker (Figure 2.1). Several boreholes were also drilled along the western flank of the esker into the surrounding till mantle and underlying bedrock. In addition, borehole data were supplemented by GPR profiles across the surface of the esker (EBA Engineering Consultants Ltd., 1995b). Although the report goes into little detail concerning the esker sediments or ground ice encountered at the Airstrip esker, approximately 5.5 m of massive ice was encountered in borehole BH-E3 on the esker (Figure 2.1). GPR profiles obtained at that time further suggested that massive ice could be laterally extensive beneath the surface of the esker.

GSC Investigations, August 1995

On August 18, 1995, Dr. Stephen Wolfe of the Geological Survey of Canada, visited the Airstrip esker quarrying site and sampled massive ground ice along the esker flank in an attempt to determine the origin of the ice. Field work consisted of detailed description of the exposed ice together with shallow coring and sampling of the ice, sediments and surface waters. At that time, massive ice was exposed at the surface of the active pit from near the top of the esker to the base, covering a distance of over 32 m (Figure 2.1). The ice was present along slope for a distance of over 100 m and surface samples were obtained across a 32.5 m transect (Figure 2.2). The ice was cored to a depth of 1.7 m near the base of the esker and to 0.80 m near the top (Figure 2.3). In general, ice samples obtained were relatively free of sediment. Trace amounts of sediment, where it occurred, was similar to the overlying sands and gravels and occurred in bands inclined up to 50° to the horizontal.

Ice samples collected on August 18, 1995 were analysed for oxygen and deuterium isotope concentrations (Table A1), major cation and anion composition (Table A2), elemental concentrations, electrical conductivity and pH (Table A3). The pH of the massive ground ice samples ranged from 5.7 to 6.7 and averaged 6.2, comparable to the value of 6.2 obtained for the Airstrip Lake. Electrical conductivities of the sediment-free ground ice were commonly very low (ranging from 4 to 22 µmhos/cm) and were comparable to that of the Airstrip Lake (19 µmhos/cm), but were up to 119 µmhos/cm when associated with sediment. In these instances, because of the very low conductivity of the ice, even small amounts of dissolved elements from the included sediment increased the electrical conductivity considerably. Despite the similarities between the ground ice and the Airstrip Lake water mentioned above, there were considerable differences in the elemental composition of the waters. In particular, the ground ice contained higher concentrations of Fe, Mn, Co, Ba, La, Pb and U than the lake water, among other elements, suggesting that the water source for the ice and the lake water may be different. In addition, core samples obtained from the upper part (samples 121 to 124) of the esker are considerably more enriched in these elements, compared to samples obtained from the lower part of the esker (samples 100 to 106). This further suggests that,

either the upper and lower ice in the esker may have different origins, or that the upper ice has been affected by an additional groundwater water source.

These differences are further reflected in the oxygen and deuterium isotope analysis (Figure 2.4). The oxygen isotope value of a sample from Airstrip Lake, relative to Standard Mean Ocean Water (SMOW), is -18.74‰. In comparison, most of the ground ice samples obtained from the exposed massive ice have values of between -28.2‰ and -30.2‰, possibly indicating a much colder water source for the ice. However, ground ice samples obtained near the top of the esker have values of between -22.0‰ and -25‰, and are intermediate between the Airstrip Lake water and snow (Figure 2.4).

The oxygen isotope analysis suggests two different sources of water for the ice contained in the esker; one source for the lower ice having values between -28‰ and -30‰, and a second source for ice near the surface having values between -25‰ and -22‰. This analysis appears to be confirmed by the cation and anion analysis of the water and by dissolved elements in the water. Dissolved sulphate (SO_4^{-2}) in the ground ice near the surface of the esker ranges between 4.5 and 45.7 ppm (comparable to the values of 2.9 and 35.8 ppm for modern waters in the Airstrip Lake and downstream of the esker). In contrast, the SO_4^{-2} concentrations for the lower ground ice are all less than 0.8 ppm. The same observations are generally true for NO_3^{+2}, Ca^{+2} and Mg^{+2}.

2.2.2 Misery Lake Esker

The Misery Lake esker extends for approximately 30 km, trending north-northwest to connect to the larger east-west trending Lac de Savage esker system approximately 8 km northeast of Koala Camp. The southernmost limit of the Misery Lake esker is a proposed location for aggregate resource extraction in conjunction with BHP's development activities in the Misery Lake region. Esker deposits in this area traverse complex surficial terrain including bedrock, till, organic deposits and numerous small lakes (Figure 2.5). The south end of the system appears kame-like, with

several distinct hills comprising the terminus of the deposit. In this vicinity, the summit of the esker is relatively flat, and ice wedge polygons are apparent in several areas. The deposits appear to be wave-washed in this area, possibly resulting from higher post-glacial water levels in Lac de Gras as suggested by Ward et al. (1995). Farther north, the esker appears to dam a small lake for a length of approximately 500 m (Figure 2.5). In this area, the top of the esker is narrow and the eastern flanks are steep.

2.2.3 Carat Outwash Terrace

An extensive glaciofluvial deposit resides immediately north and east of Carat Lake. The deposit has been identified by Canamera Geological Ltd. as an aggregate resource and location for an airstrip and tank farm for diamond exploration purposes. The deposit includes a local sandy outwash terrace and a more extensive coarse-grained esker deposit, representing the southerly portion of a large north to northwest trending esker complex. This southern portion of the esker system has been referred to as the Jericho Esker Complex in previous reports (Canamera Geological Ltd., 1995, 1996).

The outwash terrace north of Carat Lake covers an area of approximately 75 hectares (Figure 2.6). Presently, a borrow pit area is located at the south end of the terrace, adjacent to Carat Lake, with a tank farm located approximately 250 m north of the borrow pit. An airstrip is also located on the terrace adjacent to the previously proposed location of borrow site C (Figure 2.6).

The outwash terrace is interpreted to have formed after deposition of the Jericho Esker Complex, with the delta likely forming adjacent to a glacial lake with an inferred lakeshore elevation of 450 m (Canamera Geological Ltd. 1995). In addition, the presence of several lakes with circular shorelines abutting the terrace sediments indicates that terrace sediments were likely deposited adjacent to melting ice blocks. Ice was also likely present in Carat Lake during the formation of the terrace.

2.3 SUBSURFACE CONDITIONS

2.3.1 Drilling and Sampling Procedures

Drilling was conducted with a mobile CME 750 drill rig on rubber tires with top drive head. Boreholes were dry-cored with 6-inch diameter augers and a 4-inch CRREL barrel or an MS-3200 drill bit, depending upon sediment type. Core and auger cutting retrieved were described and sampled by GSC staff. Extruded CRREL samples were measured, described and subsampled for moisture content, grain size of the sediments and for isotopic analysis and electrical conductivity of porewaters. A brief sediment type description, and the presence and type of ground ice, where observed, was logged.

2.3.2 Airstrip Esker

From March 19 to 21, 1996 the Geological Survey of Canada along with Indian and Northern Affairs Canada conducted geotechnical drilling from the surface of the esker along a transect consistent with previous boreholes (Figure 2.1). Three boreholes were drilled in order to obtain data on massive ground ice and enclosing sediments (see Table A4 for analyses). The borehole data was further supplemented with approximately 1.2 km of GPR profiles and 2.0 km of resistivity profiles.

The three boreholes drilled on the Airstrip esker ranged in depth from 7 to 16 m (Figures 2.7 to 2.9). Sand and gravel dominated the sediments, with layers of silty sand in all holes (Table A4). The sands and gravels were typically well-graded with distinct but frequent changes in stratigraphy. Except where massive ice occurs, the sand and gravel layers typically did not contain visible ice and moisture contents were typically less than 25% (Table A4).

Borehole INAC-01 encountered approximately 5 m of massive ice beginning at a depth of

about 9 m (Figure 2.7). Close to sediment contacts, the ice contained fine sand and silt layers along horizontal and vertical fractures, indicative of thaw contacts. Contacts between the ice and sediment were oxidized. Otherwise, the ice was clear to cloudy and commonly bubble-rich with flattened bubbles to 2 mm in diameter.

Borehole log INAC-01 (Figure 2.7) also depicts oxygen isotope concentrations and electrical conductivities of the porewaters. The $\delta^{18}O$ values in Unit 1 of the borehole are relatively enriched (-26.8‰) in the upper part of the unit (isotopes could not be obtained from the sediment above 2.4 m due to the low moisture content) compared with $\delta^{18}O$ values in the lower portion of Unit 1 residing in the -29‰ range. The $\delta^{18}O$ values for the massive ice in Unit 2 are slightly depleted, ranging from -28‰ to -29‰. Porewaters contained within bands of sediment in Unit 2 also tend to be less negative ($\delta^{18}O$ -26.9‰ to -27.9‰) than the enclosing ice. In general, the massive ice also has very low electrical conductivities (<10 µS/cm), except where it is in contact with sediment bands, suggesting that solute concentration in the ice is low. Similarly, ground ice samples collected in the summer of 1995 revealed that dissolved cations (Na^{+}, K^{+}, Ca^{+2}, Mg^{+2}) in the lower massive ice were all less than 1 ppm (Table A2).

The co-isotope plot of δD(SMOW) versus $\delta^{18}O$(SMOW) (Fig. 2.10) indicates that the porewater and ground ice samples from INAC-01 are considerably more depleted in both isotopres relative to waters from other sources in the Slave including surface waters, aufeis, snow and wedge ice (Table A5). These background water samples were collected in the summer of 1995 from various sources in the north Slave region in the Kikerk Lake and Coppermine map sheets. The figure indicates that waters from INAC-01 possibly have a "colder" water source than other waters sampled in the region.

Approximately 1.2 m of massive ice was encountered in borehole INAC-2, starting at a depth of 1.1 m (Figure 2.8). The ice occurred within well-graded gravels, and the shallow depth suggests that it is presently located within the active layer. However, overlying sediments had previously been removed by quarrying activities so that the ice was previously at a greater depth than

present. Drilling terminated at a depth of 9.2 m and no other massive ice was encountered in the hole. Oxygen isotopic concentrations obtained from the INAC-2 borehole were similar to those in INAC-1, residing in the -29‰ to -30‰ range. Finally, no massive ice was obtained from borehole INAC-03 drilled to 7.0 m depth (Figure 2.9). However, no samples were obtained from 3 to 7 m depth due to a slurry created by the high moisture content of the sediments.

2.3.3 Misery Lake Esker

Five boreholes were drilled at the south end of the Misery Lake esker from March 22 to 24, 1996. The borehole data was further supplemented with approximately 3.0 kilometres of resistivity profiles with the Ohm Mapper (Figure 2.5).

The five boreholes drilled on the Misery Lake esker ranged in depth from 4 to 11 m (Figures 2.11 to 2.15). Sand and gravel dominated the upper 1.5 to 5 m of sediment, ranging from clean poorly-graded sands to well-graded gravels. In several of the boreholes (INAC-04, 05, 06), a grey, coarse silty sand diamicton was encountered that had the appearance of till. The diamicton occurred at an average depth of 4.5 m below the surface, and in two of the holes (INAC-04 and INAC-05) the unit continued to the termination of the hole. Each of these three holes was located near the summit of the esker, while the two other holes (INAC-07 and INAC-08) were located east of the main deposit on comparatively flat surfaces. Massive ice was encountered in only one borehole (INAC-08), at a depth of approximately 6.2 m. At all other locations, the ice contents were low, and moisture contents were typically less than 20%.

Borehole INAC-04 encountered approximately 5 m of clean but well-graded sand and gravel, overlying at least 3 m of sandy diamicton (Figure 2.11). Similarly, approximately 4 m of relatively clean sand and gravel, overlying at least 6.5 m of sandy diamicton, was encountered in INAC-5 (Figure 2.12). Moisture contents were slightly higher in the diamictons, compared to the overlying sands and gravels, probably as a result of the increased proportion of fine sediments. Borehole

INAC-06 encountered approximately 3 m of coarse sand and gravel, over approximately 1.5 m of silty-sand with some gravel. The silty-sand unit, in turn, was underlain by at least 5 m of medium to coarse sand with gravel (Figure 2.13). Borehole INAC-07 encountered approximately 2 m of gravel, underlain by a medium sand with increasing silt content a depth (Figure 2.14). Drilling terminated at a depth of approximately 4 m on probable bedrock. Borehole INAC-08 was located approximately 15 m south of the small lake adjacent to the Misery Esker (Figure 2.5). The borehole encountered approximately 1 m of well-graded gravel, underlain by 4 m of fine-grained fluvial sands with fine silt laminae. Sandy beds in this unit were very steeply dipping (60° to the horizontal), indicative of post-depositional displacement. The presence of ice wedge polygons in this area, and in the vicinity of INAC-07, suggests that ice wedge growth may be responsible for the displacement. This sandy unit was underlain by approximately 1 m of gravel that, in turn, was underlain by ice. Approximately 60 cm of ice was encountered before the auger stem on the drill broke. Thus, the maximum thickness of the underlying ice is unknown. Oxygen and deuterium isotopes from this borehole are the most negative encountered during this project. Oxygen isotopic concentrations from the ice and the overlying fine-grained steeply dipping sands are in the range of -35‰. These values would likely rule out a modern source for these waters.

2.3.4 Carat Outwash Terrace

On March 25 and 26, 1996 the Geological Survey of Canada along with Indian and Northern Affairs Canada conducted geotechnical drilling from the surface of the outwash terrace, in the vicinity of borrow site A, southeast of the tank farm (Figure 2.6). This borehole was further supplemented by approximately 4.5 line kilometres of resistivity profiles with the Ohm Mapper and 3.5 line kilometres of GPR profiles.

Borehole INAC-09, on the Carat Lake outwash terrace, was drilled to a depth of approximately 16 m until problems occurred with drilling operations. Medium to fine sand dominated the borehole for the upper 11 metres (Figure 2.16). A fining-downward sequence of sands

graded into a 2 m thick unit of medium to fine sand with grey silt. Moisture contents remained fairly consistent throughout the sandy unit, ranging from approximately 24 to 30% with a trend towards increasing moisture content with depth. Sediments were well-bonded, with excess ice evident upon thawing.

Massive ice was encountered in the borehole at a depth of approximately 13 m. The ice contained inclusions of grey silt, occurring as small aggregates in distinctly parallel bands. Approximately 3 m of massive ice was drilled prior to the termination of drilling. The borehole log also depicts oxygen isotope concentrations and electrical conductivities of the porewaters (Fig. 2.16). As in borehole INAC-1, the $\delta^{18}O$ values in Unit 1 of INAC-9 are highest in the upper part of the unit (~-20‰), compared with $\delta^{18}O$ values in the lower portion of Unit 1 lying in the -27.5‰ range. The $\delta^{18}O$ values for the fine sands in Unit 2 are slightly more negative (-28.5‰ to -29.05‰) while the underlying massive ice in Unit 3 is less negative, averaging about -25‰. The massive ice tends to have higher electrical conductivities than the BHP esker ice (40 to 130 µS/cm).

The co-isotope plot of δD(SMOW) versus $\delta^{18}O$(SMOW) from INAC-9 (Fig. 2.17) shows three distinct clusters from INAC-09. Porewaters from the upper portion of Unit 1 are comparable to surface waters, aufeis and ice wedge samples found in the north Slave region. This suggests that the upper 3.5 m of Unit 1 may have been influenced by surface waters. This is most likely due to modern or past active layer thicknesses up to 3.5 m deep. Interestingly, the most negative porewaters are from the lower portion of Unit 1 and from Unit 2 which, like the porewaters in INAC-1, suggest a cold-water source, while the waters from the massive ice in INAC-9 (Unit 3) are more enriched in $\delta^{18}D$ and $\delta^{18}O$ not unlike modern-day snow. Unfortunately, the isotopic evidence alone does not provide conclusive evidence for either a segregated or glacial origin for the ice.

Very little gravel was encountered in the borehole, suggesting that it was located near the distal end of the outwash deposit. In addition, the fining-downward sequence of sediments is consistent with a previous interpretation of a prograding delta (Canamera Geological Ltd. 1995). GPR profiles (see section 3) further suggest that the upper sediments are deltaic, as prominent foreset

beds are visible at the distal (southern end) of the deposit.

The thick sequence of sediments overlying the ice, suggests that sediments were deposited into relatively deep water. Interpretation by Canamera Geological Ltd. (1995), place the inferred glacial shoreline at an elevation of 480 m asl, suggesting a local water depth of between 15 to 20 m. It is clear that large blocks of stagnant glacial ice were probably present during deposition of the outwash sediments, as is evident by the numerous thaw lakes in the area, and it is possible that the sediments buried large blocks of ice which were subsequently preserved by permafrost.

2.4 REFERENCES

BHP Diamonds Inc. 1995. NWT Diamonds Project Environmental Impact Statement, IV Volumes.

Brown, R.J.E. 1967. Permafrost in Canada. Geological Survey of Canada, Map 1246A, scale 1:7,603,200.

Canamera Geological Ltd. 1995. Lytton Minerals Limited Jericho Diamond Project: Bulk sample Class A Land Use Application. Report submitted to Indian and Northern Affairs Canada.

Canamera Geological Ltd. 1996. Lytton Minerals Limited Jericho Diamond Project: Submission in support of Class A Land Use Application. Report submitted to Indian and Northern Affairs Canada.

Dredge, L.A., Ward, B.C and Kerr, D.E. 1994. Glacial geology, and implications for drift prospecting in the Lac de Gras, Winter Lake, and Aylmer Lake map areas, central Slave Province, Northwest Territories. In Current Research 1994-C; Geological Survey of Canada, p. 33-38.

EBA Engineering Consultants Ltd. 1995a. NWT Diamonds Project: Tailings Management Plan and Preliminary Design of Retention Structures. Submitted to BHP Diamonds Inc. EBA Report 0101-94-11580.2.

EBA Engineering Consultants Ltd. 1995b. Koala Mine Airport Esker Evaluation. Submitted to BHP Diamonds Inc. EBA Report 0101-94-11439.3.

Kerr, D.E. Dredge, L.A., Ward, B.C and Gebert, J.S. 1995. Quaternary geology and implications for drift prospecting in the Napaktulik Lake, Point Lake and Contwoyto Lake map areas, northwest Slave Province, Northwest Territories. *in* Current Research 1995-E; Geological Survey of Canada, p. 201-209.

Ward, B.C, Dredge, L.A. and Kerr, D.E. 1995. Surficial geology, Lac de Gras, District of MacKenzie, Northwest Territories. Geological Survey of Canada, Map 1870A (North), scale 1:125 000

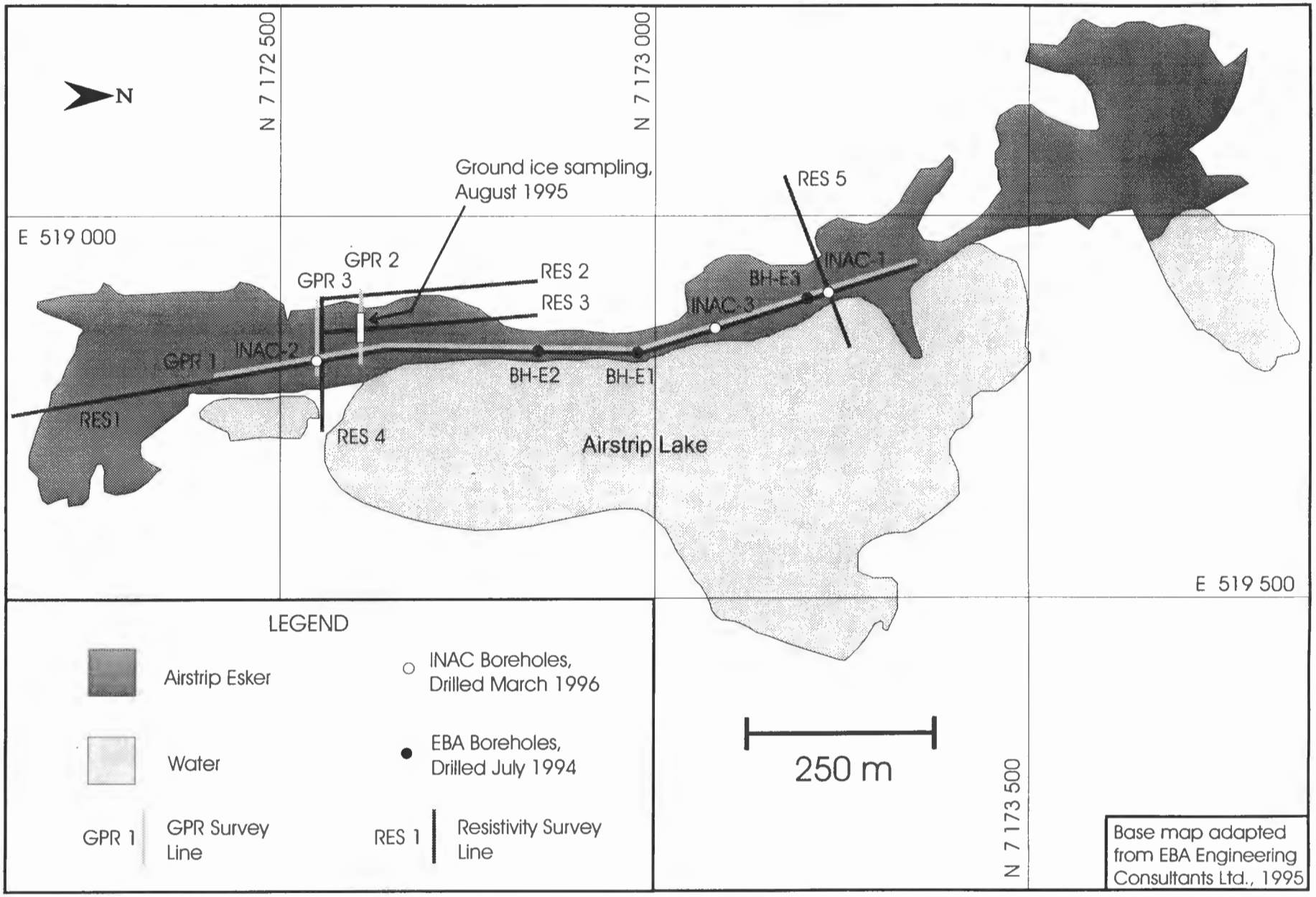

Figure 2.1. Borehole locations, ground ice sampling and geophysical surveys on BHP Airstrip esker.

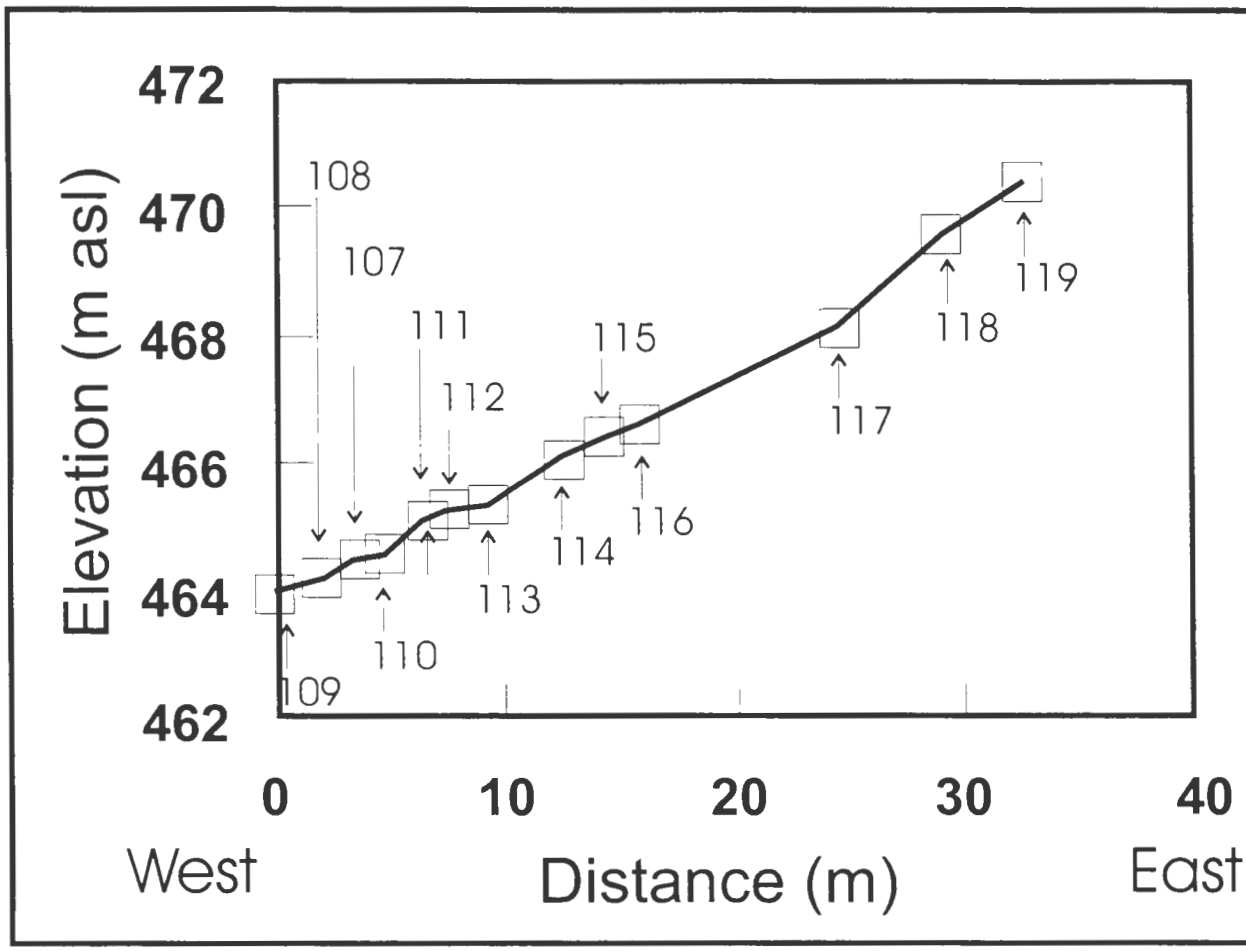

Figure 2.2. Location of massive ice and sediment surface samples from flank of Airstrip esker (refer to Figure 2.1 for location of sampling transect).

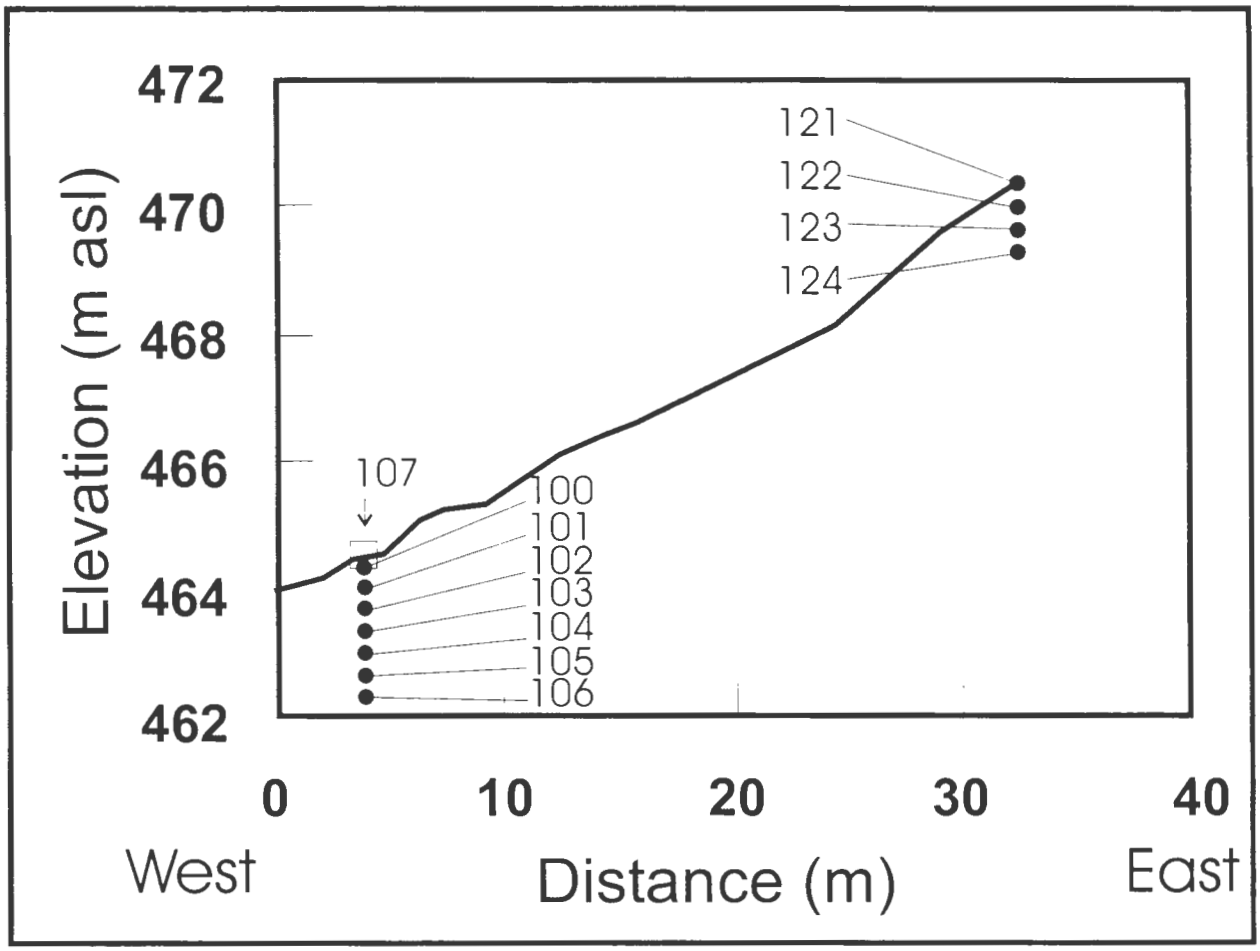

Figure 2.3. Location of massive ice and sediment borehole samples from flank of Airstrip esker (refer to Figure 2.1 for location of sampling transect).

Figure 2.4 Isotopic concentrations of Airstrip esker flank and other waters.

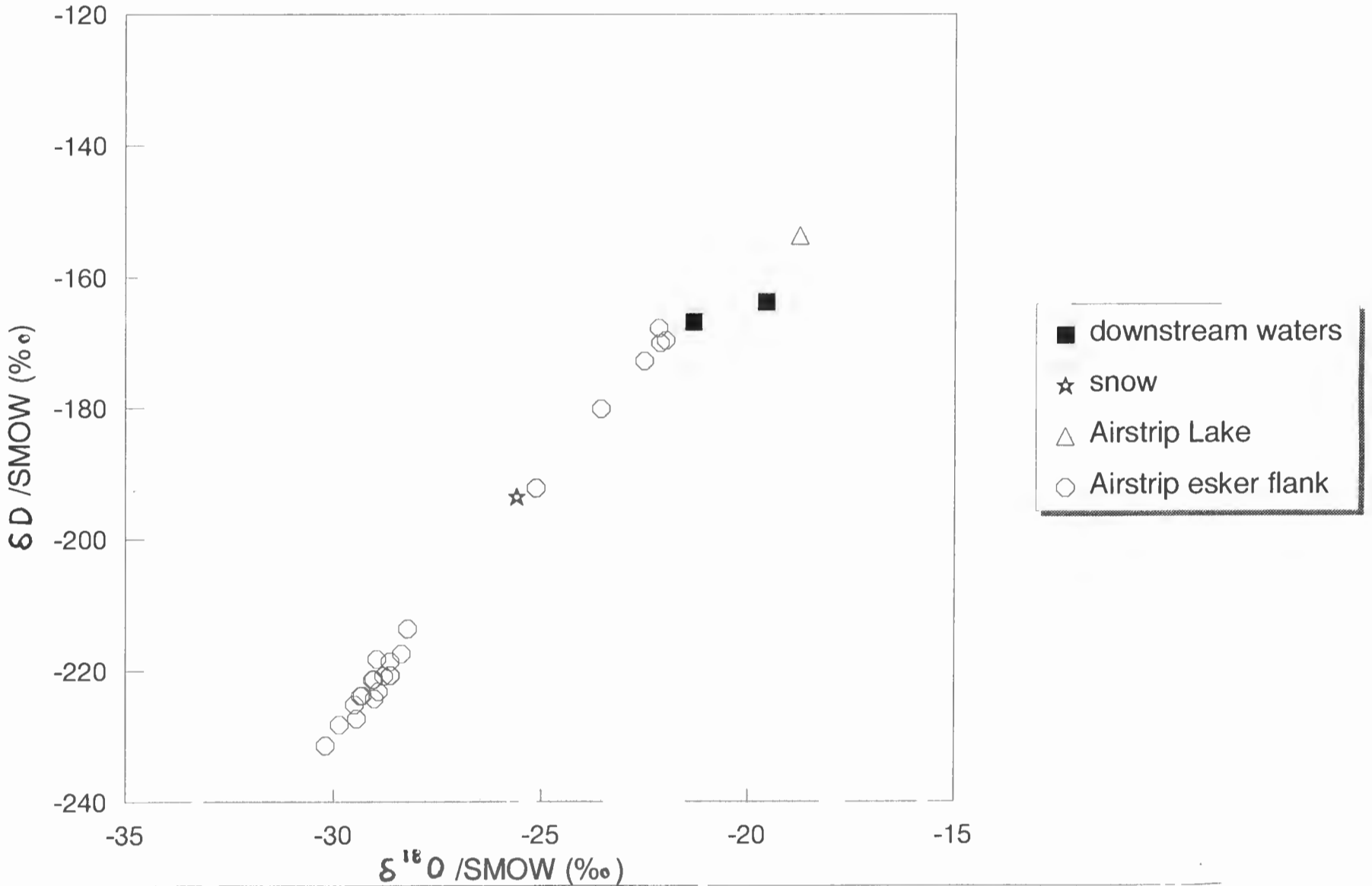

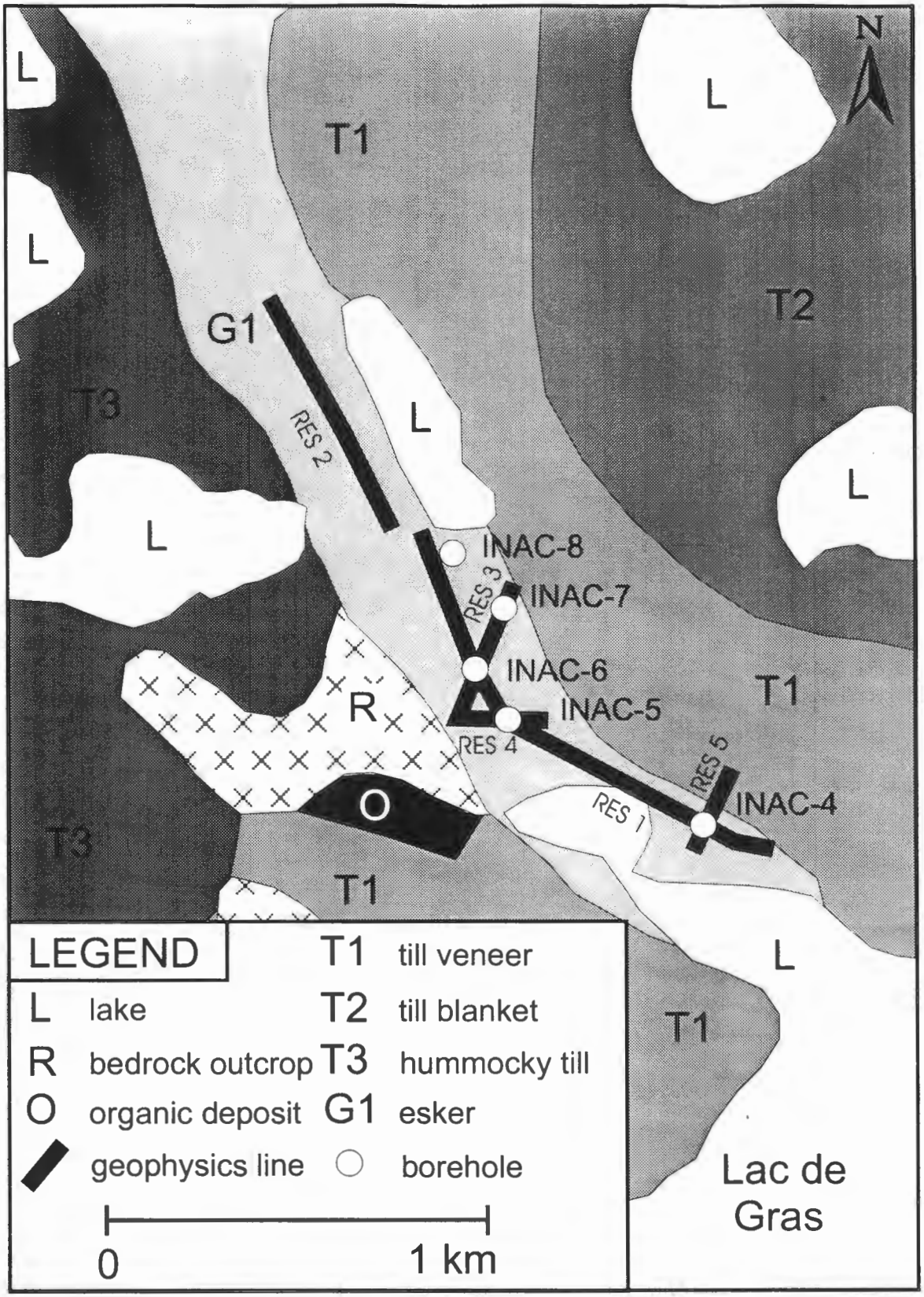

Figure 2.5 Surficial geology, geophysics and borehole locations in the Misery Lake Esker region (surficial geology after Ward et al., 1995).

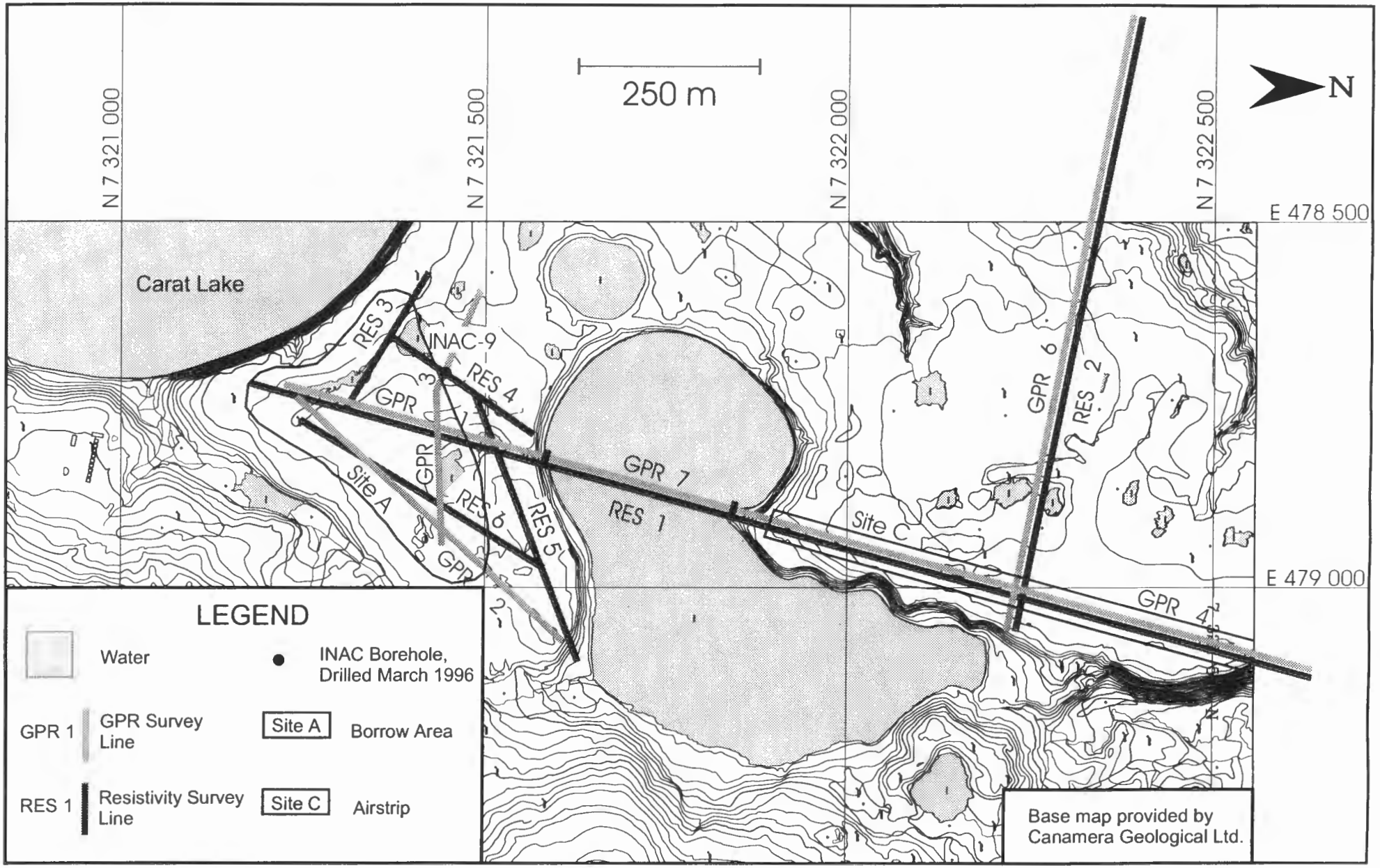

Figure 2.6 Borehole location and geophysical survey lines on the Carat outwash terrace.

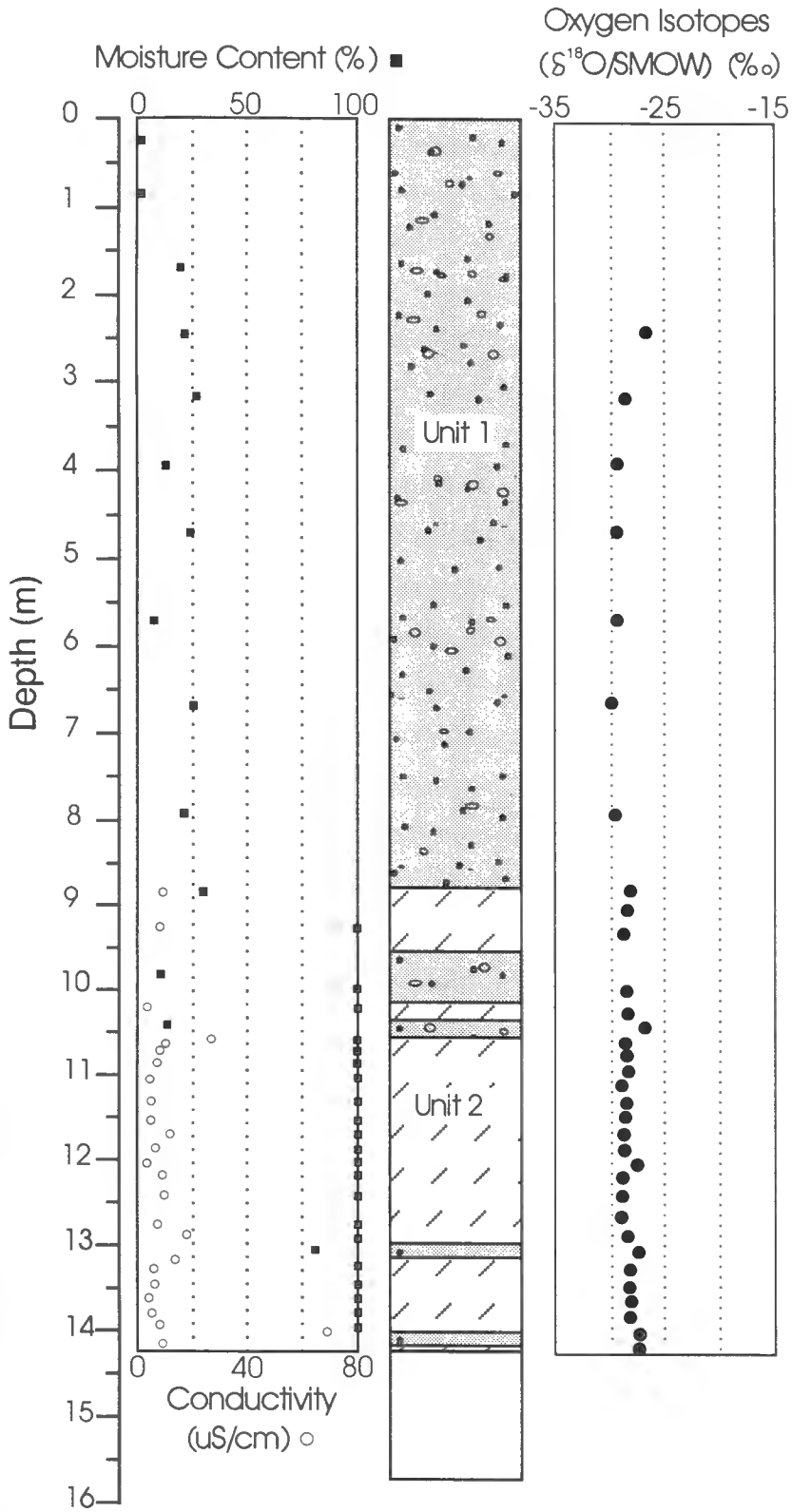

SAND, medium to coarse, SP-SW with trace silt and frequent gravelly beds. Nbn/Nbe

ICE, clear to cloudy, with cylindrical flattened bubbles to 2 mm. SAND layers(SP-SM), medium to coarse with silt and occasional gravelly beds and coarse sand (SW). Contacts between sand and ice abrupt and oxidized, silt included in ice below contacts along fracture planes.

Coarse-grained sediments, no samples, drilling ending at refusal.

EOH, possible bedrock @ 15.85 m

Figure 2.7 Borehole log INAC-01.

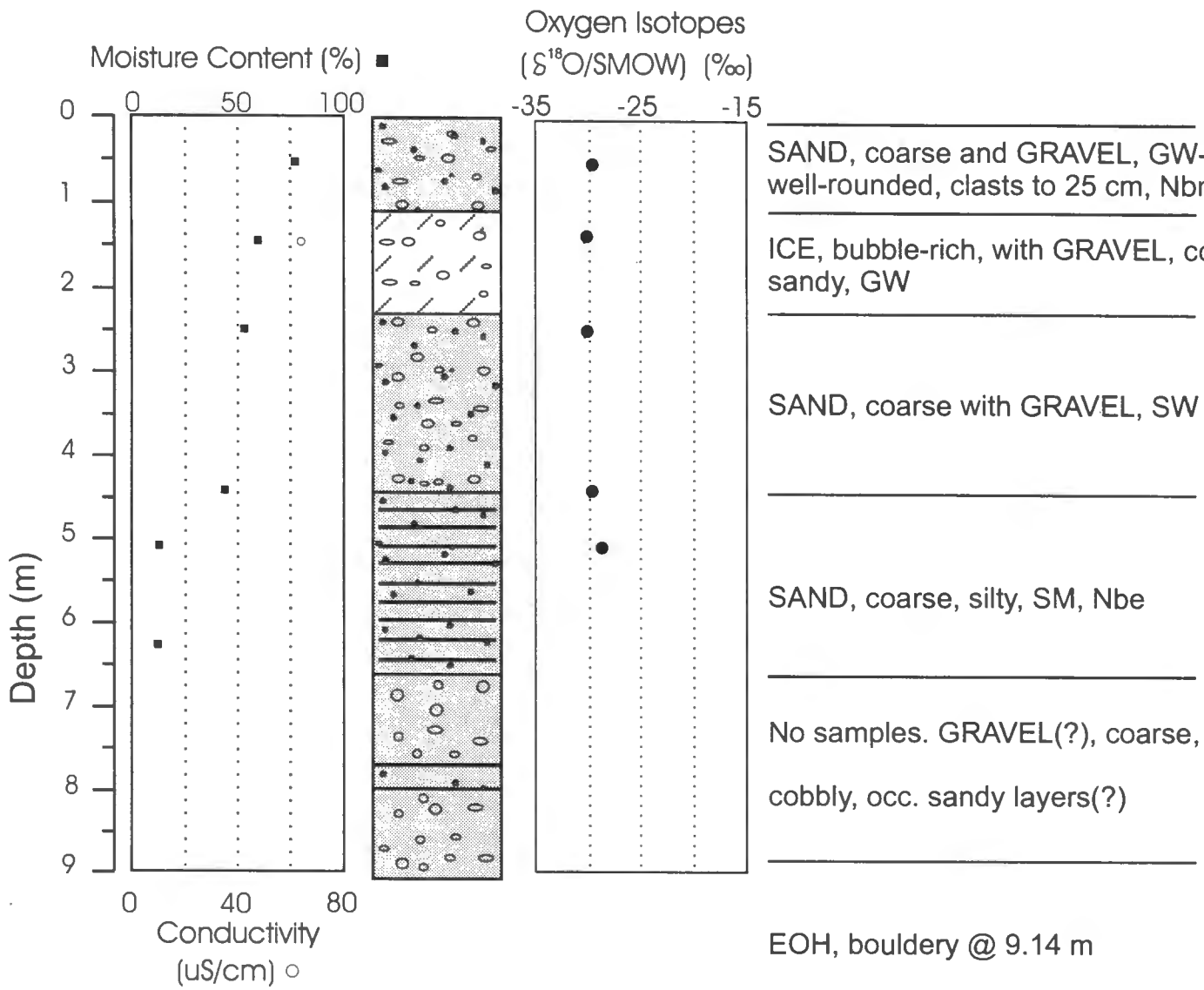

Figure 2.8 Borehole log INAC-02.

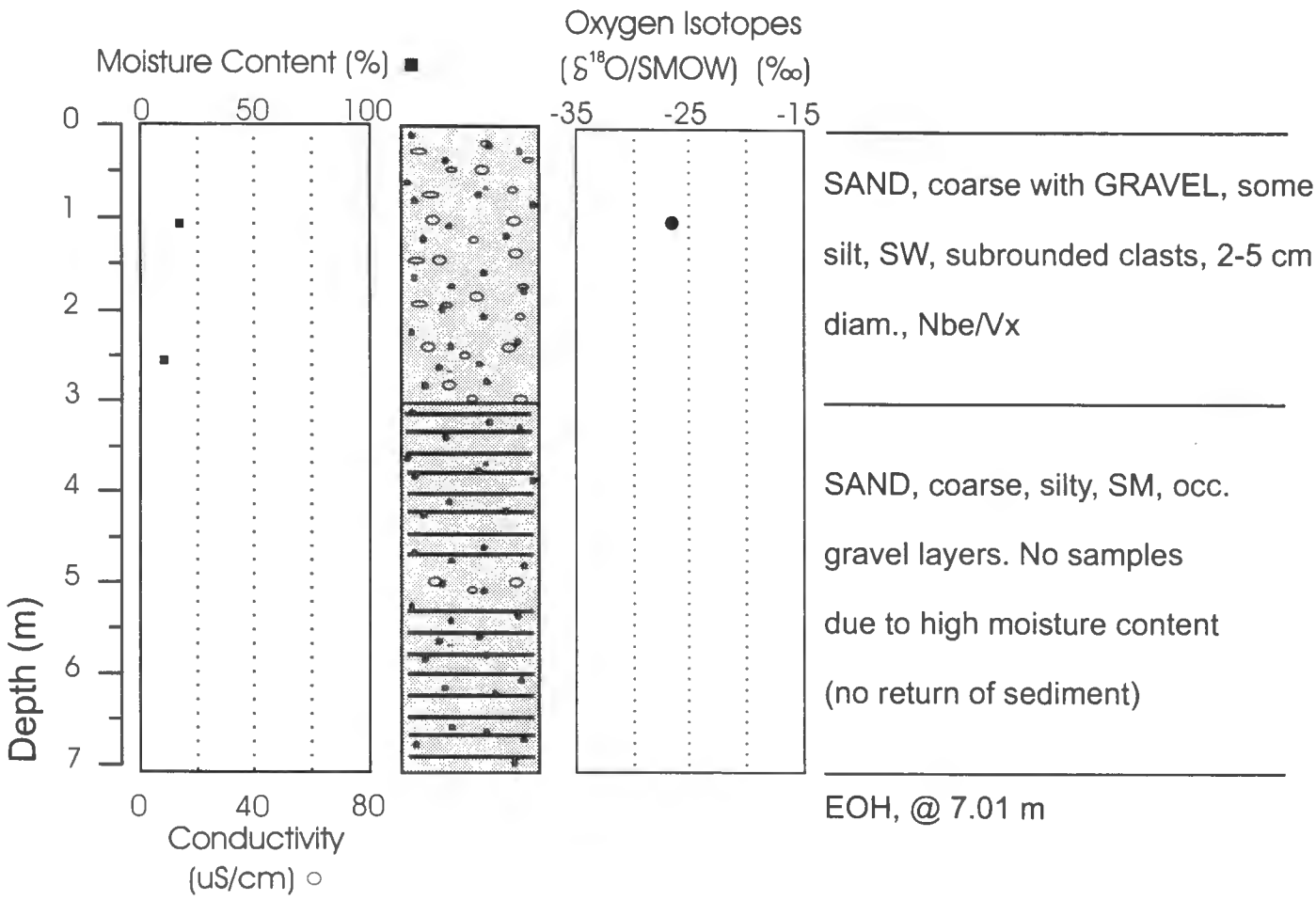

Figure 2.9 Borehole log INAC-03.

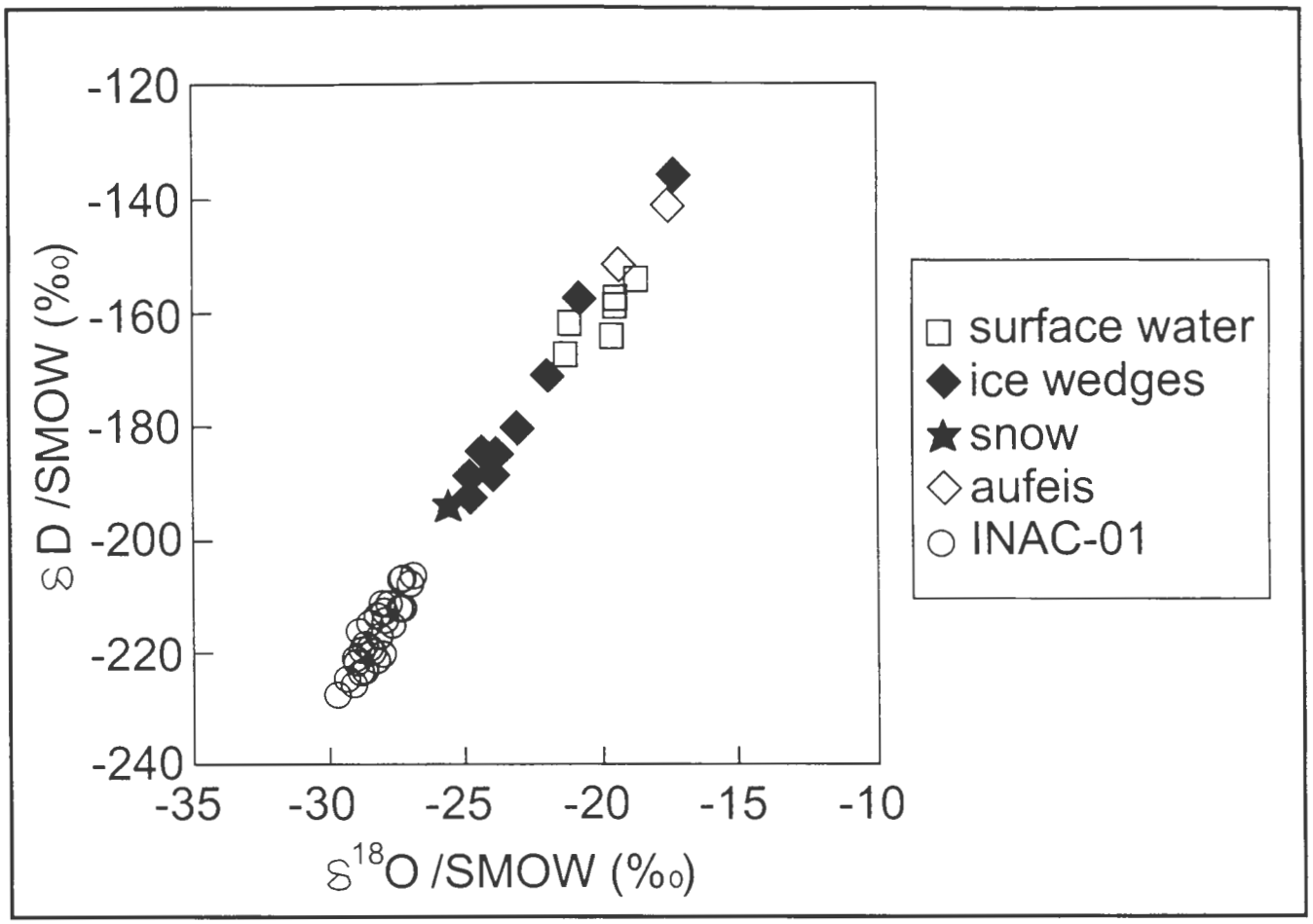

Figure 2.10. Co-isotope plot of δ D (SMOW) versus δ^{18}O (SMOW) from INAC-01.

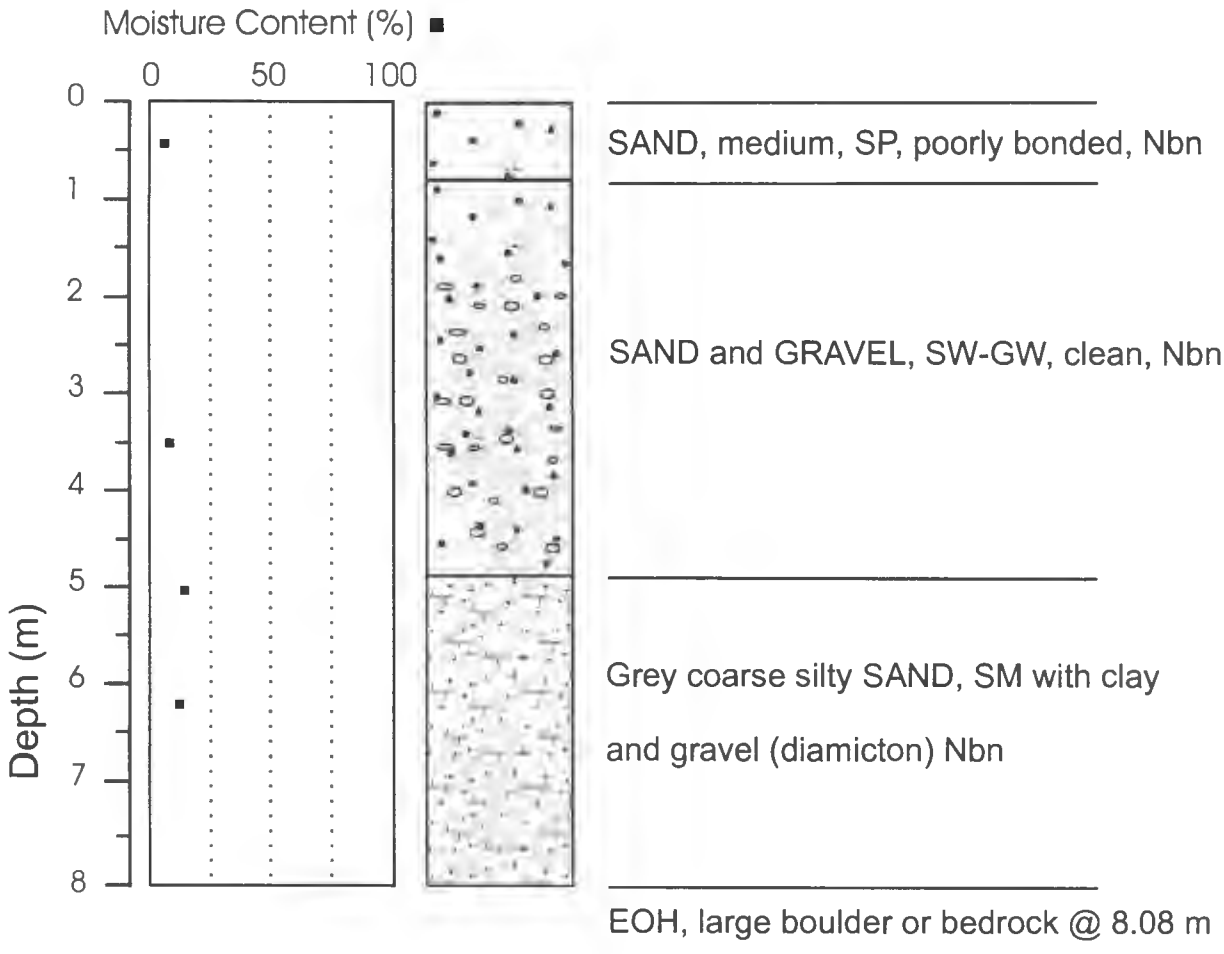

Figure 2.11 Borehole log INAC-04.

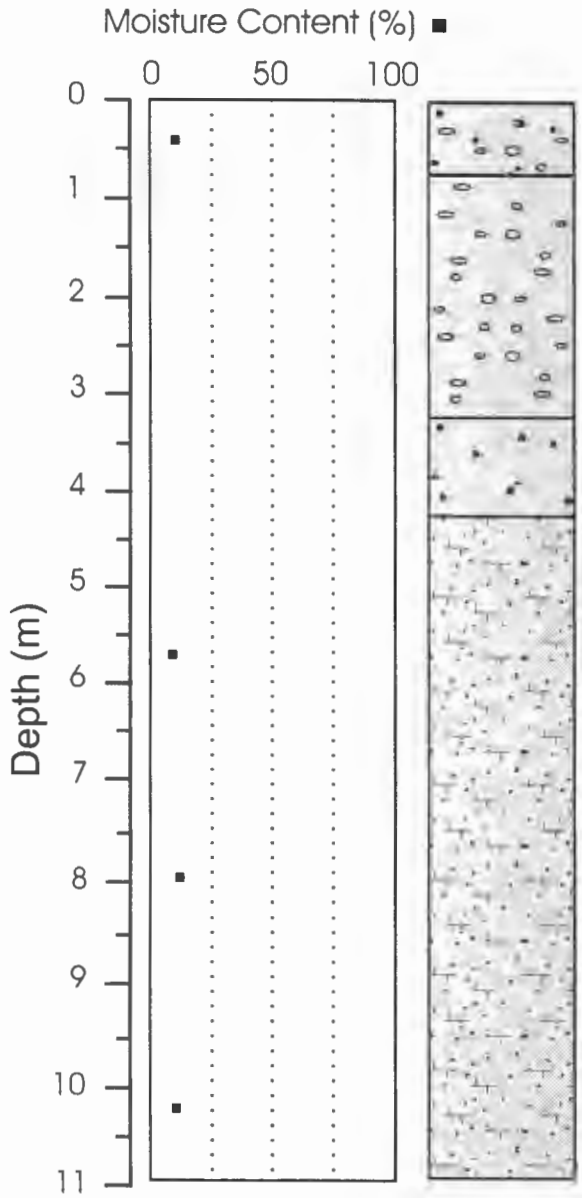

GRAVEL and sand, GW, organics (peat), dry to slightly moist, non-bonded

GRAVEL, GP, clean, clasts 1-2 cm avg, 4 cm max., very dry, becoming finer with depth

SAND, coarse, SW, with silt

SAND, coarse with silt, SM, trace clay; sub-rounded to sub-angular clasts, 2 cm avg., 4 cm max., occasionally very coarse, grey, becoming finer with depth (diamicton)

Nbn

EOH, large boulder or bedrock @ 10.97 m

Figure 2.12 Borehole log INAC-05.

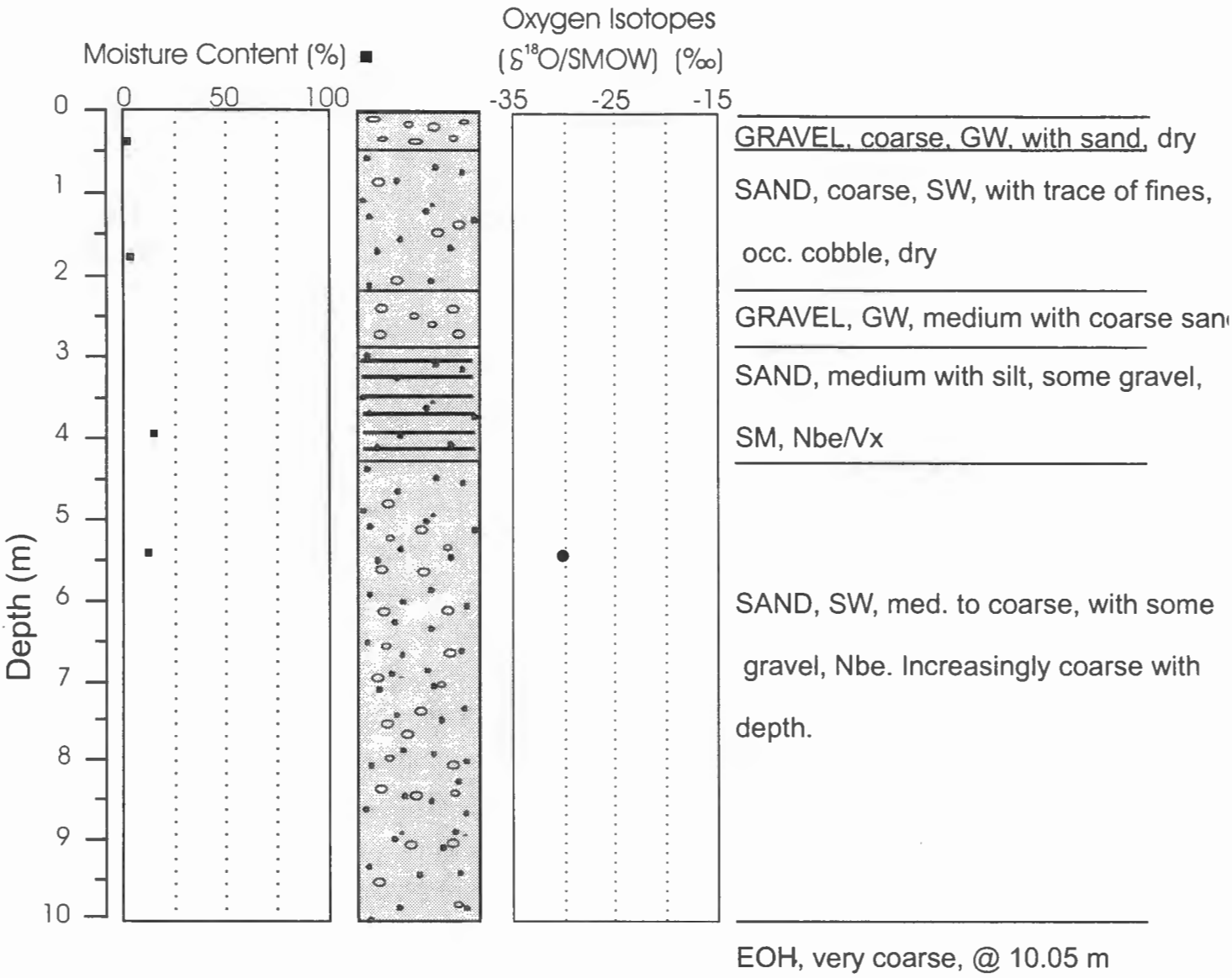

Figure 2.13 Borehole log INAC-06.

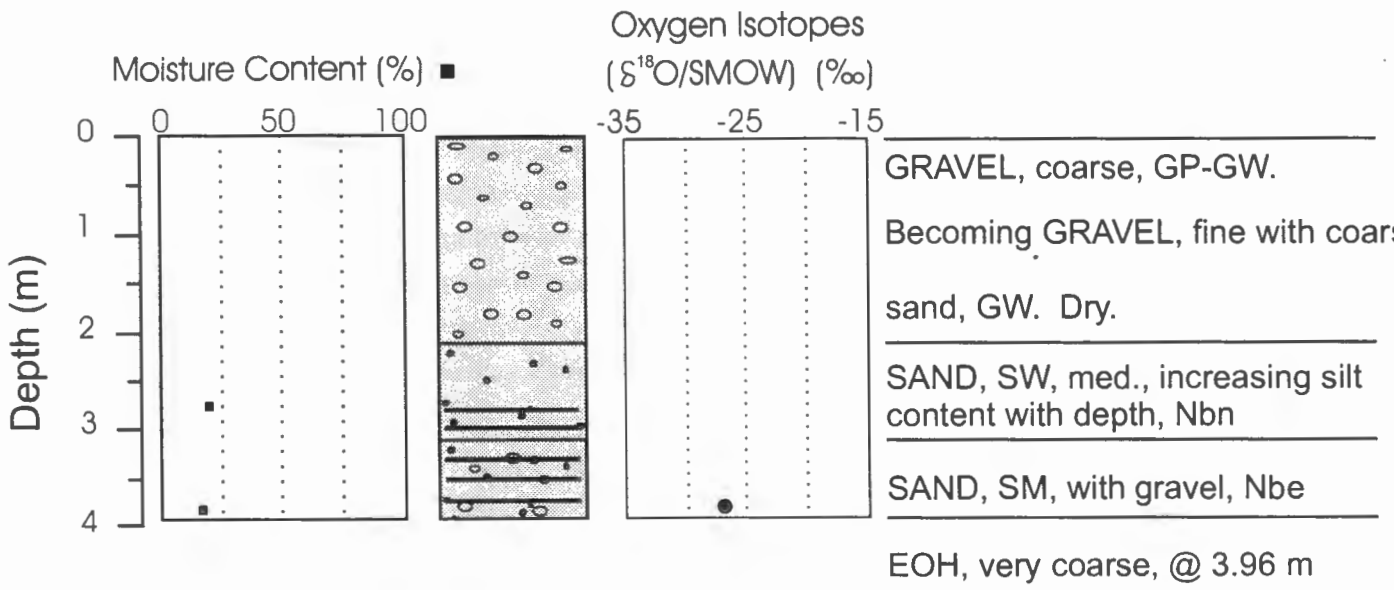

Figure 2.14 Borehole log INAC-07.

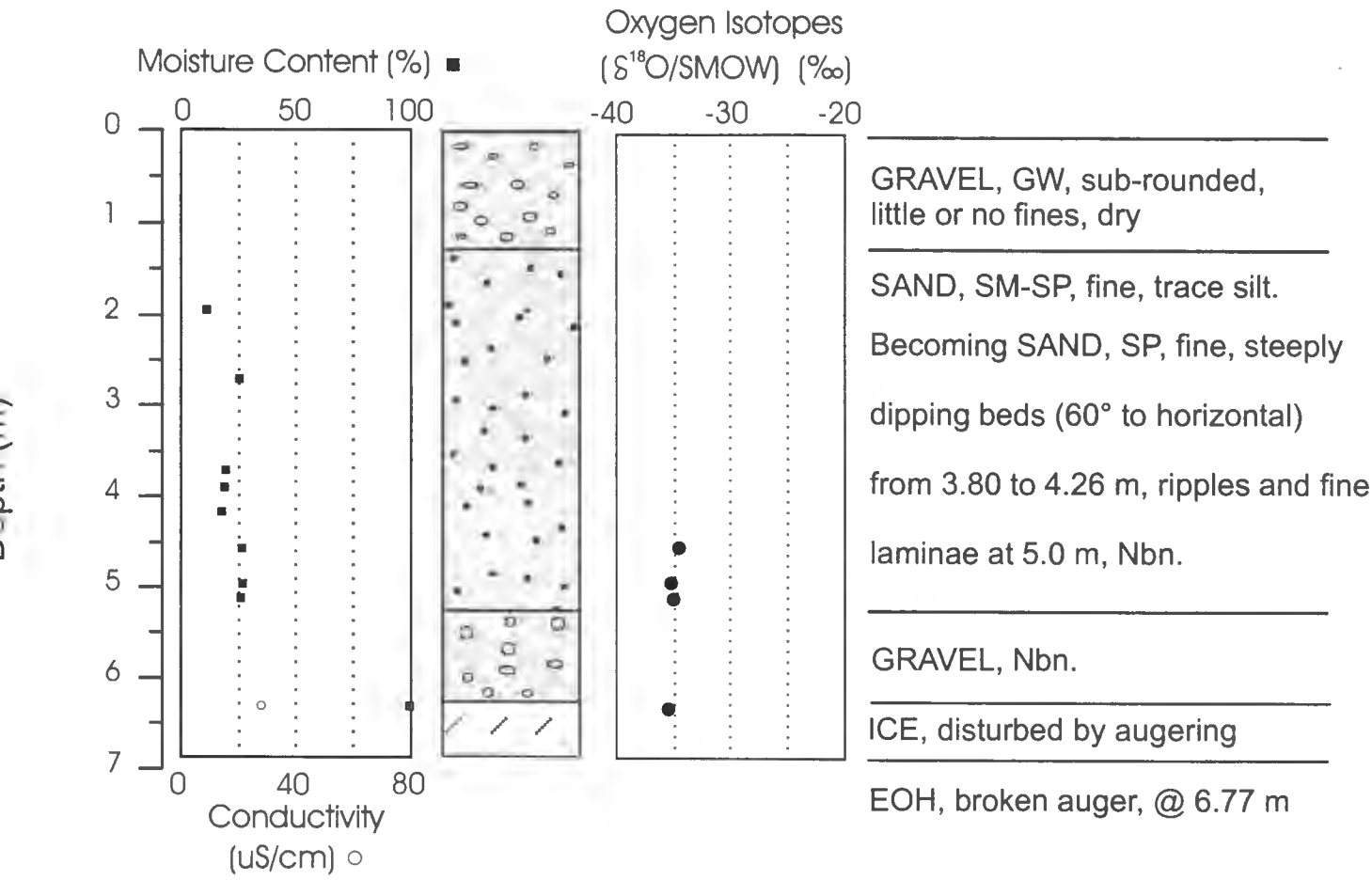

Figure 2.15 Borehole log INAC-08.

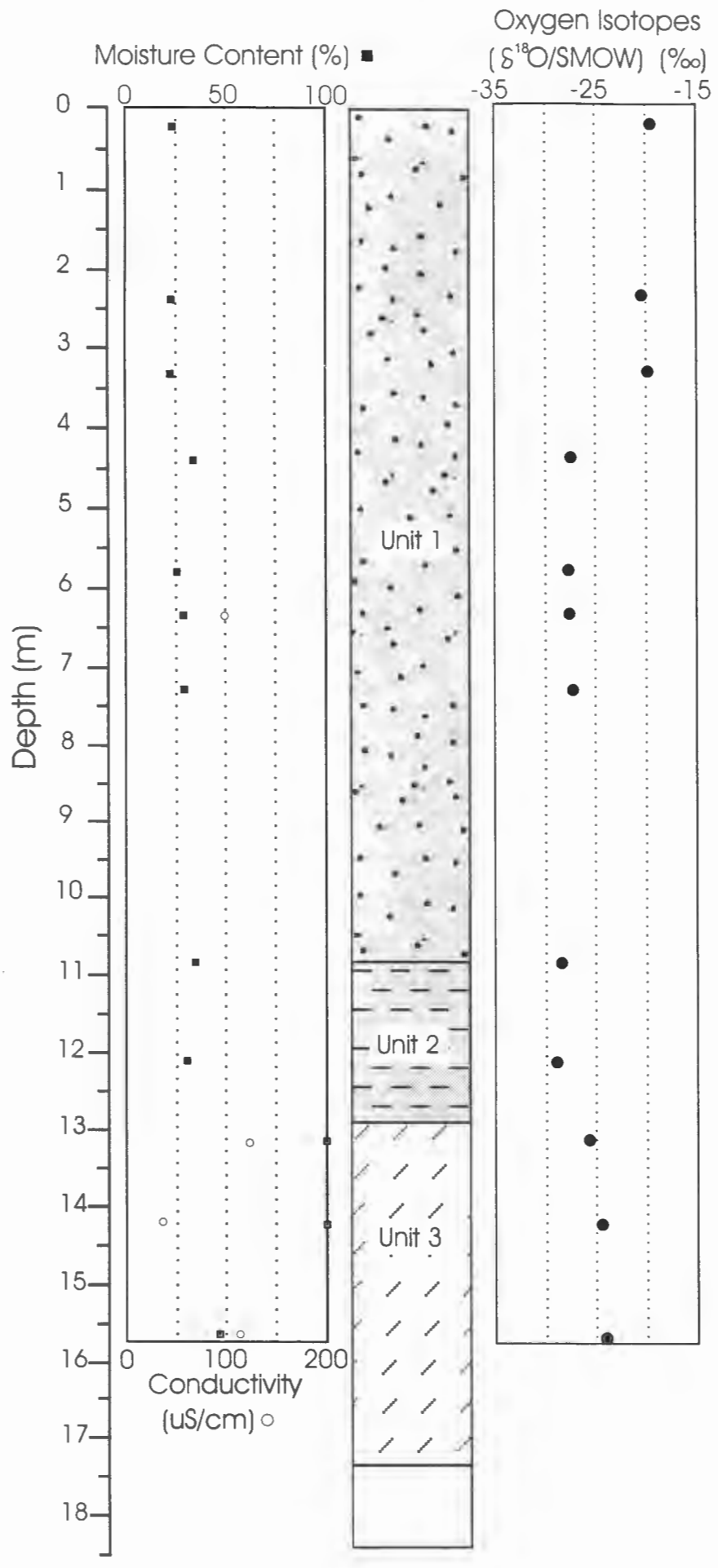

SAND, SP-SW, medium, with some coarse sand. Increasing fine sand with depth. Well bonded, Nbe

SAND, SP-SM, medium to very fine with silt, well bonded, Nbe/Vx

ICE, with grey silt, ML, inclusions occurring as small aggregates in distinct parallel bands. Occasionally sediment-rich with silt and fine sand (ML-SM).

No samples

EOH @ 18.44 m

Figure 2.16 Borehole log INAC-09.

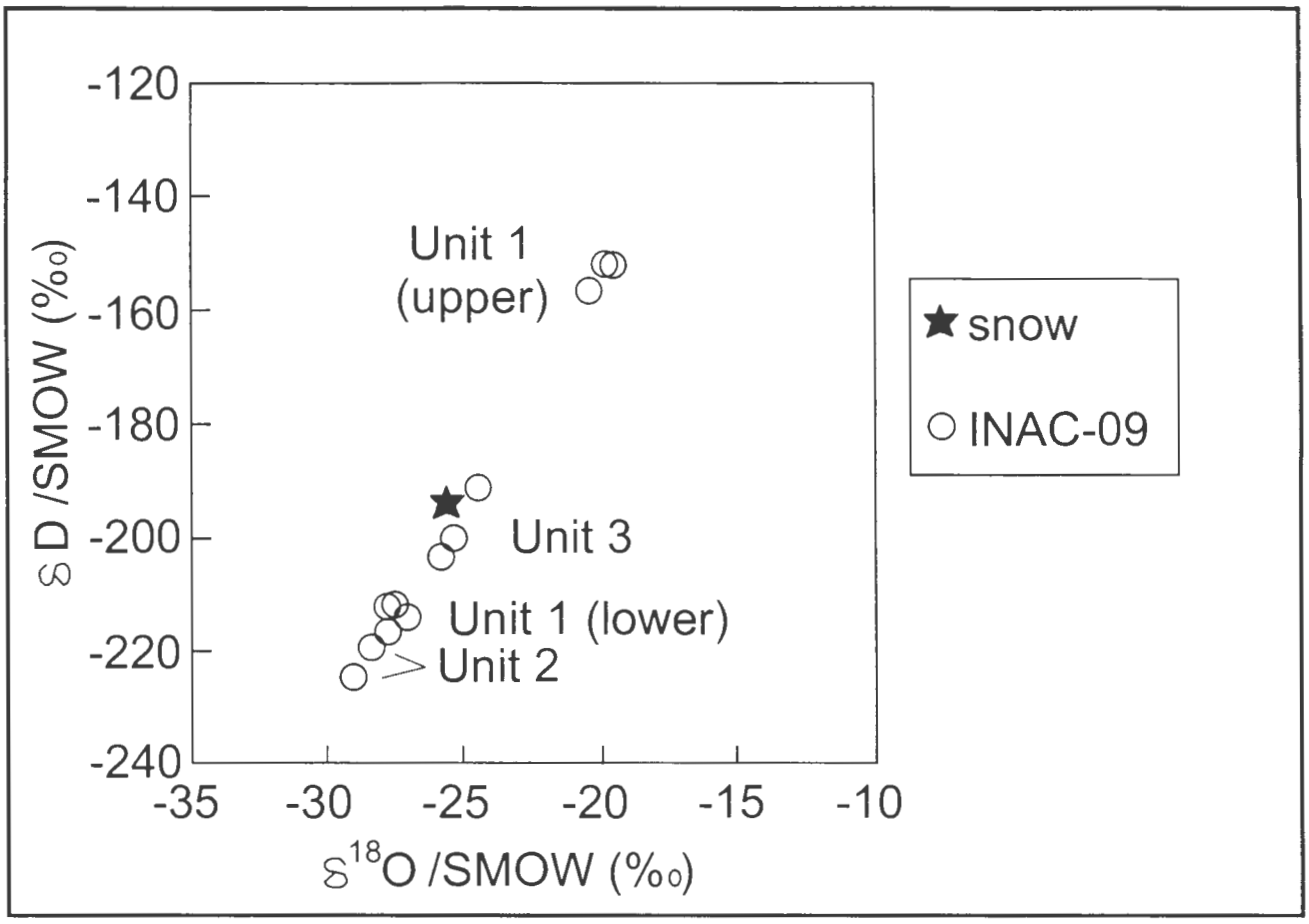

Figure 2.17. Co-isotope plot of δ D (SMOW) versus δ^{18}O (SMOW) from INAC-09.

3. GROUND PENETRATING RADAR (S. Robinson; M. Burgess; S. Wolfe)

3.1 INTRODUCTION

Ground penetrating radar (GPR) surveys were conducted between March 16-25, 1996 at the BHP Diamonds, Inc. Airstrip esker and the Canamera Geological Ltd. outwash terrace. Both deposits are presently utilized as aggregate resources for diamond mine infrastructure construction. The purpose of the GPR surveys was to provide a continuous subsurface profile of high resolution to delineate potential massive ground ice bodies, map the subsurface sediments, and provide data for estimating the granular material available for extraction.

Two boreholes at the north end of the Airstrip esker penetrated a significant thickness of massive ground ice previously identified by EBA Engineering Consultants Ltd. (1995) and overlain by sand and gravel. Other boreholes further south on the esker did not encounter significant massive ground ice. However, previous excavation by BHP Diamonds Inc. on the western flank of the esker towards the southern end had exposed sections of massive ground ice that may be identified in the GPR surveys. At the Carat Lake esker-delta complex, massive ground ice identified in the GPR surveys was confirmed in a geotechnical borehole. In addition, a second discrete body of massive ground ice was identified on GPR profiles, east of the Carat Camp airstrip.

3.2 GPR BACKGROUND AND METHODS

Ground penetrating radar (GPR) surveying has been shown to be a fast, reliable and relatively inexpensive technique for non-destructive, high-resolution mapping of subsurface materials to depths of 3 to 30 m, depending upon the electrical properties of the materials (Davis and Annan, 1989). GPR principles are similar to those of the reflection seismic method, the difference being that GPR utilizes an electromagnetic (EM) energy source, rather than acoustics. With the GPR reflection technique, an energy pulse is transmitted into the ground and a portion of this energy is reflected

back to a receiver at the surface from an interface with contrasting electrical properties (Figure 3.1). The remaining EM energy continues to travel downwards through the ground with additional portions reflected at subsequent interfaces. The two-way travel time to these reflectors is measured by the GPR unit. If the propagation velocity of the energy pulse is known, the depth to each reflector can be calculated. In air, the propagation velocity is the speed of light (0.3 mns^{-1}). In the subsurface, however, velocity is dependent upon the electrical properties of the material. This velocity is some fraction of the speed of light, typically between 0.03 and 0.16 mns^{-1}. Higher velocities are typical of dry or frozen soils, while lower velocities are typical of wet materials. Propagation velocities are typically calculated by conducting a common mid-point (CMP) survey (see below).

Each energy pulse transmitted at a survey position is called a trace. A collection of traces from evenly spaced survey positions (moving both antennas the same distance in the same direction and maintaining a constant antenna separation) allows the construction of a cross-section, or profile, through the ground. Drill cores yield only point-source information, while a GPR profile provides a continuous subsurface profile with high resolution. A plotted profile contains a horizontal axis representing survey position and vertical axes indicating two-way travel time and interpreted depth in the ground. In conjunction with borehole or other ancillary information, the profile permits interpretation of subsurface characteristics.

Electrical contrasts in the ground can be caused by changes in material density, water content, temperature, groundwater chemistry, or mineralogy. Thus, common geologic causes of subsurface reflectors are material boundaries (overburden/rock, sand/clay, sediment/ice, etc.), the water table, changes in water content, frozen/unfrozen interfaces, cavities, boulders, and ice lenses. Fractures or faults within rock and sedimentary structure are also commonly mapped using GPR.

The choice of antenna frequency is important when conducting a GPR survey. Higher frequency antennas (100 or 200 MHZ) provide high-resolution in the near-surface, while lower frequency antennas (25 or 50 MHZ) yield greater depth penetration but with an accompanying loss in resolution. Practical experience has shown that higher frequency antennas tend to be more

sensitive to changes in the subsurface, typically returning a greater number of reflectors than lower frequency antennas and occasionally obscuring the primary reflectors. The choice of antennas should take into account the depth of penetration, as well as the degree of resolution required.

Ground penetrating radar technology has been used for sediment and permafrost mapping for several years. Sedimentary structure in unfrozen lacustrine deltas has been mapped by Jol and Smith (1991; 1992), fluvial sediments by Moorman *et al.* (1991), and glaciofluvial sediments by Beres *et al.* (1995). Surficial deposits in permafrost regions have been mapped by Pilon *et al.* (1992). Coarse grained deposits containing massive ground ice have been surveyed by Dallimore and Davis (1987) and Robinson *et al.* (1993). Other permafrost-related geotechnical studies include investigation of slopes along pipeline routes (Robinson and Moorman, 1995; Burgess *et al.*, 1995) and the monitoring of arctic road and airport runway performance (LaFleche *et al.*, 1988; Judge *et al.*, 1991). Mapping the stratigraphy and ice component of coarse-grained, perennially frozen sediments represents one of the most optimum environments for the application of GPR technology. The frozen, coarse grained nature ensures that signal penetrations will be deep, without the attenuation that often limits depth of penetration in unfrozen or fine-grained sediments.

3.3 EQUIPMENT AND DATA COLLECTION METHODS

The pulseEKKO IV ground penetrating radar unit was used for survey data collection presented in this report. This system is operated by a laptop computer, and the antennas are connected to the control unit by fibre optic cables. Antennas with centre frequencies of 50 MHZ were used for the majority of surveys. One section of survey line was repeated using the 100 MHZ antennas. All surveys utilized the 1000V transmitter. Due to extremely cold operating temperatures, the radar unit, power supply, and laptop computer were placed in an insulated box with hot-water bottles providing a heat source.

A station (or trace) spacing of 0.5 m was used for all surveys. Antenna separation was

maintained at 1.0 m, with one test line conducted using a 2.0 m spacing. A total time window of 800 ns was collected for each trace, and each plotted trace represents the average of 64 individual pulses per station. Topographic surveys were conducted along sections of survey lines with major elevation changes. The topography of the ground surface was incorporated into the plotted profiles.

Several common mid-point (CMP) surveys were conducted at selected sites to calculate propagation velocities. This technique involves collecting several traces (usually 20-30) in which the spacing between transmitter and receiver is successively increased about a "common mid-point". As the distance from the mid-point is consistently increased, reflections from that mid-point arrive at a later time. The velocity (V in mns^{-1}) in the ground to a reflector can be calculated from a plot of the square of the antenna separation (X^2 in metres) versus the square of the two-way travel time (T^2 in nanoseconds) to that reflector, where the velocity is the square root of the slope of the line of best fit.

Data editing and processing consisted only of that available through the pulseEKKO software. Minor temporal down-trace filtering was applied to smooth out high frequency noise. Due to the low frequency of antennas used, this required a maximum averaging of only 3 points in most cases. Trace-to-trace averaging filters were generally not applied as sedimentary structures such as dipping beds tend be removed. Due to energy losses with depth, the relative strength of later returns was amplified by using an automatic gain control. Only a very minimal amount of gain addition was required due to the deep signal penetration in the frozen coarse-grained sediments. Radar traces collected in error have been removed. All profiles are plotted in wiggle-trace format.

3.4 DATA INTERPRETATION TECHNIQUES

Once the profiles are plotted with appropriate filters, gain, and topography applied, the results may be analysed. The first reflection received in each trace is the air wave travelling through the air between the transmitter and receiver. As this first wave arrival remains constant throughout the

survey and travels at high speed, it serves as a zero marker reference for the ground surface. The next arrival is the ground wave, travelling directly from the transmitter to the receiver through the surface skin of the ground. As the propagation velocities through the ground are always slower than through the air, the ground wave arrives slightly later than the air wave, however they often appear as one with thicker waves where ground velocities are high. The succeeding waves to arrive are from interfaces within the ground and they arrive in order of depth (shallowest first). In the case of very shallow structure, reflectors may be indistinguishable from the ground wave.

Geometric distortion, caused by antenna separation, must be accounted for during profile interpretation. The greater the antenna separation (up to 2 m when using 50 MHz antennas), the greater the near-surface distortion due to the sub-vertical energy path. With this in mind, the returns from the near surface (upper 2 to 3 m) are presented with a slightly compressed depth scale. However, as this report deals with penetrations up to 30 m deep, this becomes a minor consideration.

The pattern of reflections on the profile provides clues as to the nature of material encountered in the survey. Continuous line returns are expected from continuous, relatively smooth interfaces. In this study, continuous reflections would be expected from the sediment-bedrock contact, ice-sediment-bedrock contacts, continuous internal stratigraphy, and other abrupt lithological contacts. The extent and thickness of massive ground ice can often be mapped based upon stratigraphic relationships and contrasts in radar patterns with the enclosing sediment (Robinson *et al.*, 1993). Borehole data is typically required for confident interpretation of the presence of massive ground ice.

As the radar waves are not focussed directly downwards, hyperbolic reflections are produced when the survey approaches, passes over, and continues past a small body that has considerably different electrical properties than the surrounding material. Large boulders within the sediment or fractures within bedrock or ice can cause such reflections, as can interference from borehole casing and instrumentation. These hyperbolic interference reflectors can be distinguished as they should be steeply dipping at 45° (when corrected for vertical exaggeration). The limbs of hyperbolic reflectors

can also be used to measure the ground velocity. This method assumes that all reflections in the hyperbolic reflector originate from the same point, and successive antenna moves simply increase the distance from that point.

Chaotic returns may be the product of thin layers or small point reflections within the ground. In this study, these may be from joints in bedrock, sediment or ice lensing, or small cobbles. Some reflections may appear to be a combination of semi-continuous and chaotic returns, and may be caused by larger, more extensive joints, sediment bedding, or ice lenses. The number of chaotic reflectors within a sedimentary unit can be used as a qualitative measure of unit heterogeneity.

In order to provide confident interpretations of subsurface condition, borehole logs or other ancillary data (ground temperatures, nearby exposures, knowledge of local surficial geology, etc.) must be used in conjunction with ground penetrating radar profiles. Radar interpretation is often very subjective. However, if the user has a good idea of the survey objective, a geological model, and an understanding of the equipment and its limitations, much of the uncertainty can be removed. Research over the past 10-15 years has shown that certain geological conditions yield often predictable radar results. For instance, radar propagation velocities are often high (0.09-0.16 mns^{-1}) in frozen material with a fairly high ice content. The higher velocities enable the entire pulse width to be reflected by an interface faster, with a higher frequency (narrower) return sensed at the receiver. Signal losses are also lower in frozen material, generally resulting in signal penetration to depths greater than those possible in most unfrozen sediments. Slower propagation velocities, common in unfrozen wet materials, cause the pulse to "drag", resulting in a thicker, smeared reflector. When this knowledge is combined with the information on the nature of reflectors, a clearer picture of ground conditions emerges. For example, a frozen silt with numerous ice and clay lenses would appear as a zone of chaotic, narrow reflectors, probably with fairly deep penetration. Certain materials are also known to attenuate the signal more rapidly than others. For instance, penetration in clay may be limited to a few metres, perhaps slightly more if the clay is well frozen. Some material may yield few reflectors, yet with reflectors common at the contact with a different material at greater depth. This type of response indicates that the material is very homogeneous (not causing any reflectors) and

likely coarse-grained (low attenuation allowing reflectors at greater depth).

3.5 SURVEY DESIGN

3.5.1 Airstrip Esker

Using 50 MHz antennas, one survey transect was conducted along the north-south length of the esker and two east-west transects crossing the esker towards the southern end (Figure 2.1). The north-south profile (GPR 1) was 928 m long, and each of the cross profiles (GPR 2 and 3) were 100 m long. The surveys passed over all boreholes drilled in the esker by both EBA Engineering Consultants Ltd. (1995) and Indian and Northern Affairs Canada (INAC, this study). A 100 m section of the esker known to contain massive ground ice was also surveyed using the 100 MHz antennas.

3.5.1 Carat Outwash Terrace

A series of 50 MHz surveys with a 1-m antenna separation were conducted across two sections of the outwash terrace (Figure 2.6), totalling 3.5 km. Surveys generally followed the same lines used for the Ohm Mapper and EM surveys. One test section was re-surveyed using a 2-m separation.

3.6 INTERPRETATION OF SURVEY RESULTS

3.6.1 Airstrip Esker

In order to convert two-way travel times into a depth scale, a CMP profile was conducted near the north end of the Airstrip esker. In addition, propagation velocities were calculated at various depths and locations from the limbs of hyperbolic reflectors. Propagation velocities ranged from 0.145 to 0.162 mns^{-1}, with an average of 0.154 mns^{-1} (n=5). This mean velocity was used for all profile plots at the Airstrip esker.

Occurrence of Massive Ground Ice

Massive ground ice was noted in two boreholes near the north end of the esker. These boreholes were at the 821 m (EBA BH-E3) and 843 m (INAC-01) positions of line GPR 1 (Figure 3.2). The boreholes contained massive ice at depths of 6.85 to 12.65 m and 8.99 to 14.30 m respectively.

These depths correlate with strong, semi-continuous reflectors that are interpreted to represent the top and bottom of the ice body (Figure 3.2). Within the ice body several chaotic reflectors are found that are interpreted to represent sand and silt banding as noted in borehole INAC-01 (Figure 2.7). It is important to note that core logging in the EBA boreholes was not as detailed as the INAC boreholes and little stratigraphic data is available from BH-E3. There appears to be an abrupt discontinuity in the surface of the ice body at about 841 m of line GPR 1, which is in part masked by interference from a hyperbolic reflector that may be a large boulder.

Both borehole logs indicate coarse-grained sand with some interspersed sand and gravel lenses above the ice body. This is characterized on the radar profile as more continuous, wavy reflectors. Immediately beneath the ice body, borehole logs indicate 3.5 and 1.5 m of gravelly sand

in BH-E3 and INAC-01, respectively, overlying granitic bedrock. The separation of these sediments from the bedrock reflectors is difficult. In BH-E3, a strong reflector appears at about 14 m depth, however it is unclear if this represents the ice-sand or sand-bedrock contact.

The prevalence of continuous wavy reflectors representing bedded sediment north of about the 860 m position likely marks the northern lateral boundary of the ice body at about 40 m north of borehole INAC-01. As there appears to be no definitive reflectors marking this change in radar pattern, the actual boundary of the ice body is probably near-vertical. South of borehole BH-E3 the surface of the ice body appears to rise towards the surface, as does the bedrock reflector. The edge of the ice body is interpreted to be at about the 750 m position as shown by the "pinching-out" of the ice surface reflector. Thus, the top of the ice body is interpreted to range between 4 and 9 m below the surface, with the base between 10 and 16 m below the esker surface. Maximum thickness appears to be about 7 m, and the lateral extent along the profile appears to be about 125 m in this vicinity.

Other sections of the radar profiles may contain significant volumes of ground ice. Lines GPR 2 and 3 show a zone of chaotic reflectors between the interpreted bedrock surface and overlying esker sands and gravels (Figure 3.3). Massive ice is known to be exposed on the lower flanks of the esker, suggesting that the zone between these two reflectors is ice-rich. Based upon the chaotic reflector pattern typical of massive ice, a few other small sections of the line GPR 1 profile possibly also contain massive ground ice. These sections are noted on the profiles, however, this interpretation is impossible to confirm without drilling.

Bedrock Topography

The upper surface of the granitic bedrock is commonly characterized by a sharp reflector immediately below which chaotic and hyperbolic reflectors dominate (Figure 3.2). The hyperbolic reflectors are likely caused by fracturing within the granite. The bedrock reflector should also be

below the continuous, wavy reflectors typical of the overlying sediment. Boreholes INAC-01, BH-E1, and BH-E3 intersected bedrock at depths of 15.85, 15.55, and 16.30 m respectively. All of these depths correlate well with bedrock depths interpreted from the GPR profiles. Interpreted bedrock topography varies from 10 to 20 m below the esker surface. On cross profiles at the southern end of the profile, the interpreted bedrock reflector remains 4 to 7 m below the base of the esker (Figure 3.3).

In some sections of the line GPR 1 profile, the bedrock reflector is more difficult to pinpoint, especially at the southern end of the esker between 85 and 230 m. Along this section, it is interpreted to lie either at a depth of about 10 m, or between 16 and 18 m. It is possible that the overlying material disrupts the pattern of the bedrock reflectors at depth (Figure 3.2). This reflector differs from the continuous wavy patterns of the sands and gravels, and may be either a body of massive ground ice or possibly bouldery till. Such an interpretation is impossible to confirm without drilling. One borehole was drilled at approximately 140 m of line GPR 1, and intersected massive ice between 1.1 and 2.3 m, and alternating silt and coarse gravel to the end of the borehole at 9.14 m.

Sedimentology

Boreholes drilled in the esker generally show alternating beds of coarse sand (with some silt or gravel) and coarse gravel with some cobbles. However, without very detailed borehole logs and GPR surveys of different frequencies, it is impossible to determine which reflectors are attributed to each sedimentary unit. Nevertheless, stratigraphic patterns of sedimentary bedding are plainly visible on the profiles (Figure 3.2). Boulders within the sediment are typified by hyperbolic reflectors, with boulders located at the crest of the reflectors.

The very continuous and slightly wavy reflectors seen through much of the profile at depth likely indicate stratified coarse sand and gravel deposits. These reflectors appear to comprise the majority of the deposit, except near the surface between about the 370 and 500 m positions. In this

zone, a bowl of less continuous and more chaotic reflectors occurs, likely indicating a fill zone of finer sands and gravels. A more chaotic pattern of reflectors near the surface in the vicinity of borehole INAC-02 is also apparent where gravel, sand and ice are present in discrete layers. Borehole INAC-03 (695 m position) also shows alternating sand and gravel to 7 m. The radar profile at this point indicates a lack of continuous stratigraphy.

3.6.2 Carat Outwash Terrace

In order to convert the two-way travel times to a depth scale, a CMP profile was conducted over each of the two main survey areas. In addition, propagation velocities were calculated at various depths and locations from the limbs of hyperbolic reflectors. Propagation velocities ranged from 0.148 to 0.167 mns^{-1}, with an average of 0.154 mns^{-1} ($n=10$). This mean value was used for all profile plots.

Carat Lake Region A

Three surveys were conducted over the glaciofluvial borrow site designated as Carat A (lines GPR 1, 2, and 3 in Figure 2.6). The surveys were planned to intersect several boreholes to be drilled by INAC following the geophysical surveying. However, due to equipment problems, only one borehole was drilled (INAC-09). This borehole, located at the 273 m position of Carat A line GPR 3, contained medium sand to 10.80 m, silty sand from 10.80-12.85 m, and massive ice from 12.85 to 18.44 m (Figure 2.16). Drilling difficulties resulted thereafter, and it is unlikely that borehole INAC-09 terminated at the bedrock contact, suggesting that massive ice likely continues to a greater depth than 18.44 m.

Occurrence of Massive Ground Ice

Massive ground ice was noted at depths of 12.85 to 18.44 m in borehole INAC-9 drilled at the 273 m position of line GPR 3 (Figure 3.5). Interpretation of the radar profile from this section shows a laterally continuous body at approximately the same depth, overlain by a fairly chaotic sedimentary unit. It appears that there may be a 3 to 4 m thick sedimentary unit immediately underlying the ice between the 175 and 250 m position. The interpreted ice body continues past the end of line GPR 3 to the west, thickening towards the end of the line. This same unit is found on GPR 1 (Figure 3.4), which runs roughly north to south down the centre of the deposit. The northeast trending survey GPR 2 slightly to the east does not appear to contain the massive ice body (Figure 3.4). Towards the west, the character of the ice body, as depicted on line GPR 3, appears to change (Figure 3.5). Borehole INAC-09 indicates that sand and silt banding may occur within the ice body, and is likely the cause of radar reflectors within the eastern portion of the ice body. At the western end of line GPR 3, the lack of radar reflectors within the ice body suggests that sediment banding may not be present in the ice.

Bedrock Topography

The radar reflector representing the bedrock surface has been delineated on all radar profiles. Over the majority of the surface area, bedrock appears to range from 16 to 22 m below the ground surface. Towards the eastern part of the Carat A borrow area, the bedrock reflector rises gradually and approaches to within about 3 or 4 m of the ground surface as depicted in line GPR 2 (Figure 3.4). At the south end of the Carat A borrow site there appears to be a fault within the bedrock that dips steeply towards the south. This fault is depicted in both lines GPR 1 and 2 in Figure 3.4.

Sedimentology

Several interesting zones are noted on the radar profiles from a sedimentological perspective. Immediately to the south of the interpreted ice body in line GPR 1, the upper 7 m of sediments dip steeply southward in a manner typical of deltaic foreset deposits (Figure 3.4). These deltaic sediments are underlain by about 7 m of sediment that generally conforms to the bedrock topography. These lower sediments also appear to conformably overlie the southern edge of the ice body and, in fact, parallel the upper surface of the ice (line GPR 1 in Figure 3.4). Further to the south, the thickness and the dip of deltaic sediments increases, perhaps in response to the deepening of the bedrock surface and potential increase in water depth during time of deposition. The lower sediments conforming to the bedrock topography maintain a thickness of about 7 m in this area. There is a definite lack of boulders in this sequence of deltaic sediments and the sediments are generally interpreted as being coarse to medium sand, or finer.

Towards the north end of the Carat A area, several continuous reflectors form a bowl, suggesting a small basin or depression filled with sediment (line GPR 1 in Figure 3.4). Field observations indicate the area to be a small pond. Deeper reflectors appear to be continuous with the interpreted surface of the ice body. In general, reflectors above the ice body are hyperbolic and chaotic. These reflectors may represent boulders or fractures in the sediments overlying the ice.

It appears from lines GPR 1 and 3 that there may be a 3-4 m thick sedimentary unit underlying portions of the ice body (Figures 3.4 and 3.5). This interpretation is based upon the presence of several continuous flat-lying reflectors that would probably not be found within bedrock. However, there is no borehole information to confirm this interpretation.

3.6.3 Carat Lake Region C

Two surveys were conducted over the glaciofluvial borrow site designated as Carat C (lines GPR 4, and 6 in Figures 3.6 and 3.7). The surveys were planned to intersect several boreholes that were to be drilled by INAC following GPR surveying. This site was also the planned location for an airstrip (now constructed). As with region A, a propagation velocity of 0.154 mns^{-1} has been used for all profile plots.

Occurrence of Massive Ground Ice

Although no boreholes were drilled in Site C at the time of initial GPR surveys, there is strong radar evidence for a large ground ice body between the 175 and 275 m positions of line GPR 6 (Figure 3.7). The reflectors outlining the ice body display the same double reflector observed above the ice on lines GPR 1 and 3 at Site A (Figures 3.4 and 3.5). The apparent rise in bedrock topography beneath the interpreted ice body may be caused by high propagation velocities in ice. The deep penetration of the GPR signal into the underlying bedrock is also indicative of ice overlying the bedrock. The presence of massive ground ice at this location was subsequently confirmed by a drilling program for granular evaluation in the summer of 1996.

There appears to be no other location in the Carat C region that contains massive ground ice, however based upon the high frequency and chaotic nature of reflectors, there are two zones that may contain ice-rich sediment. These are on line GPR 4 between 480 and 520 m and 625 and 680 m (Figure 3.6). Both of these interpreted areas lie between about 4 and 12 m depth. Without boreholes in the area, however, this interpretation is not confirmed.

Bedrock Topography

Bedrock is delineated as a discontinuous reflector comprised of the crests of numerous hyperbolic diffraction reflectors, caused by fractures at the bedrock surface. Over most of the Carat C region, the bedrock is approximately 20 m below the surface of the deposit. The greatest depth to bedrock occurs at about the 320 m position of line GPR 4 (Figure 3.6). Towards the west of the deposit, bedrock is found between 12 and 16 m below the ground (i.e. rising slowly between 300 and 600 m on line GPR 6). At the western edge of line GPR 6, the radar survey continues off the edge of the glaciofluvial deposit and across a small valley. The bedrock rises to the surface about 100 m from the end of the survey. This observation is consistent with observations of bedrock at the ground surface nearby.

A small lake separates Carat Lake regions A and C (Figure 2.6). Surveying was continued across the lake in an effort to map lacustrine sediment and bedrock topography beneath the lake. Bedrock is interpreted to be almost immediately beneath a shallow sediment layer within the lake (except at a few places, the sediment thickness is likely too small to be mapped with 50 MHz antennas).

Sedimentology

Two main sedimentological units are evident in Site C. The upper sediments (to approximately 15 m depth) are characterized by semi-continuous and, at times, chaotic reflectors. However, several very continuous reflectors also occur in this zone, most notably between 4 and 6 m depth, extending most of the way along line GPR 6 (Figure 3.7). Southward dipping beds are also found between the 675 and 715 m positions of line GPR 4 while northward dipping beds are noted to the north on line GPR 4, between the 220 and 270 m positions.(Figure 3.6). Adjacent to the interpreted body of ground ice on line GPR 6 (Figure 3.7), the sedimentary contact appears conformable with the upper surface of the ice. The chaotic nature of the reflectors, combined with

both northerly and southerly dipping beds suggest that this upper unit was deposited under fluvial environment, most likely as a deltaic or alluvial fan deposit.

A second unit, overlying the bedrock surface, appears much more continuous on the radar record, especially on line GPR 4 (Figure 3.6). The signal is not greatly attenuated in this zone as the bedrock reflector at depth remains strong, suggesting that the material is exceptionally homogeneous, and without boulders. The unit may be composed of fine-grained sand or silt, as observed in the INAC-9 borehole. Several weak but continuous reflectors appear to follow the bedrock topography.

3.7 REFERENCES

Beres, M., Green, A., Huggenberger, P. and Horstmayer, H., 1995. Mapping the architecture of glaciofluvial sediments with three-dimensional georadar. *Geology*, 23(12), p. 1087-1090.

Burgess, M.M., Robinson, S.D, Moorman, B.J., Judge, A.S., and Fridel, T.W., 1995. The application of ground penetrating radar to geotechnical investigations of insulated permafrost slopes along the Norman Wells pipeline. *Preconference Proceedings, 48th Canadian Geotechnical Conference*, Vancouver, B.C., p. 999-1006.

Dallimore, S.R., and Davis, J.L., 1987. Ground probing radar investigations of massive ground ice and near surface geology in continuous permafrost. In: *Current Research*, Part A, Geological Survey of Canada Paper 87-1A, p. 913-918.

Davis, J.L., and Annan, A.P., 1989. Ground penetrating radar for high resolution mapping of soil and rock stratigraphy. *Geophysical Prospecting*, 37, p. 531-551.

EBA Engineering Consultants Ltd. 1995. NWT Diamonds Project: Tailings Management Plan and Preliminary Design of Retention Structures. Submitted to BHP Diamonds Inc. EBA Report 0101-94-11580.2.

Jol, H.M., and Smith, D.G., 1991. Ground penetrating radar of northern lacustrine deltas. *Canadian Journal of Earth Sciences*, 28, p. 1939-1947.

Jol, H.M., and Smith, D.G., 1992. Ground penetrating radar: recent results. *Canadian Society of Exploration Geophysicists Recorder*, December, 1992, p. 15-20.

Judge, A.S., Tucker, C.M., Pilon, J.A. and Moorman, B.J. 1991. Remote sensing of permafrsot by ground penetrating radar at two airports in arctic Canada. *Arctic*, 44, Supp. 1., p. 40-48.

LaFleche, P.T., Judge, A.S., Moorman, B.J., Cassidy, B., and Bedard, R., 1988. Ground probing radar investigations of gravel roadbed failures, Rea Access Road, N.W.T. In: *Current Research*, Part D, Geological Survey of Canada Paper 88-1D, p. 129-135.

Moorman, B.J., Judge, A.S., and Smith, D.G., 1991. Examining fluvial sediments using ground penetrating radar in British Columbia. In: *Current Research*, Part A, Geological Survey of Canada, Paper 91-1A, p. 31-36.

Pilon, J.A., Allard, M., and Seguin, M.K., 1992. Ground probing radar in the investigation of permafrost and subsurface characteristics of surficial deposits in Kangiqsualujjuaq, northern Quebec. In: *Ground Penetrating Radar* (J. Pilon, ed.), Geological Survey of Canada Paper, 90-4, p. 165-175.

Robinson, S.D., and Moorman, B.J., 1995. Ground penetrating radar surveys along the Norman Wells pipeline route, 1989-1995: A summary of results. *Geological Survey of Canada Open File Report 3094*, Ottawa.

Robinson, S.D., Moorman, B.J., Judge, A.S., and Dallimore, S.R., 1993. The characterization of massive ground ice at Yaya Lake, Northwest Territories using radar stratigraphy techniques. In: *Current Research*, Part B, Geological Survey of Canada Paper 93-1B, p. 23-32.

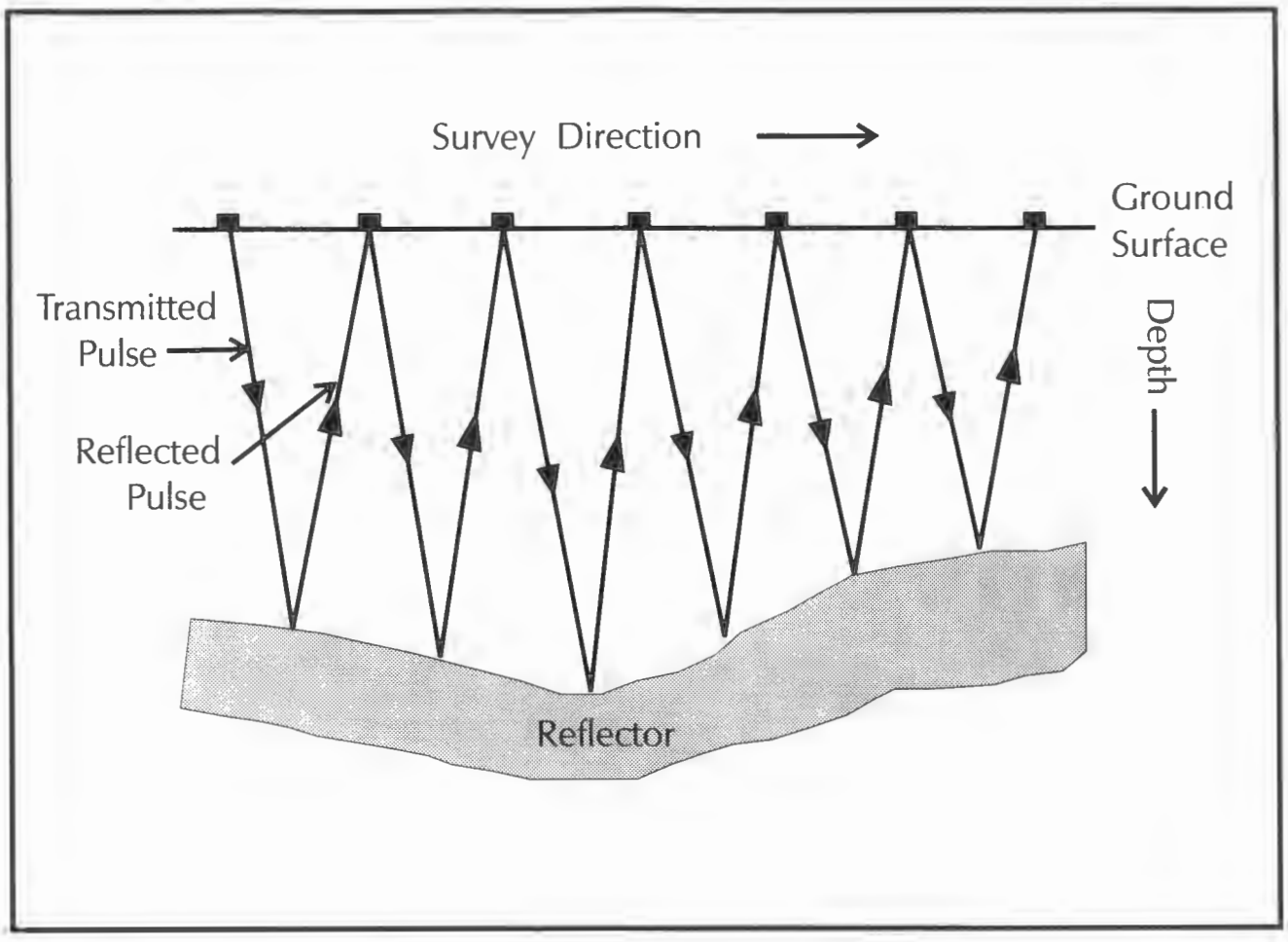

Figure 3.1 Schematic representation of GPR transmitted and reflected pulses.

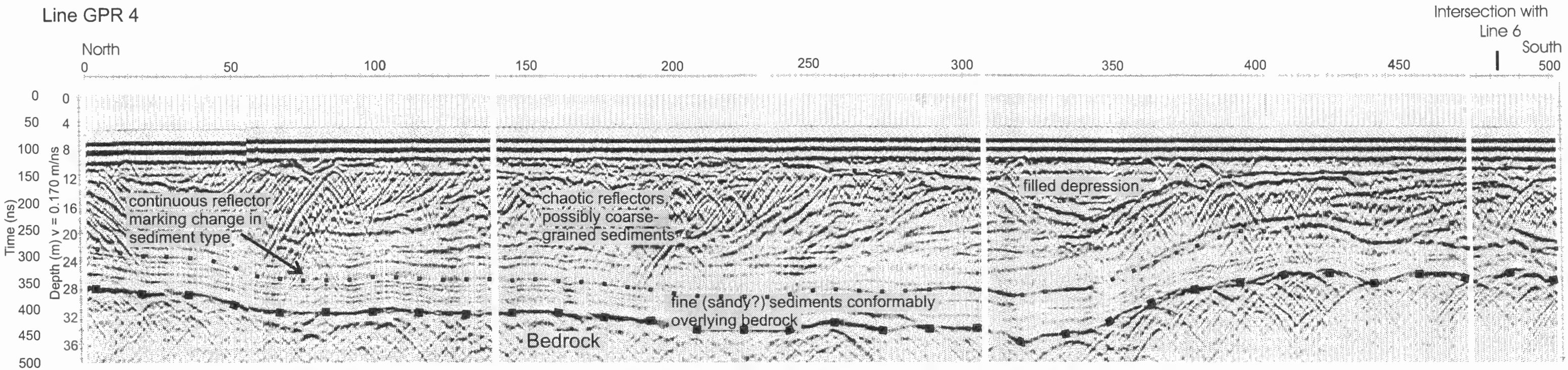

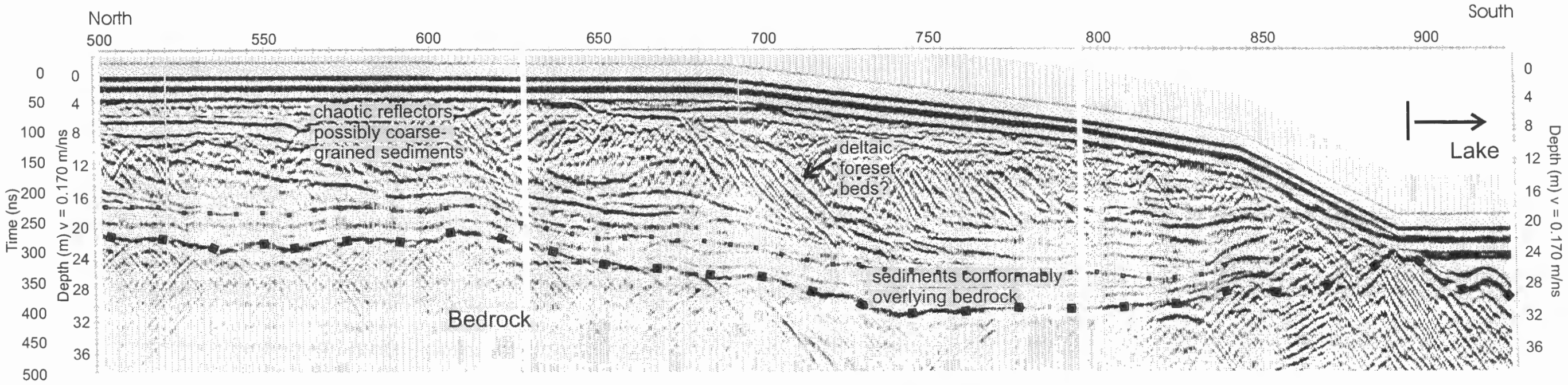

Fig. 3.6 GPR profiles of line 4 on Carat outwash terrace.

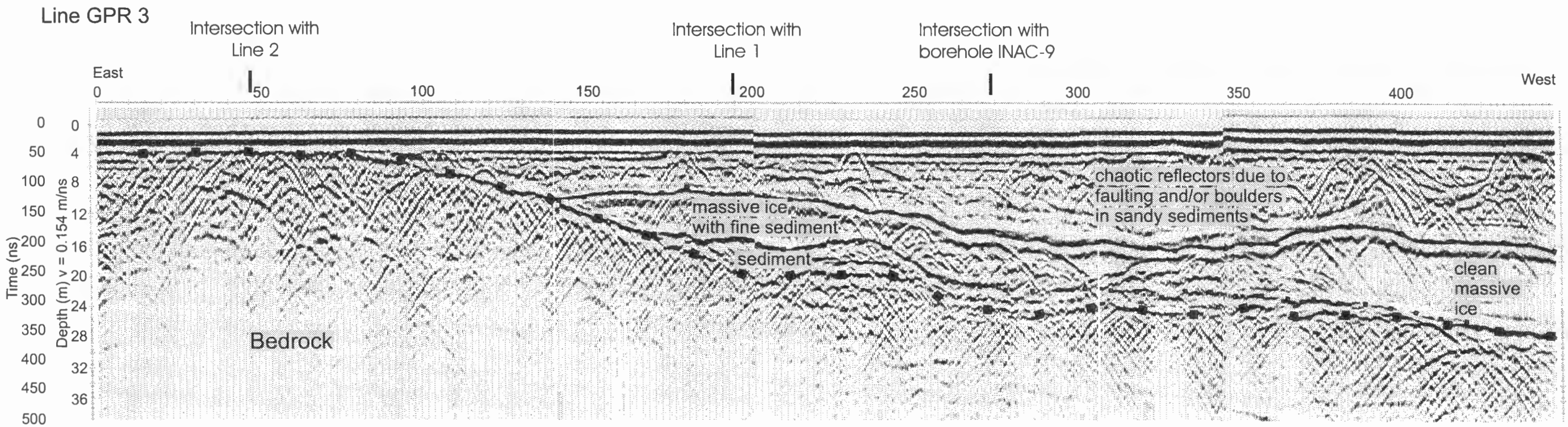

Fig. 3.5 GPR profiles of line GPR 3 on the Carat outwash terrace.

■ ■ GPR interpreted bedrock contact

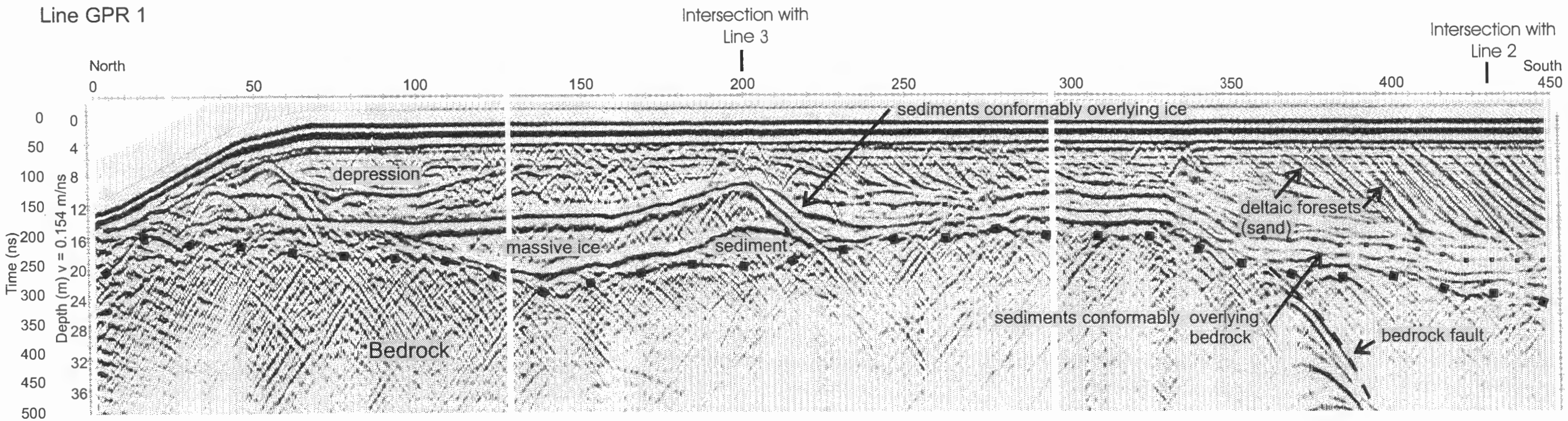

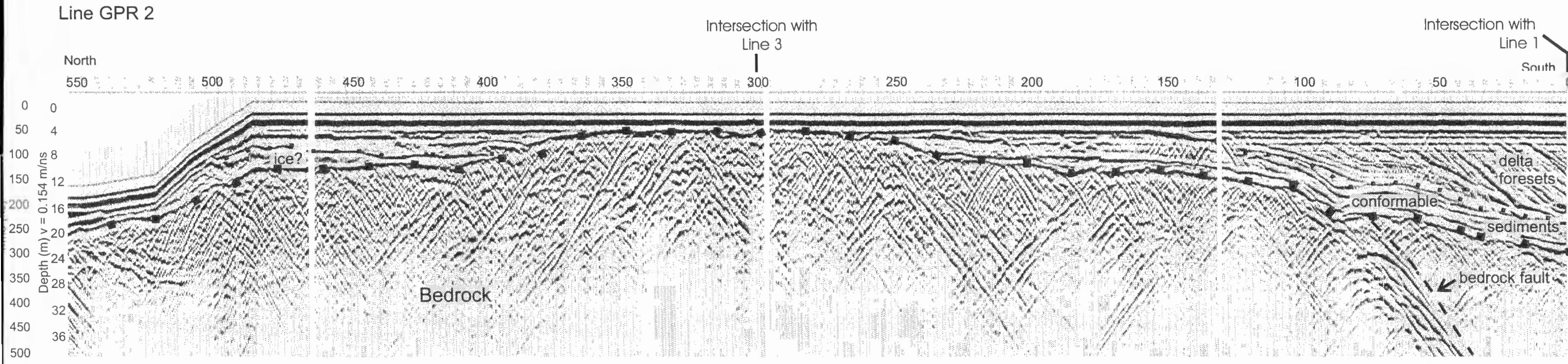

Fig. 3.4 GPR profiles of lines GPR 1 and 2 on the Carat outwash terrace.

GPR interpreted bedrock contact

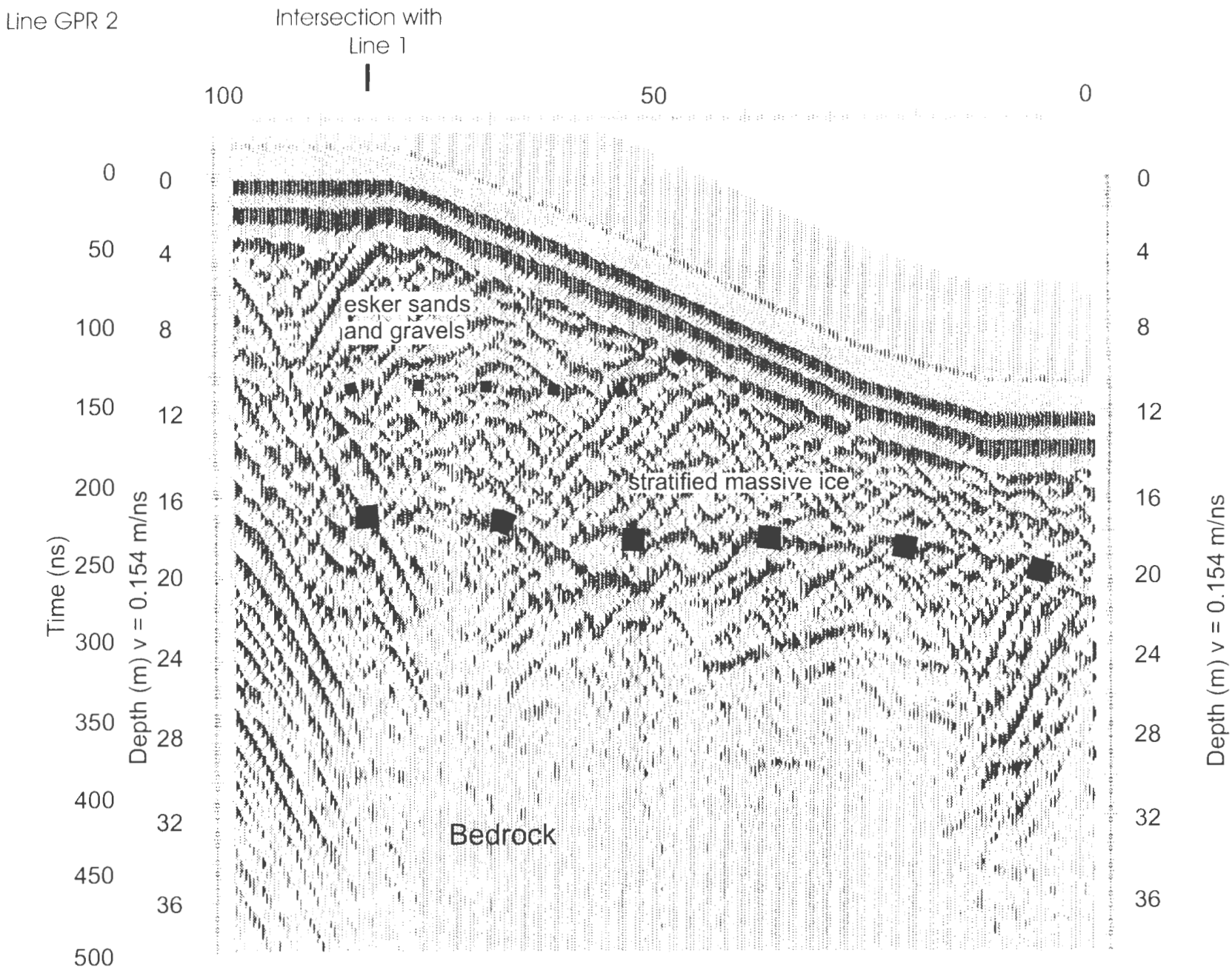

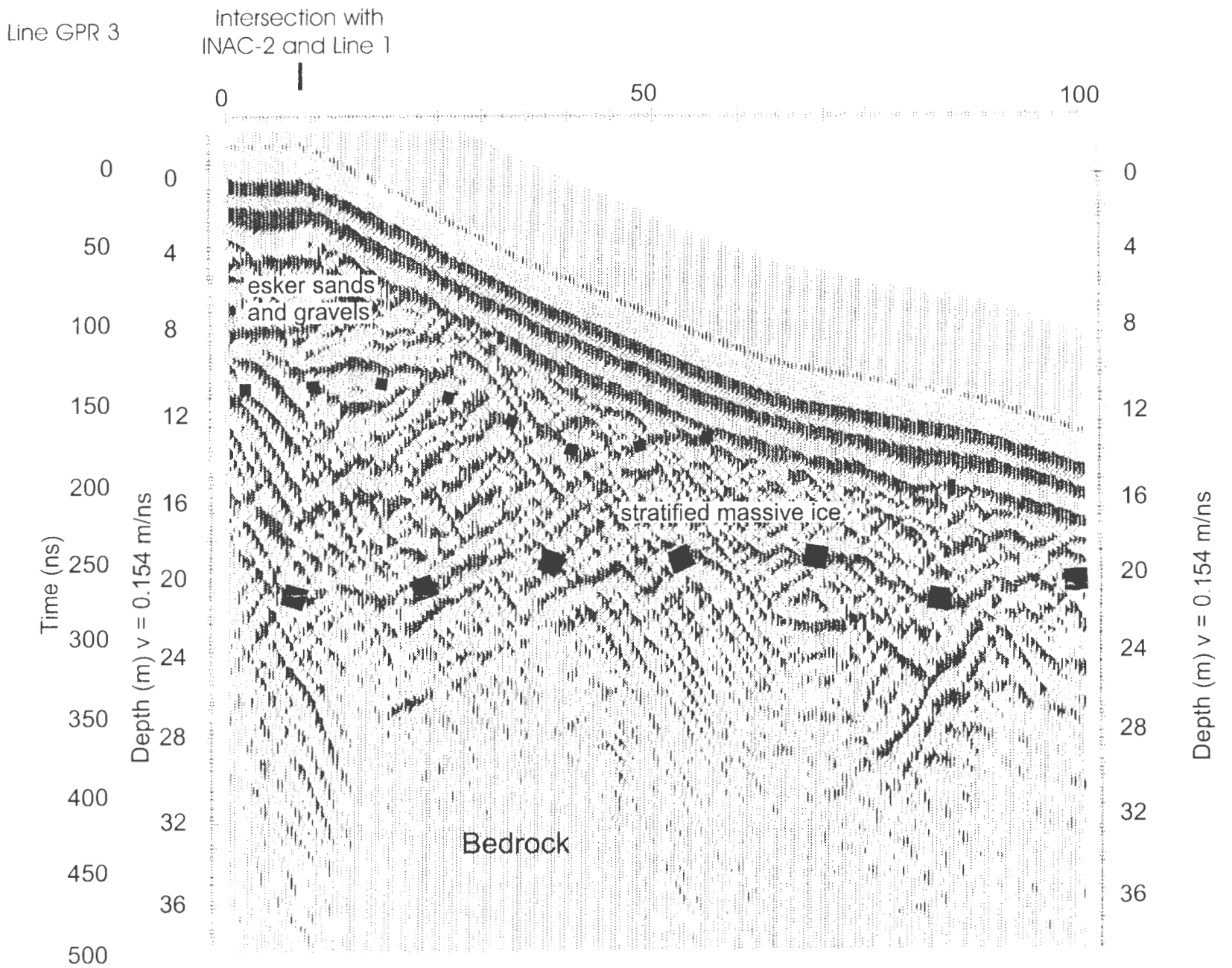

Fig. 3.3 GPR profiles of lines GPR 2 and 3 on the BHP Airstrip Esker.

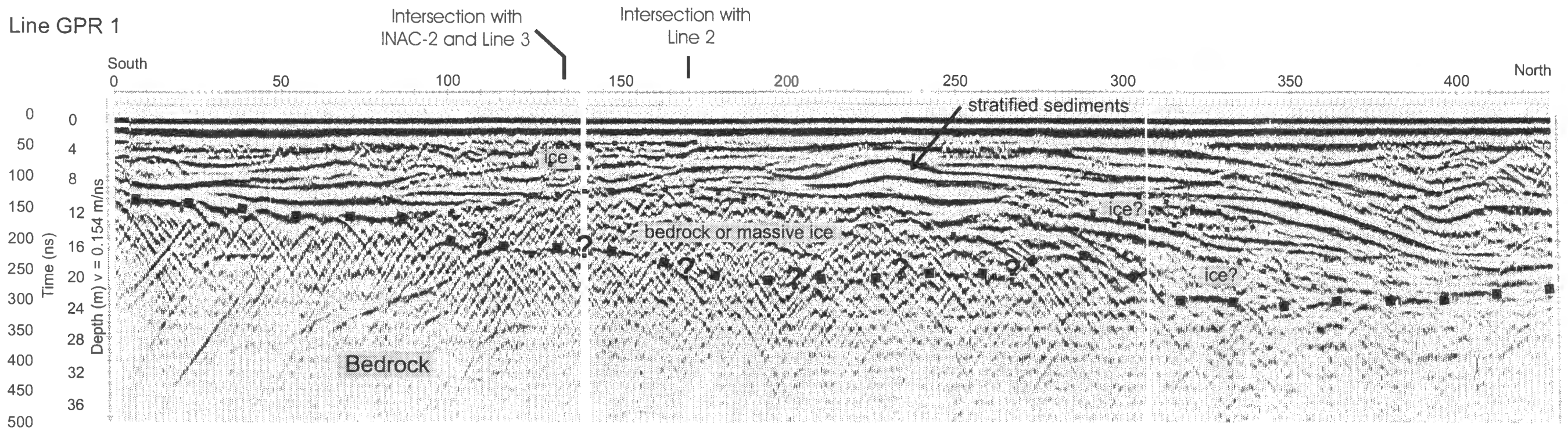

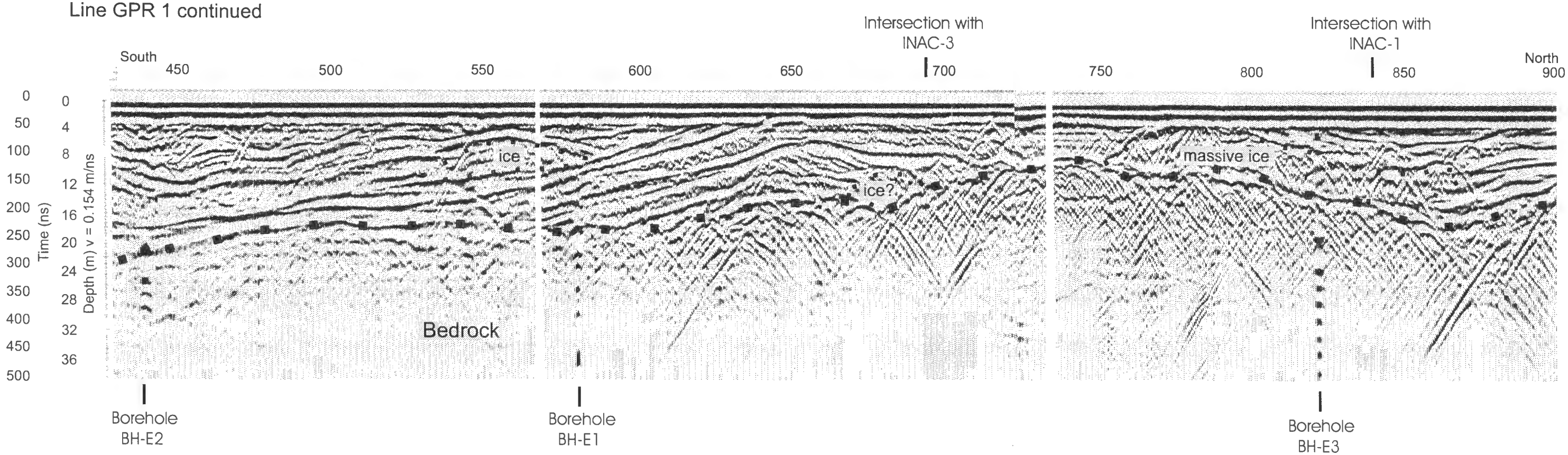

Fig. 3.2 GPR profiles of line GPR 1 on the BHP Airstrip esker.

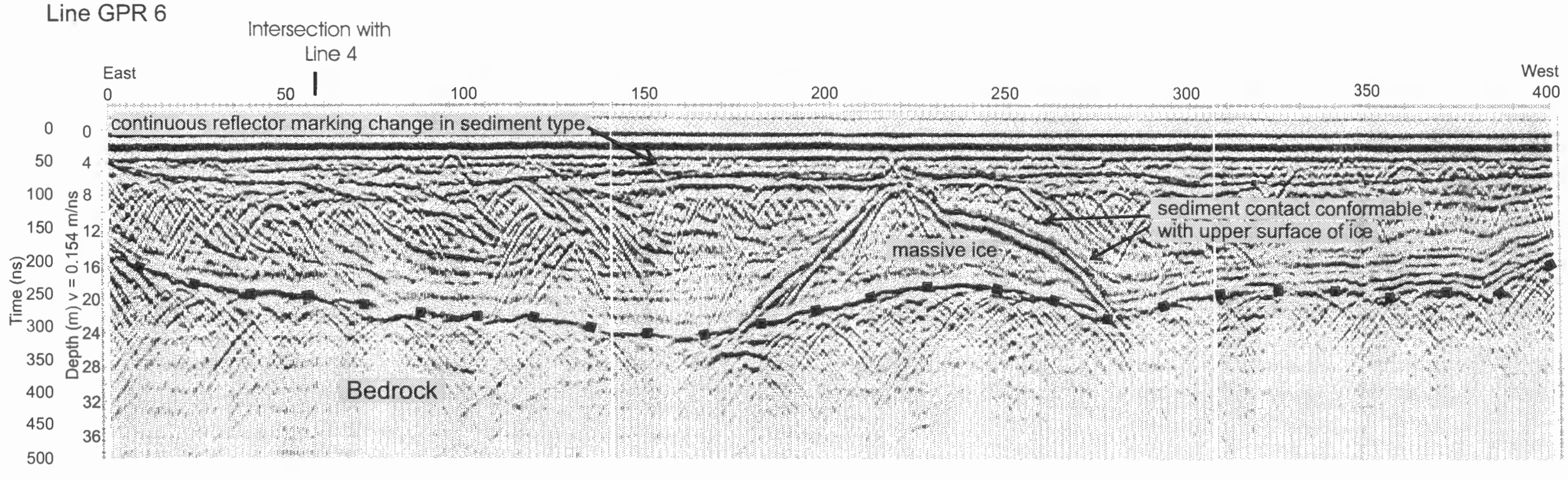

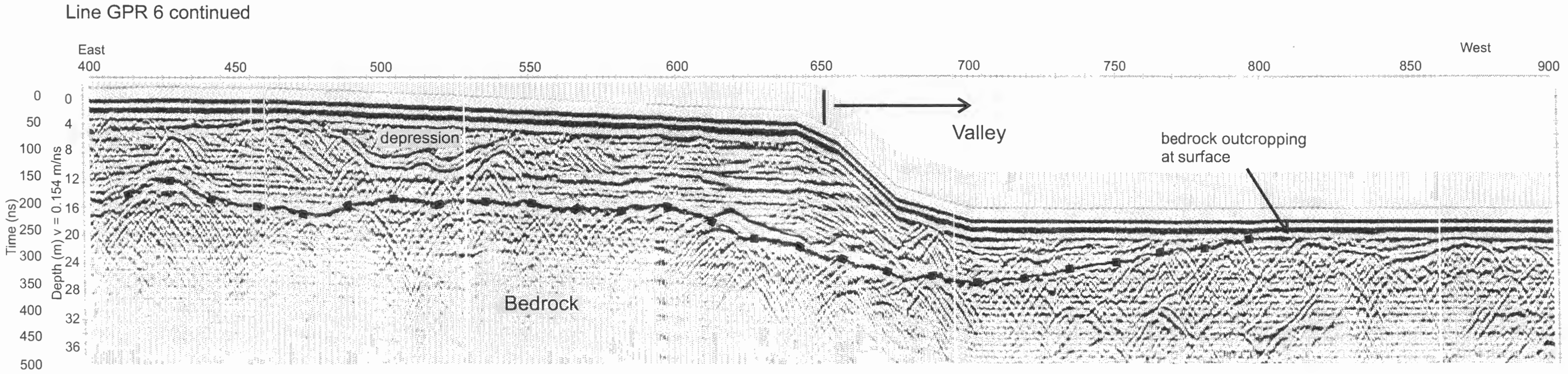

Fig. 3.7 GPR profiles of line 6 on Carat outwash terrace.

GPR interpreted bedrock contact

4. SURFACE GEOPHYSICAL SURVEYS (M. Douma; C. Hyde)

4.1 BACKGROUND AND METHODOLOGY

The surveying equipment consisted of an electromagnetic GEONICS EM-34 unit, and a prototype capacitive-coupled resistivity system (Ohm Mapper) currently under evaluation by the Geological Survey of Canada and a geophysical instrument manufacturer.

The EM-34 is a two-coiled inductive measuring system with a variable coil spacing of 10, 20 or 40 m. This system can be used to measure conductivities to depths of 60 metres. The instrument is operated by two people with the two 630 mm diameter coils lying flat on the ground or held vertically at ground level. For the present study, coil spacings were 10 and 20 metres, and both horizontal and vertical dipole measurements were recorded. This arrangement allows a sounding, or vertical conductivity profile to be constructed. From the sounding, it may be possible to model the distribution of sediments, frozen ground, or massive ice in the substrate.

The Ohm Mapper capacitive-coupled resistivity system is deployed by spreading four collinear antennas over the ground. One antenna pair is connected to a transmitter which generates a 16 kHz signal. The other antenna pair is connected to a receiver, which is essentially a sensitive and very stable voltmeter. The electrical potential is measured in the receiver antenna from which an apparent resistivity can be calculated. The layout of the antennas is essentially the same as a conventional resistivity survey, except that by replacing steel stakes with antennas, the speed of the survey is substantially increased, particularly in conditions of frozen ground where driving electrodes is very difficult. By optimal choice of antenna size and spacing between transmitter and receiver antennas, the field system can be designed to measure apparent resistivities from shallow depths (1-2 metres) to greater depths (>30 m). In this operation the antenna dipole spacing for both transmitter and receiver was 10 metres and the spacing between the two antennas was 20 metres.

4.2 INTERPRETATION OF RESULTS

4.2.1 Airport Esker

A 1475 metre long Ohm Mapper survey was conducted parallel to the axis of the Airstrip esker, near the BHP Koala Camp (line RES 1 in Figure 2.1). Most of the line is coincident with the GPR line discussed in Chapter 3 of this report, and crosses the three INAC boreholes drilled during this program, as well as the earlier EBA holes. Two shorter lines (RES 2 and 3) parallel and offset 50 and 100 metres to the west of line RES 1 were surveyed to measure resistivity of the esker flank. An east-west line (RES 4) connects the three north-south lines. A second line perpendicular to the esker, through the INAC-01 borehole at the north end of the site, was run to measure the resistivity over Airstrip Lake, adjacent to the esker (RES 5).

The main survey line, along the axis of the esker, shows more variability in resistivity than might have been expected for this type of feature (Figure 4.1). Rather than being fairly uniform, with high resistivity characteristic of well-bonded material or massive ice, the profile shows significant portions where the resistivity falls around 20000 ohm-m, high enough to imply frozen conditions, but perhaps also reflecting the effect of the underlying material. Comparison of the Ohm Mapper trace (at an arbitrarily selected vertical scale) with the GPR results reveals a significant correlation between the methods, with respect to proximity of the granitic bedrock (Figure 4.2). Even in the presence of 5-6 metres of massive ice in the section, such as at the north end of the line, the resistivity values are probably over-printed by the bedrock. At the southern end of the esker near the INAC-2 borehole, resistivity values rise to 40 000 ohm-m (Figure 4.2). This area corresponds to the ambiguous zone in the GPR trace where the depth to bedrock is interpreted to lie either at about 10 m, or between 16 and 18 m depth below the surface. The resistivity profile suggests that, rather than the area being a zone of massive ice or till, the depth to bedrock could be relatively shallow (approximately 10 m) in this area.

The resistivity profiles for RES 2 and 3 (Figure 4.3) show similar values to RES 1, except

at their northern ends which terminate on or at the edge of a small pond west of the esker. Line RES 4 (Figure 4.3) crosses the esker from the south end of RES 2 in an easterly direction, past INAC-02, and down onto a small isthmus between Airstrip Lake and a small pond. Again, presence of water is detected as a resistivity low. RES 5 crosses the esker, from east to west, past borehole INAC-01. Like RES 4, the profile shows that the esker is homogeneous across its axis.

4.2.2 Misery Lake Esker

Misery lines RES 1 and 2 (Figure 4.5) are resistivity profiles along the axis of the Misery Lake esker. Resistivities are consistent with massive ice or frozen ground with more than 30% ice content. Based on previous work, however, a comparison with the moisture contents of the borehole samples indicates that the ice-content value could be reduced to about 20-25%. Misery lines RES 3, 4, and 5 (Figure 4.6) are oblique traverses across the main axis of the esker. The resistivity values are not substantially different from the on-axis survey, although the resistivities are depressed in the presence of ponds and lakes.

4.2.3 Carat Outwash Terrace

Surface resistivity surveys were carried out over two potential borrow areas, immediately north of the camp (Figure 2.6). For the interests of the Geological Survey of Canada, the site was an excellent one for testing a new resistivity system (Ohm Mapper) in an area of extensive perennially frozen ground.

The geophysical surveying systems were run over two long lines, one of which tied the two borrow sites together over an intervening lake, and four shorter lines which joined together four potential drilling sites. The approximate locations of the lines are shown in Figure 2.6 based on chain distances and non-differential GPS observations.

Figures 4.6 and 4.7 show the EM-34 and Ohm Mapper data collected at the Carat Lake site. For comparison purposes, the conductivity values of the EM-34 have been converted to resistivity values. At the 20 metre separation, most EM-34 data plot in the negative domain, which is not a valid alternative. Although the EM-34 10 metre readings plot positive, these points were measured with the 20 metre cable, and thus must have a correction factor subtracted for the difference in the resistance of the 10 and 20 metre reference cables. If applied, the 10 metre values would plot negative, as well. These results confirm previous experiments that demonstrated that the EM-34 inductive electromagnetic method does not work very well in low conductivity environments, such as perennially frozen ground.

Based on the Ohm Mapper data, the average resistivity over the outwash material at the Carat Lake site (excluding a low resistivity zone) is about 34600 ohm-m, with a standard deviation of about 2400 ohm-m. Similar values have been recorded at Richard's Island, at the mouth of the MacKenzie River, where drilling and ground penetrating radar were used to map the distribution of massive ice and sediments (Dallimore and Wolfe, 1988; Douma et al. 1994). Resistivity values greater than 3000 ohm-m corresponded to the presence of massive ice greater than 10 metres thick, or to glaciofluvial sediments with ice-content > 30%. Talik zones, where the ground is unfrozen, and which may occur under lakes, were found to have resistivities below 1000 ohm-m.

The INAC-09 borehole drilled at the eastern edge of the southern outwash area uncovered about 3 metres of massive ice overlain by 13 metres of well-bonded sand. The low resistivity zone over the lake at the Carat Lake site indicates a talik along survey line RES 1 (Figure 4.7). The other lines at Carat Lake show similar resistivity values to line RES 1 (Figure 4.6) and GPR data over the area shows variable thicknesses of sediment and some zones of massive ice (Figure 4.8). The resistivity data indicates that the sediments are well-bonded with some areas of high ice content, confirmed in INAC-09 borehole. However, as with the Airstrip Esker, the Ohm-Mapper does not appear to differentiate between massive ice and frozen well-bonded sediments (Figures 4.8 and 4.9).. Instead, the resistivity profiles appear to depict the depth to bedrock, with resistivities approaching 50 000 ohm-m in areas of exposed bedrock (Figure 4.9).

4.3 REFERENCES

Dallimore, S.R. and Wolfe, S.A. 1988. Massive ground ice associated with glaciofluvial sediments, Richards Island, N.W.T. Canada. *in* Proceedings of the Fifth International Conference on Permafrost, Trondheim, Norway, Aug. 1988, Volume 2, p.1217-1222.

Douma, M., Timofeev, V.M., Hunter, J.A., and Rogozinski, A.W. 1994. A capacitive-coupled ground resistivity system for engineering and environmental applications: results of two Canadian field tests. *in* Technical Program, Expanded Abstracts with Authors' Biographies; Society of Exploration Geophysicists, International Exposition & Sixty-Fourth Annual Meeting, Los Angeles, California, October 23-28, 1994, p.559-561

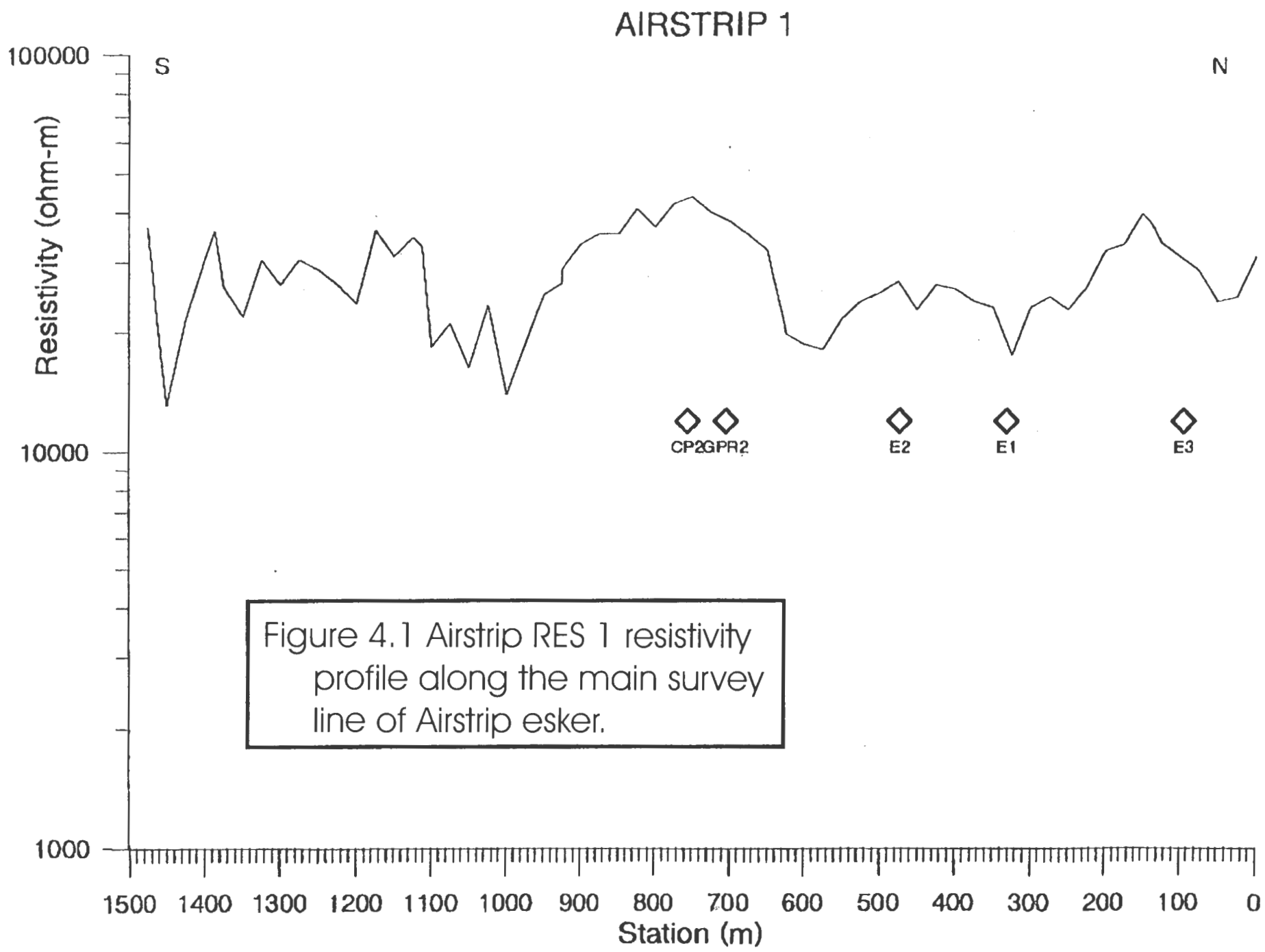

Figure 4.1 Airstrip RES 1 resistivity profile along the main survey line of Airstrip esker.

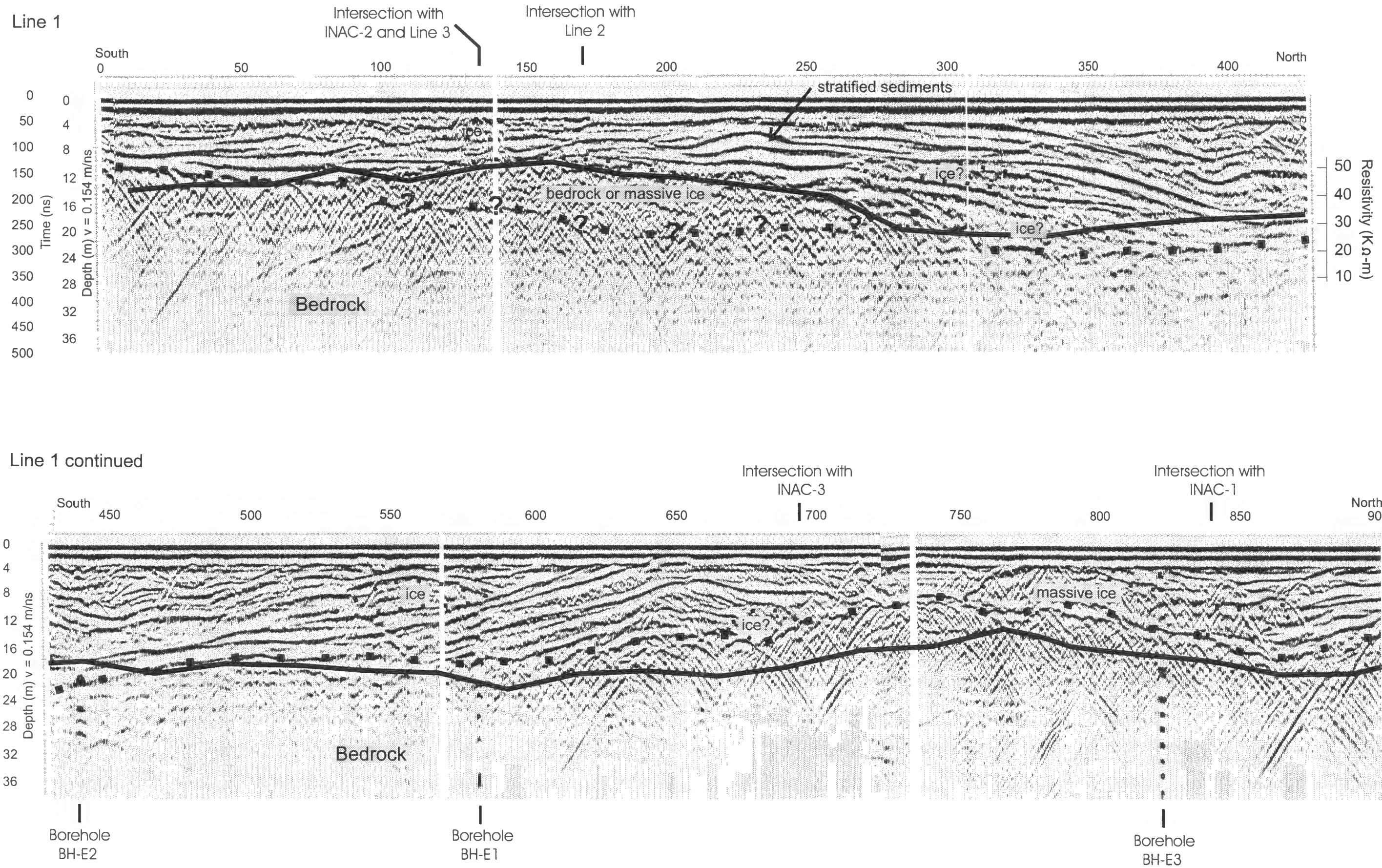

Fig. 4.2 GPR profiles of Line GPR 1 with resistivity overlay from Ohm Mapper survey on Airstrip esker.

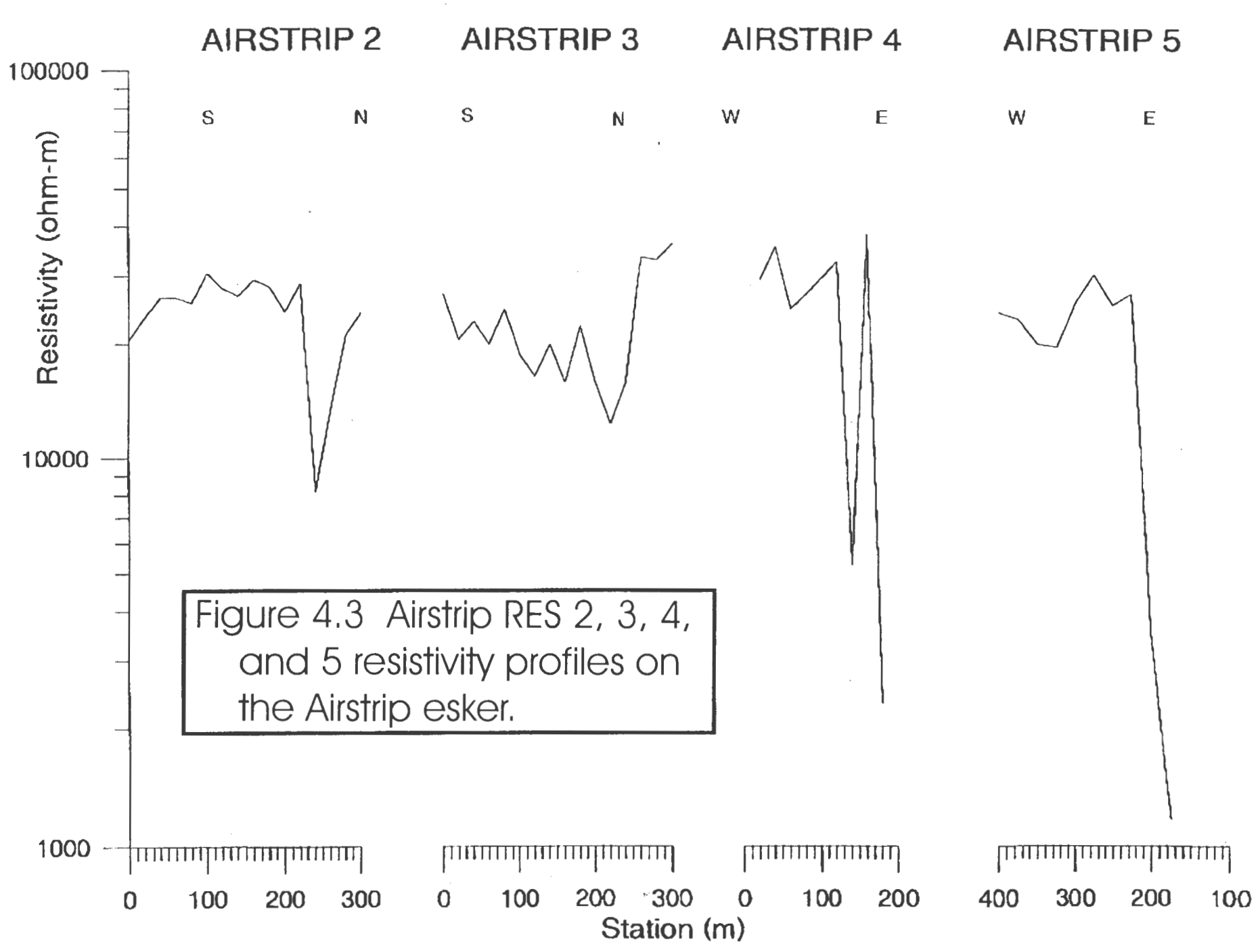

Figure 4.3 Airstrip RES 2, 3, 4, and 5 resistivity profiles on the Airstrip esker.

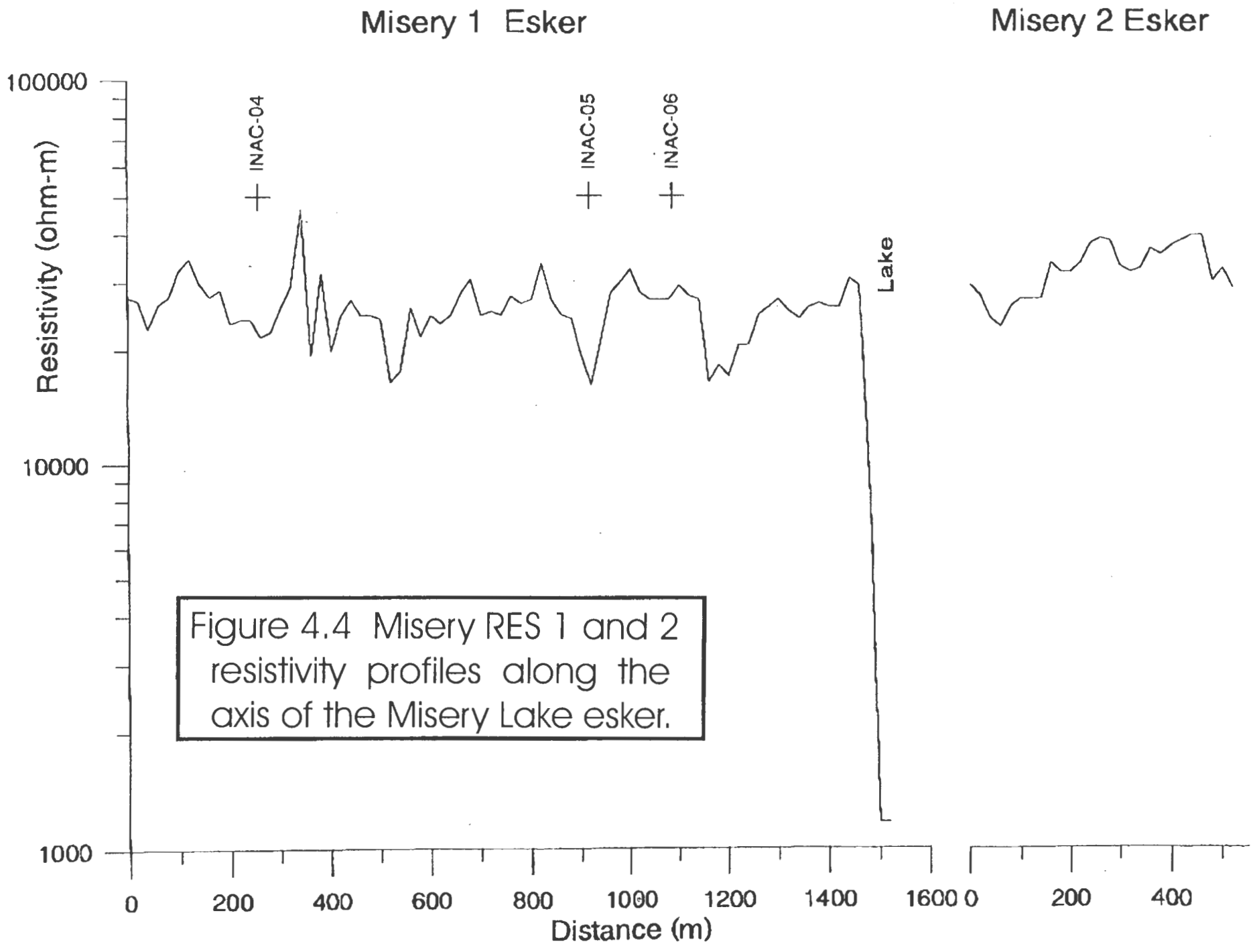

Figure 4.4 Misery RES 1 and 2 resistivity profiles along the axis of the Misery Lake esker.

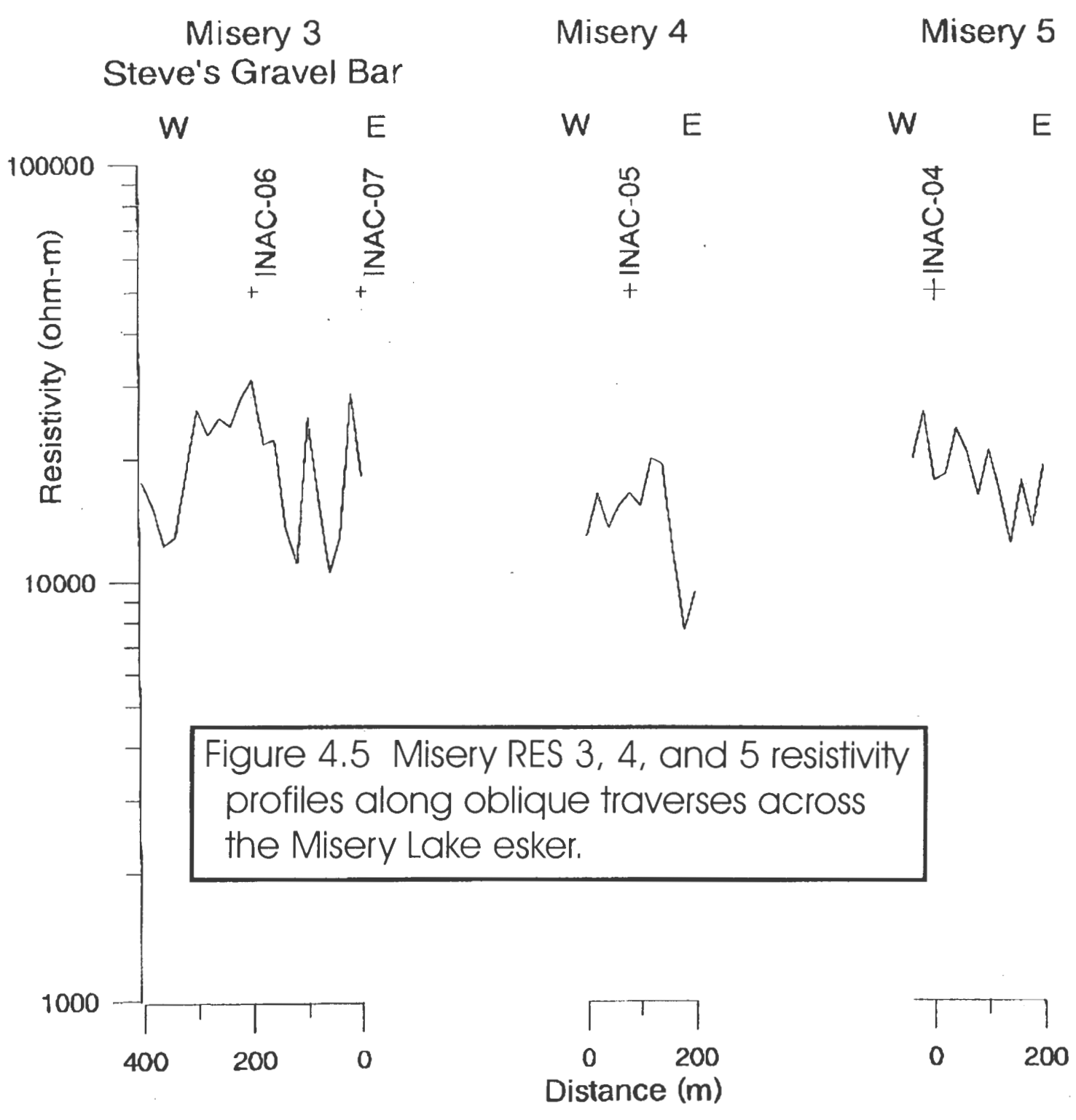

Figure 4.5 Misery RES 3, 4, and 5 resistivity profiles along oblique traverses across the Misery Lake esker.

Figure 4.6
CARAT LAKE SITE
SURFACE RESISTIVITY SURVEY

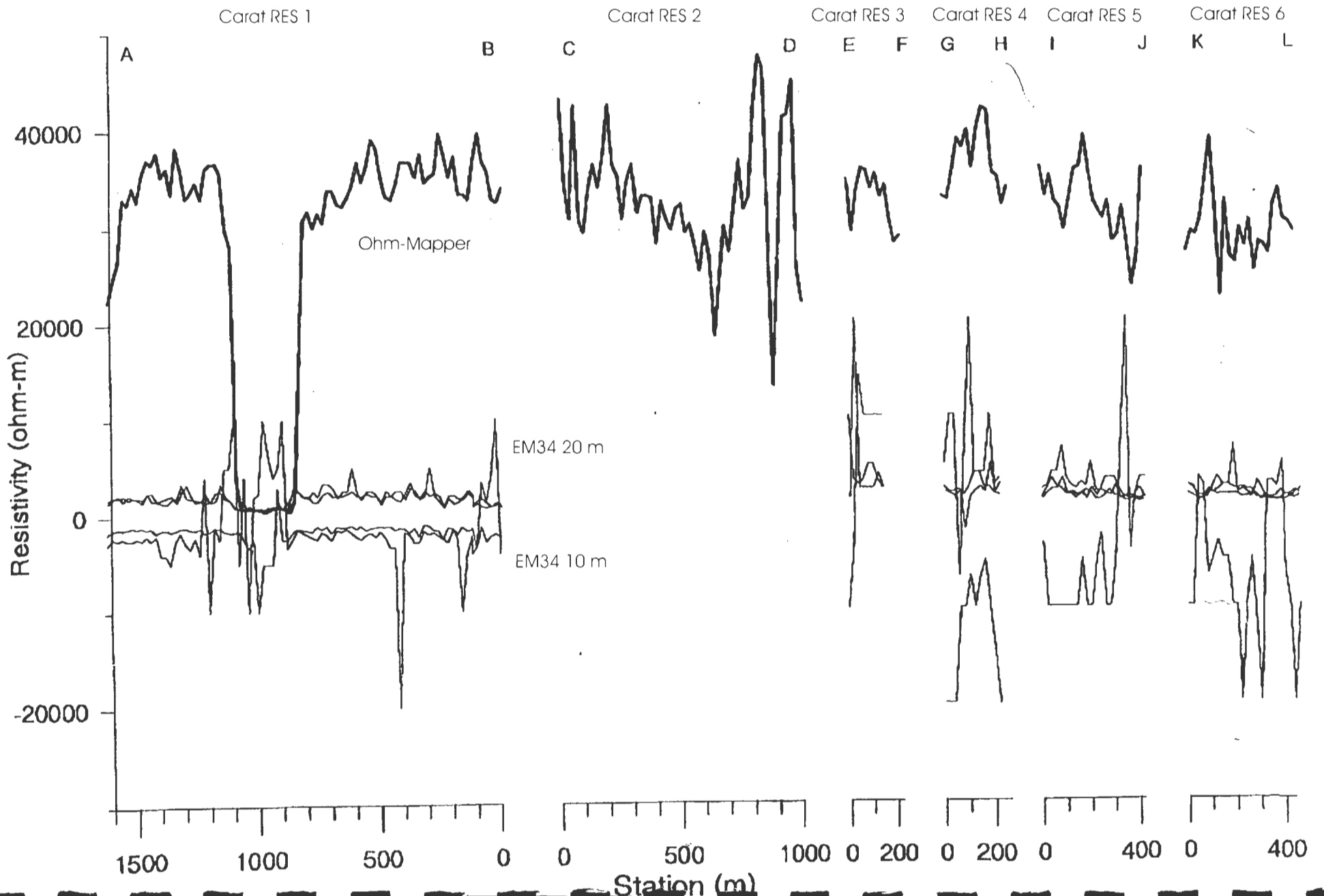

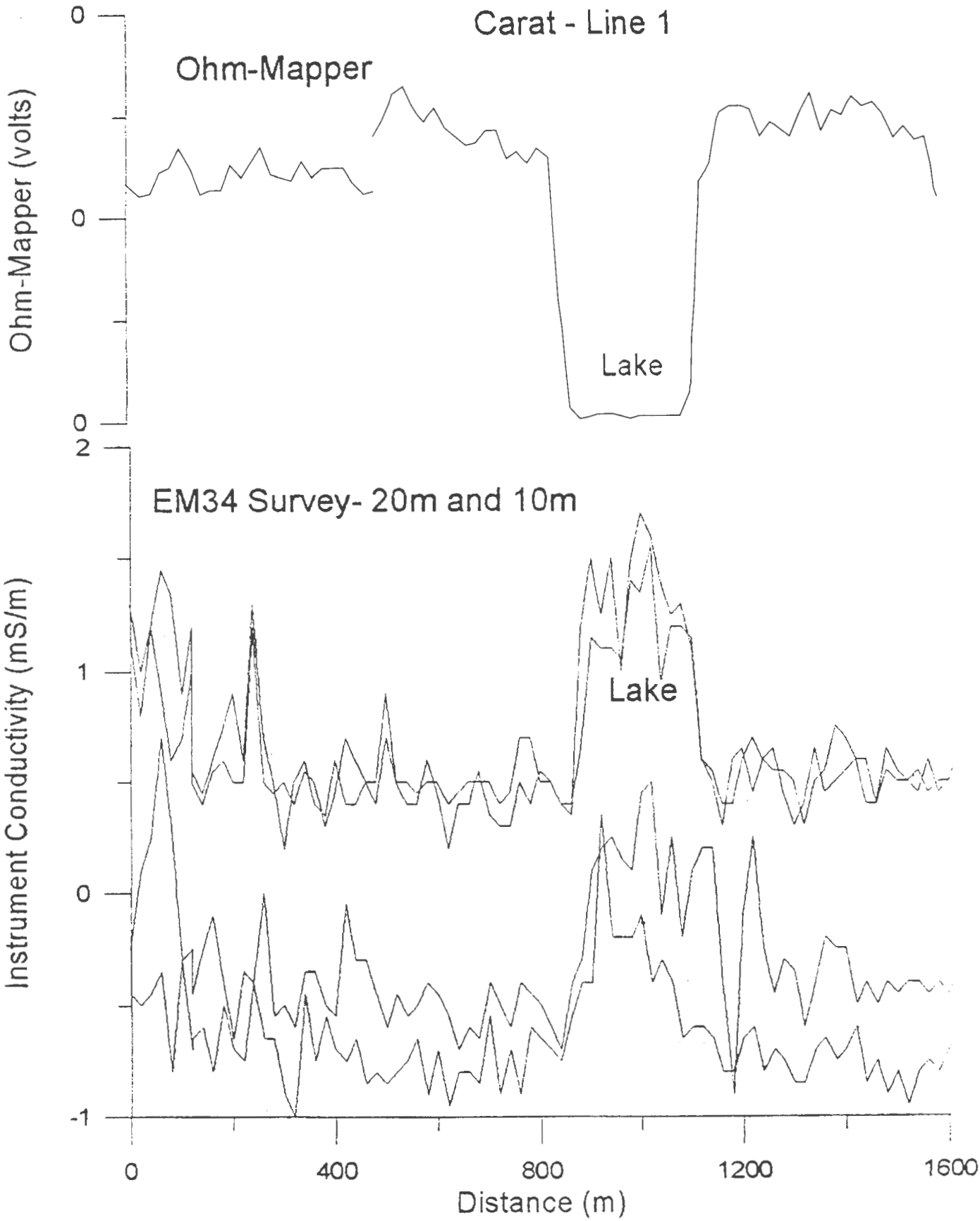

Figure 4.7 Ohm mapper and EM-34 surveys on Carat RES 1.

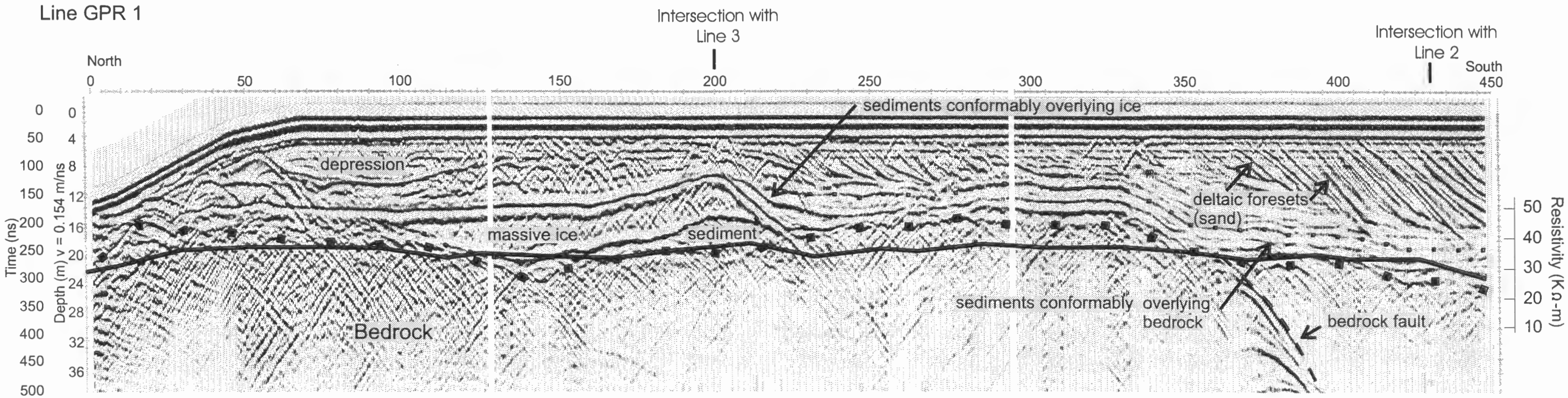

Fig. 4.8 GPR profiles of line GPR 1 with Ohm-Mapper resistivity overlay (RES 1) on Carat outwash terrace.

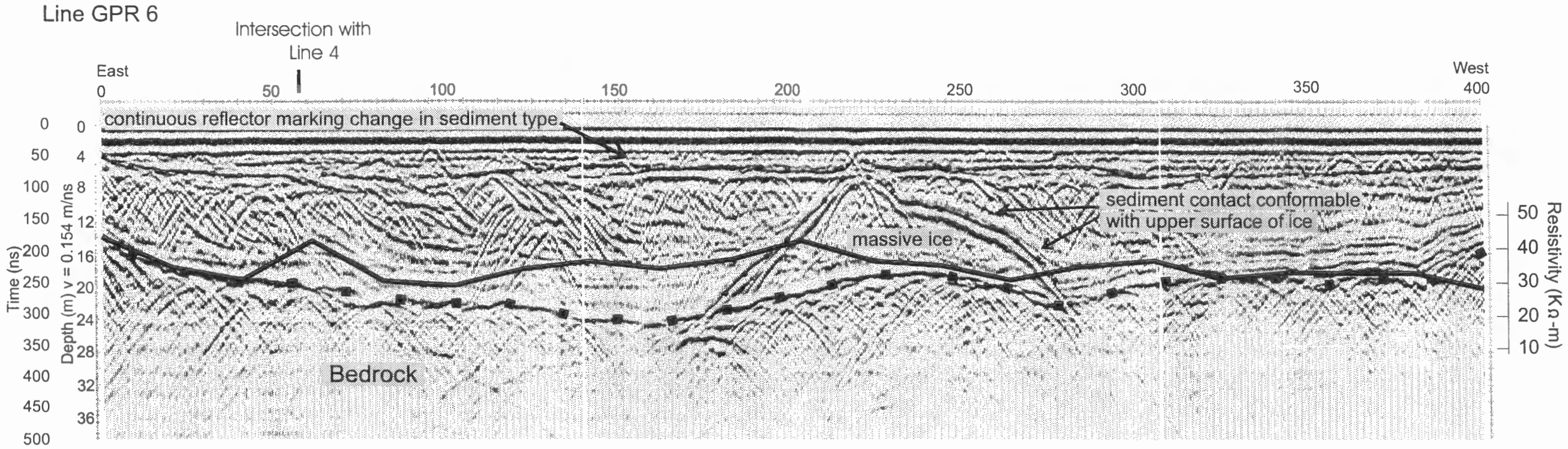

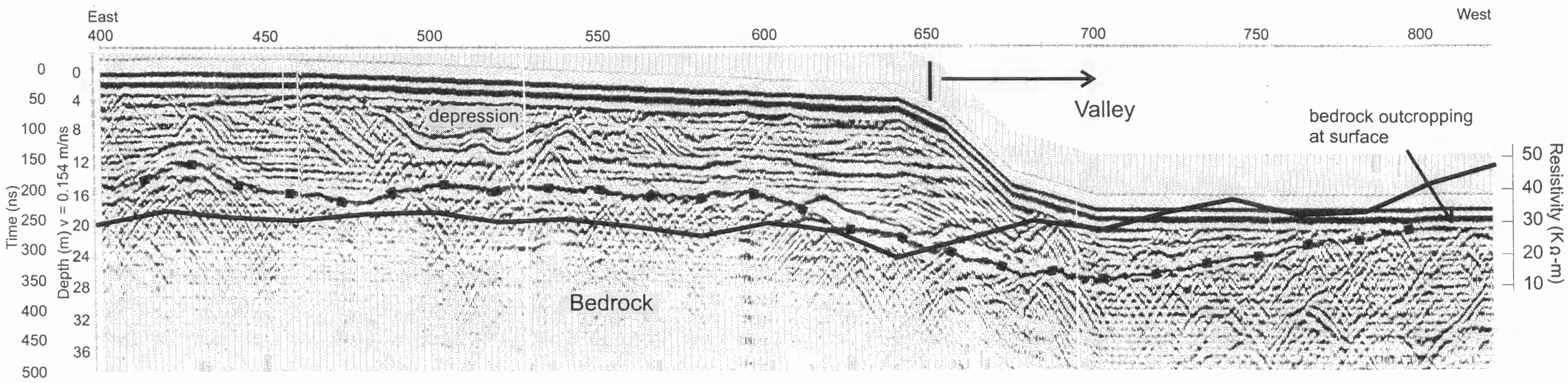

Fig. 4.9 GPR porfliles of line 6 with Ohm Mapper resistivity overlay (RES 2) on Carat outwash terrace.

■ ■ ■ GPR interpreted bedrock contact

Ohm-Mapper resistivity

5. BOREHOLE GEOPHYSICAL LOGGING (M. Douma)

Borehole geophysical logging was carried out in three boreholes at the Airstrip esker, and one borehole at the Misery Lake esker. Natural gamma, electromagnetic conductivity and magnetic susceptibility logs were run in all of the holes. The system used was the GEONICS EM-39 portable logging unit. All logging tools used for this study are passive and require no operational or site licensing.

All logs were obtained using a depth sampling increment of 2.5 cm. The natural gamma logs were taken with the high integration rate setting of the instrument, thus requiring a sample rate of 1 measurement per second. The conductivity and magnetic susceptibility logging tools were zero-calibrated before each logging run.

5.1 BACKGROUND AND METHODOLOGY

5.1.1 Natural Gamma Log

The natural gamma log measures the natural gamma radiation from earth formations. The primary instrument response is from radioactive potassium, uranium and thorium. In most unconsolidated overburden materials, high count rates are observed from silts and clays (increased K content) and lower count rates are observed in coarser grained material such as sands and gravels. Occasionally, anomalously high gamma counts have been observed in materials with large concentrations of radioactive uranium (some basal tills in central Canada and in some placer gravel deposits in the Cordilleran mountains). In general, the natural gamma log can be used in a qualitative manner to estimate the average grain size of materials. This tool measures radiation over a vertical distance of 5 cm and up to approximately 30-40 cm into the formation around the borehole. Although it is relatively unaffected by borehole fluid, its response can differ quantitatively with hole size and casing type. The overall response is attenuated by large hole diameters (15-30 cm) and steel

casing. PVC or ABS casing has minimal effect on the readings. The tool integrates the count rate over a selectable time window, hence slow speed logging yields relatively accurate repeatable results.

5.1.2 Conductivity Log

The conductivity log measures ground conductivity using electromagnetic induction techniques. The tool consists of a transmitter and receiver coil arrangement (spacing 50 cm) transmitting at a frequency of approximately 39 kHz. No contact is required with the borehole wall. Hence the tool can be used in an open hole or a plastic cased hole, either fluid-filled or dry. The tool measures the average ground conductivity between the coils and to a radius of approximately 1 metre around the hole. The tool is relatively insensitive to fluid conductivity immediately adjacent to the probe. Steel cased sections of the borehole are not logged.

5.1.3 Magnetic Susceptibility Log

The magnetic susceptibility log measures the average magnetic susceptibility of ferrimagnetic earth materials in a manner similar to the conductivity log. The two tools are similar in design and measure the same volume of material. In most earth materials the most prominent ferrimagnetic mineral is magnetite, with a susceptibility which is generally orders of magnitude higher than other oxides of iron or chromium. Hence, logs in most overburden materials are used as an indicator of heavy mineral concentrations such as differentiating different ages of sands or delineation of till units. Steel cased sections of the borehole are not logged.

5.2 INTERPRETATION OF RESULTS

5.2.1 Airstrip Esker

The borehole geophysics logs for the Airstrip esker boreholes are summarized in Figure 5.1. Individual boreholes INAC-01, INAC-02, and INAC-03 are shown in Figures 5.2, 5.3, and 5.4, respectively.

Figure 5.1 shows that the three boreholes share some common elements, although there are few borehole-to-borehole correlations. In general, the gamma logs show elevated gamma counts, greater than what would be expected from sand and gravel, which are the dominant lithologies. Gamma counts over 150 counts per second (cps) are more typical for fine grained sediments, due to high concentration of potassium-rich clay. High gamma counts in granular material may indicate potassium feldspar-rich sediment, or some contribution from radioactive minerals. Previous experience in the MacKenzie Delta shows that sand and gravel has gamma counts in the order of 40 cps, and only tills are over 150 cps. A short interval from 1.3 to 2.5 metres in INAC-02 appears to be recording an ice layer, observed during drilling. In INAC-01, the interval from 0.25 to 3 metres the gamma log appears to reflect a fining-upward sequence, mentioned in the drilling log.

Conductivity logs for INAC-02 and INAC-03 show values less than 20 milliSiemens per metre (mS/m). INAC-01 values are lower by an order of magnitude, but show more vertical variability. The only correlative event in the three boreholes is a conductivity low occurring between 3.25 and 5 metres. This anomaly does not appear to be related to lithology or ice-content.

5.2.2 Misery Lake Esker

Borehole logs for the INAC-04, Misery Lake esker borehole, are shown in Figure 5.5. Gamma count rates are not as high as the Airstrip esker boreholes, and the transition to diamicton

at a depth of about 5 metres is not recorded on the gamma log.

The conductivity log shows, with minor exceptions, values less than 1 mS/m. A very low conductivity anomaly at 3.7 m depth has no obvious explanation.

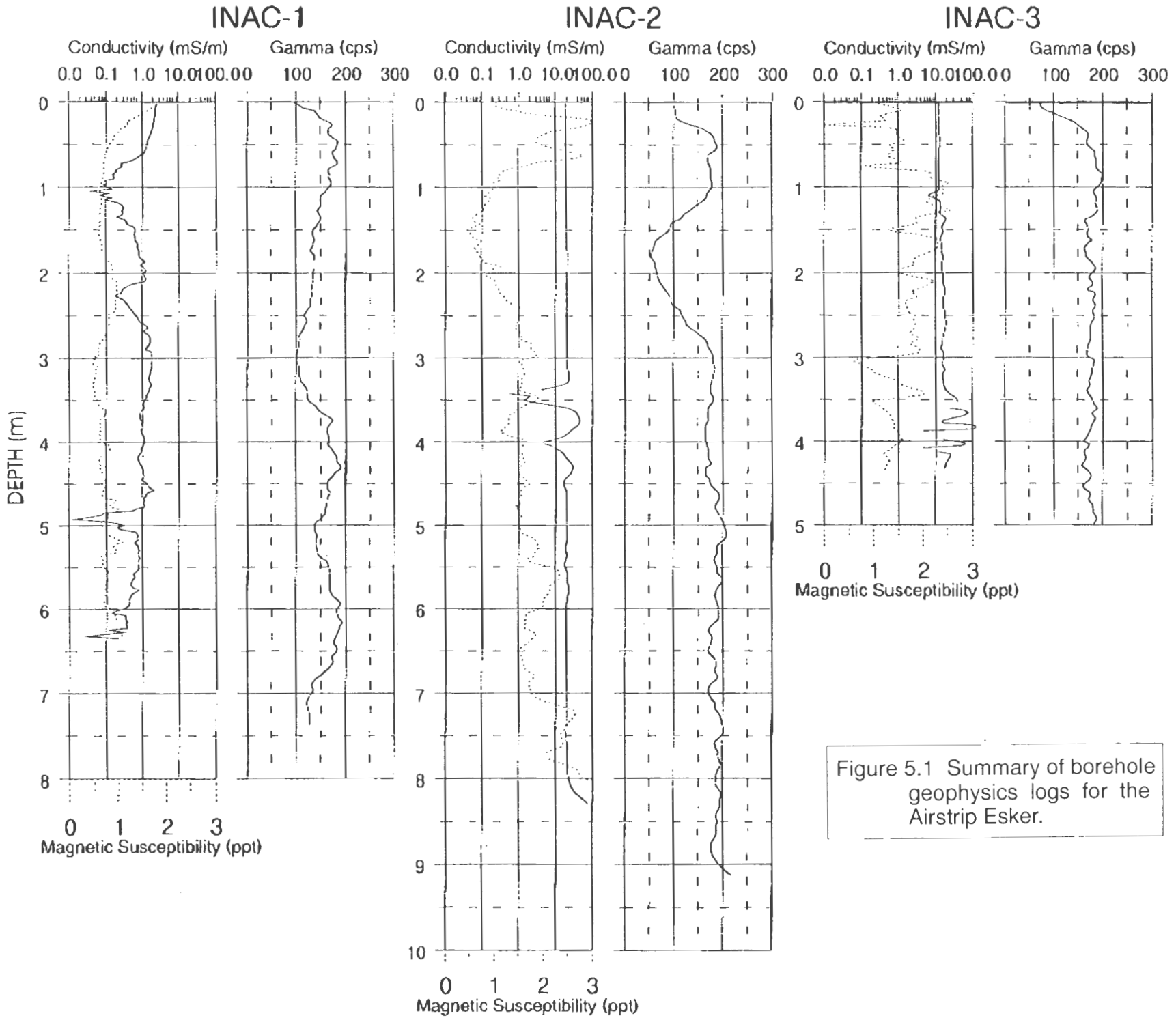

Figure 5.1 Summary of borehole geophysics logs for the Airstrip Esker.

Figure 5.2
EM-39 LOGS
BHP KOALA CAMP
INAC-1

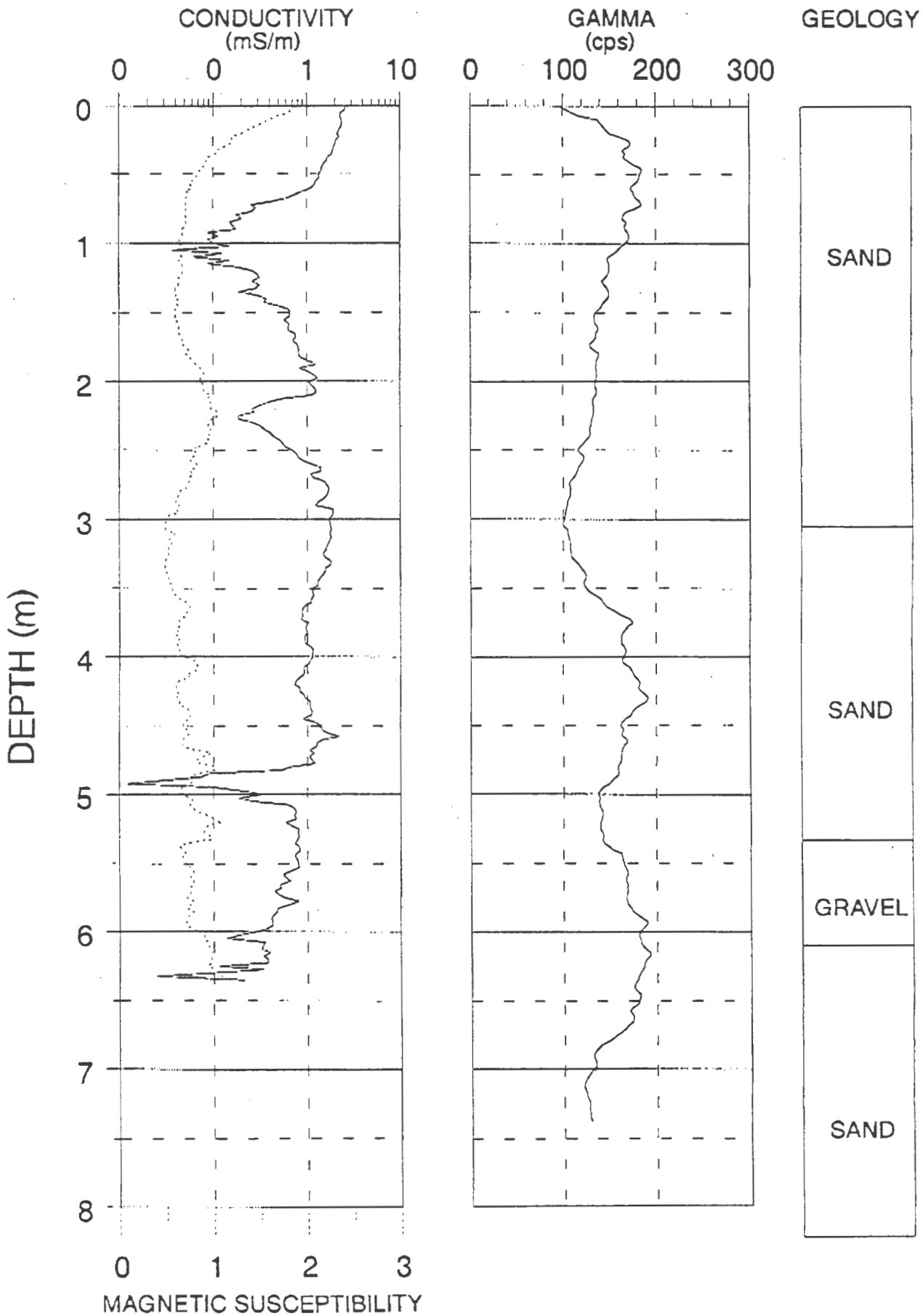

RG

Figure 5.3
EM-39 LOGS
BHP KOALA CAMP
INAC-02

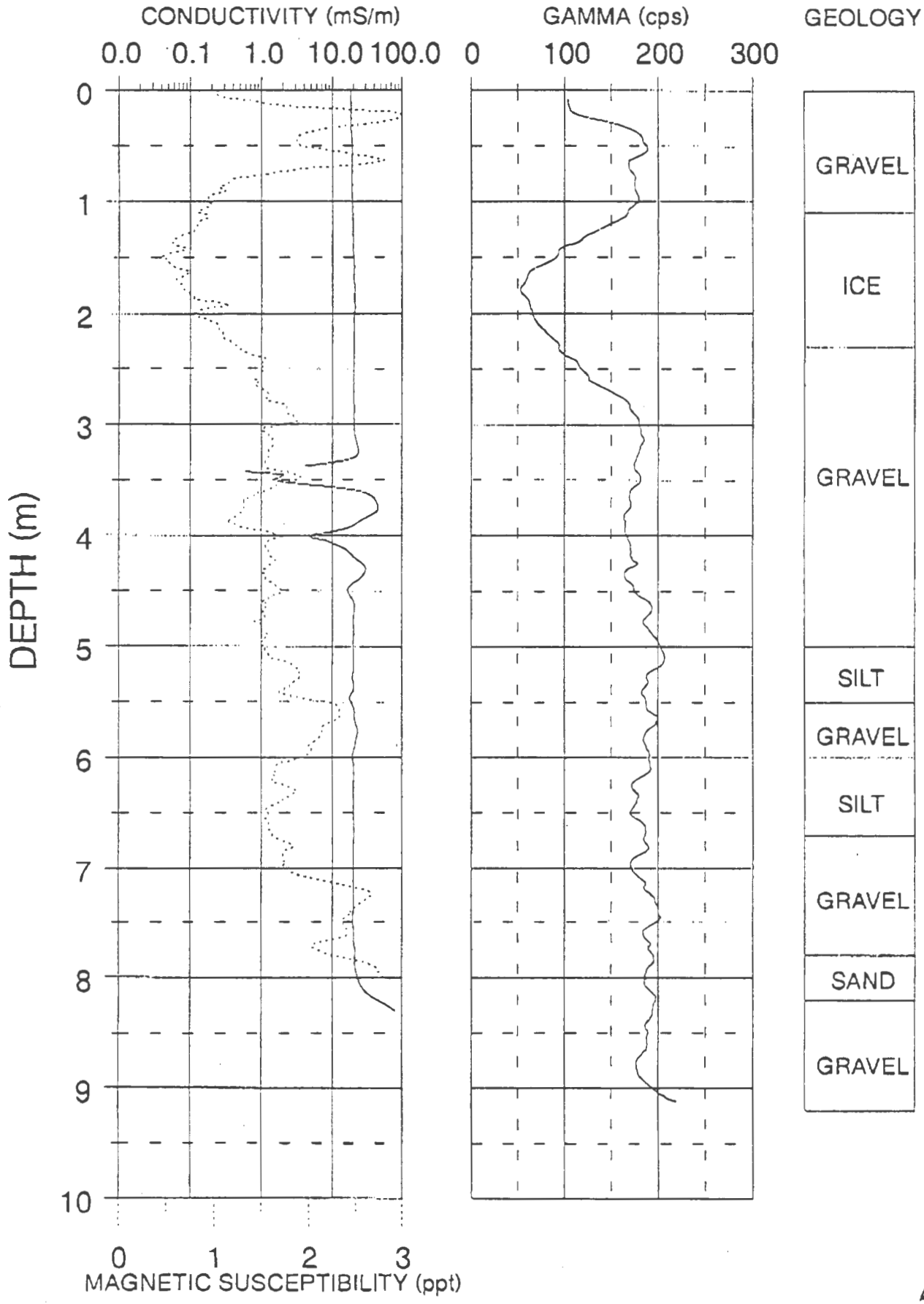

Figure 5.4
EM-39 LOGS
BHP KOALA CAMP
INAC-03

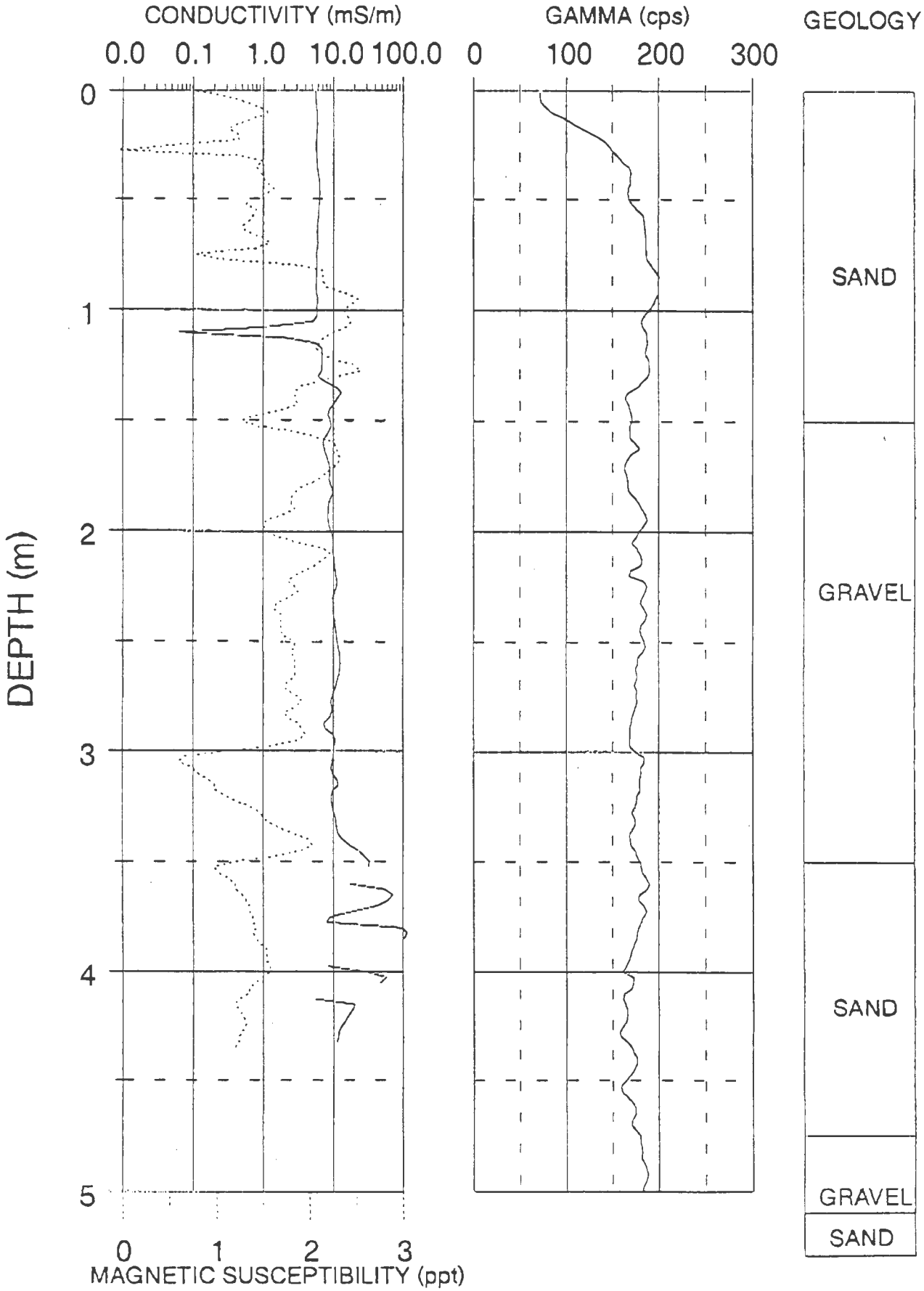

EM-39 LOGS
BHP MISERY ESKER
INAC-04

Figure 5.5

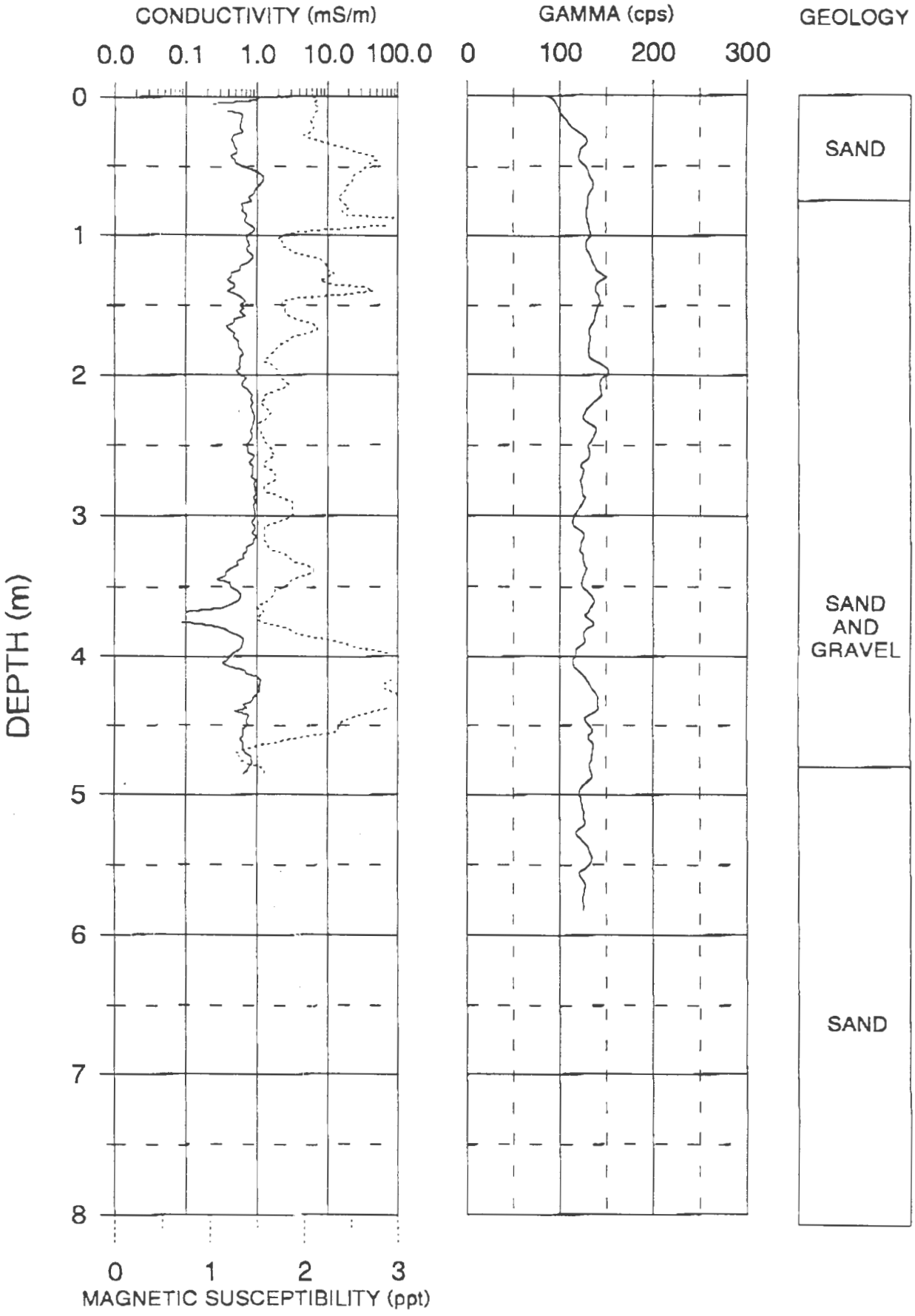

6. CONCLUSIONS (S. Wolfe)

The geological and geophysical investigations conducted at the BHP Airstrip and Misery lake eskers and the Carat Lake outwash terrace provide considerable insight into understanding of the origin, occurrence and regional distribution of ground ice in glaciofluvial sediments in the Slave Geological Province.

Sediments in the Airstrip esker are typically well-graded sands and gravels but with distinct and frequent changes in stratigraphy. In contrast, sands and gravels dominate the upper 3 to 6 m of sediment at the Misery Lake esker, ranging from clean well-graded sands to poorly-graded gravels with a sandy till-like diamicton occurring at a depth of approximately 4 m. Although massive ice is extensive in the Airstrip esker, massive ice was encountered in only one borehole in the Misery lake esker.

Massive ground ice encountered in boreholes at the Airstrip esker and Carat outwash terrace was extrapolated laterally by the GPR surveys. The top of the ice body at the Airstrip esker is interpreted to range between 4 and 9 m below the surface, with the base between 10 and 16 m below the esker surface. Maximum thickness of the ice body appears to be about 7 m, and the lateral extent along the profile appears to be about 125 m in this vicinity. Interpreted bedrock topography varies from 10 to 20 m below the esker surface. GPR profiles along the western flank of the Airstrip esker indicate that the interpreted bedrock depth remains 4 to 7 m below surface.

Results from the Ohm Mapper surveys at the Airstrip esker indicate a variable bedrock topography beneath the Airstrip esker. Comparison of Ohm Mapper traces with the GPR profiles at the Airstrip esker reveals a significant correlation, with respect to the depth to bedrock. Ohm Mapper traces at the Misery Lake esker are consistent with massive ice or frozen ground with more than 30% ice content. However, a comparison with the moisture contents of the borehole samples indicates that ice-contents probably average 20-25%.

Downhole geophysics confirmed independent interpretations in several boreholes. A short interval from 1.3 to 2.5 metres in INAC-02 appears to record the upper ice layer observed during drilling. In INAC-01, the gamma log appears to reflect a fining-upward sequence in the interval from 0.25 to 3 metres. In addition, high gamma counts in granular material may indicate potassium feldspar-rich sediment, or some contribution from radioactive minerals.

Results from the geoscience program suggest that the lower ice at the Airstrip esker was likely deposited as part of the esker system, contemporaneous with deposition of the esker sediments and has since been preserved by the presence of permafrost. Preliminary results from oxygen isotopes (ranging from -28‰ to -30‰) for the lower massive ground ice at Airstrip indicate a cold-water source for the ice, most likely of glacial or glacial meltwater origin. Less negative oxygen isotope values for ground ice encountered near the surface of the esker suggest a more modern water source for the upper ice. Massive ice observed at the Misery Lake esker is preliminarily interpreted as ice of glacial or glaciofluvial origin as oxygen isotopes are in the order of -35‰. Alternatively, this ice may have formed as permafrost aggraded into the sediments, but with source waters derived from glacial melt.

By comparison, sediments in the Carat outwash terrace show a fining-downward sequence of sands grading into a lower unit of medium to fine sand and silt. Moisture contents remain fairly consistent throughout the sandy unit, with a trend towards increasing moisture content with depth. In the borehole at the south end of the deposit (INAC-9), massive ice was encountered at a depth of approximately 13 m. Approximately 3 m of massive ice was drilled prior to the termination of drilling.

Massive ice was identified at Carat at Site A and east of the airstrip. Depth to bedrock is interpreted to range between 16 to 22 m below the ground surface. Towards the eastern part of the Carat A borrow area, the bedrock reflector rises gradually and approaches to within about 3 or 4 m of the ground surface. At the south end of the Carat A borrow site there appears to be a fault within the bedrock, dipping steeply to the south.

Results from the Ohm Mapper surveys indicate that the sediments may have a high ice content but do not differentiate between massive ice and high ice content sediment. Results from the EM-34 inductive electromagnetic method confirm that the technique does not work very well in low conductivity environments, such as perennially frozen ground.

Results from the geoscience program at the Carat outwash terrace are not conclusive, and the massive ice may be of buried glacial or glaciofluvial origin, or intrasedimental ice implaced through the process of ice-segregation during permafrost aggradation into the sediments. The thick sequence of deltaic sediments overlying the ice suggests that sediments were deposited into relatively deep water. Preservation of buried ice under this scenario would likely require rapid deposition of the overlying sediments.

7. ACKNOWLEDGEMENTS

The authors are indebted to BHP Diamonds Inc., Canamera Geological Ltd., EBA Engineering Consultants and Bruce Geotechnical Consultants for onsite support and assistance in the ground ice program. Field assistance and technical advice by Mark Nixon and Pavel Kurfurst are greatly appreciated. Partial funding for the study was obtained through a PERD project (950035-05) to investigate geophysical techniques and development in permafrost environments. We are also thankful to INAC, and particularly Stephen Traynor, for ongoing co-operation and support of this work.

APPENDIX A - Analytical Tables

Table A1. Oxygen and deuterium isotopic analysis of Airstrip Esker ground ice and surrounding waters.

Sample	Description	Depth (cm)	Values Relative to Standard Mean Ocean Water		
			Deuterium Isotopes		Oxygen Isotopes
			Values	Repeats	Values
100	Lower Ice	20-30	-213.6		-28.23
101	Lower Ice	45-53	-223.9	-219.6	-29.36
102	Lower Ice	70-75	-218.6		-28.65
103	Lower Ice	90-100	-224.3		-29.03
104	Lower Ice and Sed	120-140	-223.2		-28.93
105	Lower Ice and Sed	137-145	-221.3		-29.04
106	Lower Ice	160-170	-221.4		-29.07
107	Lower Ice	surface	-218.2		-28.97
108	Lower Ice	surface	-223.8		-29.32
109	Lower Ice	surface	-217.4	-212.5	-28.38
110	Lower Ice	surface	-225.2		-29.50
111	Lower Ice	surface	-227.4		-29.45
112	Lower Ice	surface	-220.7		-28.65
113	Lower Ice	surface	-220.8		-28.80
114	Lower Ice and Sed	surface	-231.5		-30.19
115	Lower Ice	surface	-228.3		-29.86
116	Lower Ice	surface	-220.7		-28.64
117	Upper Ice and Sed	surface	-172.9	-168.7	-22.52
118	Upper Ice and Sed	surface	-167.8	-169.1	-22.18
120	Airstrip Lake	N/A	-153.7	-155.1	-18.74
121	Upper Ice	15-25	-192.2	-192.8	-25.13
122	Upper Ice	40-50	-180.2		-23.56
123	Upper Ice	60-70	-169.7		-22.01
124	Upper Ice	75-80	-170.1		-22.14
125	Runoff from Esker	N/A	-166.9		-21.33
126	Lake west of Esker	N/A	-163.8		-19.56

Table A2. Anion and cation concentrations of Airstrip Esker ground ice and surrounding waters

SAMPLE NO		NO2	NO3	F	PO4	BR	SO4	CL
	UNITS	ppb	ppb	ppb	ppb	ppb	ppm	ppm
	D.L.	50	50	50	50	50	0.05	0.05
95 WDA-100		-50	-50	162	-50	-50	0.1	0.7
95 WDA-101		-50	56	236	-50	-50	0.8	1.7
95 WDA-102		-50	-50	-50	-50	-50	0.7	0.3
95 WDA-103		-50	-50	-50	-50	-50	0.2	0.6
95 WDA-104		-50	-50	-50	-50	-50	0.3	0.3
95 WDA-105		-50	-50	-50	-50	-50	5.5	1.2
95 WDA-106		-50	285	-50	-50	-50	0.3	0.7
95 WDA-107		-50	-50	-50	-50	-50	0.2	1.0
95 WDA-108		-50	-50	-50	-50	-50	0.7	0.5
95 WDA-109		-50	-50	-50	-50	-50	0.4	0.3
95 WDA-110		-50	-50	-50	-50	-50	0.9	0.5
95 WDA-111		-50	-50	-50	-50	-50	0.2	0.4
95 WDA-112		-50	-50	-50	-50	-50	-0.1	0.1
95 WDA-113		-50	-50	-50	-50	-50	0.3	0.6
95 WDA-115		-50	-50	-50	-50	-50	0.2	0.8
95 WDA-116		-50	-50	-50	-50	-50	0.6	0.6
95 WDA-117		-50	115	-50	-50	-50	33.0	0.4
95 WDA-118		-50	402	-50	-50	-50	4.5	0.5
95 WDA-119		-50	-50	-50	-50	-50	15.7	1.2
95 WDA-120		-50	-50	-50	-50	-50	2.9	0.9
95 WDA-121		-50	-50	-50	-50	-50	0.4	0.6
95 WDA-122		-50	539	-50	-50	-50	22.6	0.8
95 WDA-123		-50	430	-50	-50	-50	17.1	0.6
95 WDA-124		-50	634	-50	-50	-50	45.7	0.9
95 WDA-126		-50	127040	61	-50	-50	35.8	1.9

SAMPLE NO		NA AA-DIRECT 0.1% CS-LA	K AA-DIRECT 0.1% CS-LA	CA AA-DIRECT 0.1% CS-LA	MG AA-DIRECT 0.1% CS-LA
	UNITS	PPM	PPM	PPM	PPM
	D.L.	0.1	0.1	0.1	0.1
95 WDA-100		0.4	0.8	0.5	0.3
95 WDA-101		1.2	1.8	0.9	0.4
95 WDA-102		0.1	0.3	0.5	0.2
95 WDA-103		0.5	0.6	0.6	0.3
95 WDA-104		0.1	0.3	0.3	0.2
95 WDA-105		0.8	1.6	1.5	1.0
95 WDA-106		0.4	0.7	0.5	0.3
95 WDA-107		0.5	1.3	0.4	0.2
95 WDA-108		0.3	0.4	0.4	0.2
95 WDA-109		< 0.1	0.4	0.4	0.2
95 WDA-110		0.2	0.5	0.6	0.3
95 WDA-111		0.2	0.6	0.3	0.2
95 WDA-112		< 0.1	0.2	0.2	0.1
95 WDA-113		0.3	0.6	0.3	0.2
95 WDA-115		0.4	0.9	0.3	0.1
95 WDA-116		0.3	0.6	0.4	0.2
95 WDA-117		0.5	0.5	9.3	2.7
95 WDA-118		0.3	0.5	1.3	0.7
95 WDA-119		0.7	0.6	3.4	2.0
95 WDA-120		0.8	0.9	0.8	0.5
95 WDA-121		0.2	0.5	0.4	0.2
95 WDA-122		0.8	1.0	6.1	2.5
95 WDA-123		0.5	0.5	5.1	1.6
95 WDA-124		1.2	1.8	9.8	5.6
95 WDA-126		2.9	2.9	12.1	6.4
REPEATS					
95 WDA-101		1.2	1.8	0.9	0.4
95 WDA-101 R		1.0	1.8	0.9	0.4
95 WDA-109		< 0.1	0.4	0.4	0.2
95 WDA-109 R		0.1	0.4	0.3	0.2
95 WDA-126		2.9	2.9	12.1	6.4
95 WDA-126 R		3.0	2.9	12.1	6.4
CONTROLS					
BLANK		< 0.1	< 0.1	< 0.1	0.2
		< 0.1	< 0.1	< 0.1	< 0.1
OTT 94		2.6	0.7	8.5	2.2
		2.6	0.7	8.2	2.0
NBS-1643C		11.7	2.2	36.7	9.2

Table A3. PH, electrical conductivity and elemental concentrations of Airstrip Esker ground ice and surrounding waters.

Sample	Li 7 ICP-MS DIRECT ppb	Be 9 ICP-MS DIRECT ppb	Al 27 ICP-MS DIRECT ppb	Ti 47 ICP-MS DIRECT ppb	V 51 ICP-MS DIRECT ppb	Cr 52 ICP-MS DIRECT ppb
D.L.	0.005	0.005	2	0.5	0.1	0.1
95 WDA-100	0.392	< 0.005	59	1.9	< 0.1	0.3
95 WDA-101	0.841	< 0.005	24	0.8	0.3	0.7
95 WDA-102	0.138	< 0.005	19	< 0.5	< 0.1	0.2
95 WDA-103	0.247	< 0.005	9	< 0.5	< 0.1	0.2
95 WDA-104	0.348	0.011	58	3.0	0.1	0.6
95 WDA-105	4.495	0.030	80	5.9	0.3	0.5
95 WDA-106	0.469	< 0.005	11	< 0.5	< 0.1	0.5
95 WDA-107	0.349	0.018	17	0.8	< 0.1	0.8
95 WDA-108	0.213	0.009	14	0.9	< 0.1	0.4
95 WDA-109	0.381	0.014	52	3.0	0.2	0.7
95 WDA-110	1.251	0.026	63	5.0	0.2	0.5
95 WDA-111	0.776	0.014	106	8.2	0.4	0.6
95 WDA-112	0.523	0.017	77	8.5	0.4	0.9
95 WDA-113	0.338	< 0.005	26	1.4	< 0.1	0.7
95 WDA-115	0.298	0.006	18	1.1	< 0.1	0.4
95 WDA-116	1.240	< 0.005	16	0.9	< 0.1	0.4
95 WDA-117	6.347	0.038	27	1.3	< 0.1	1.4
95 WDA-118	2.555	0.026	54	2.2	< 0.1	0.4
95 WDA-119	3.212	0.025	47	2.7	< 0.1	0.9
95 WDA-120	1.227	< 0.005	17	< 0.5	< 0.1	0.3
95 WDA-121	0.386	0.009	16	1.0	< 0.1	0.6
95 WDA-122	6.594	0.014	59	3.2	0.2	0.6
95 WDA-123	3.294	0.017	19	0.9	< 0.1	0.3
95 WDA-124	19.320	0.114	506	24.3	1.2	1.4
95 WDA-126	10.212	0.159	274	0.6	< 0.1	0.2
REPEATS						
95 WDA-102	0.138	< 0.005	19	< 0.5	< 0.1	0.2
	0.143	< 0.005	18	< 0.5	< 0.1	0.2
95 WDA-108	0.213	0.009	14	0.9	< 0.1	0.4
	0.221	0.012	14	1.2	< 0.1	0.3
95 WDA-118	2.555	0.026	54	2.2	< 0.1	0.4
	2.786	0.007	61	2.6	0.2	0.5
CONTROLS						
OTT 94	0.593	0.005	57	1.7	0.4	0.2
	0.577	< 0.005	58	1.5	0.4	0.2
	0.561	< 0.005	65	1.5	0.4	0.2
	0.561	0.016	63	1.8	0.4	0.2
	0.551	< 0.005	61	1.8	0.4	0.2
	0.617	< 0.005	67	1.8	0.4	0.4

Table A3 continued.

Sample	Fe 54 ICP-MS DIRECT	Mn 55 ICP-MS DIRECT	Co 59 ICP-MS DIRECT	Ni 60 ICP-MS DIRECT	Cu 65 ICP-MS DIRECT	Zn 66 ICP-MS DIRECT
	ppb	ppb	ppb	ppb	ppb	ppb
D.L.	5	0.1	0.05	0.2	0.1	0.5
95 WDA-100	150	12.2	0.95	1.8	7.0	34.1
95 WDA-101	96	23.1	1.83	6.3	17.9	82.3
95 WDA-102	64	8.7	0.33	1.1	3.5	12.9
95 WDA-103	50	13.3	0.47	2.1	5.5	28.7
95 WDA-104	211	9.9	0.60	2.0	5.9	16.7
95 WDA-105	249	51.2	2.47	6.9	8.8	28.2
95 WDA-106	41	15.2	1.26	2.5	5.3	30.6
95 WDA-107	73	10.5	0.48	3.8	7.9	41.0
95 WDA-108	43	4.5	0.20	1.3	3.1	15.9
95 WDA-109	122	7.1	0.33	2.1	3.9	18.0
95 WDA-110	165	20.4	1.07	2.9	3.6	13.1
95 WDA-111	263	6.6	0.33	1.8	5.1	13.8
95 WDA-112	206	4.5	0.19	1.1	3.1	7.4
95 WDA-113	83	7.1	0.25	2.7	4.5	24.3
95 WDA-115	76	5.0	0.25	2.0	4.7	24.2
95 WDA-116	56	17.9	1.03	3.9	4.0	10.1
95 WDA-117	98	189.7	11.84	41.7	12.7	36.1
95 WDA-118	125	49.3	6.91	18.7	9.4	17.0
95 WDA-119	116	78.7	6.40	29.0	7.9	27.7
95 WDA-120	16	7.7	0.22	1.4	4.1	20.0
95 WDA-121	97	10.6	0.74	2.4	5.2	22.6
95 WDA-122	203	135.0	20.70	52.7	15.1	49.2
95 WDA-123	103	104.6	11.42	31.7	7.2	27.8
95 WDA-124	1038	437.5	35.48	88.4	12.6	56.8
95 WDA-126	31	201.7	6.58	12.5	3.1	38.6
REPEATS						
95 WDA-102	64	8.7	0.33	1.1	3.5	12.9
	51	8.7	0.32	1.2	3.7	13.0
95 WDA-108	43	4.5	0.20	1.3	3.1	15.9
	56	4.5	0.23	1.4	3.4	17.0
95 WDA-118	125	49.3	6.91	18.7	9.4	17.0
	123	59.1	7.46	19.7	10.2	18.6
CONTROLS						
OTT 94	100	3.6	< 0.05	0.8	1.2	1.2
	86	3.5	0.05	0.8	1.3	1.2
	98	3.6	0.06	0.8	1.3	1.2
	104	3.5	< 0.05	0.8	1.2	1.2
	98	3.6	0.05	0.8	1.5	1.3
	109	3.5	< 0.05	0.8	1.7	1.1

Table A3 continued.

Sample	As 75 ICP-MS DIRECT	Rb 85 ICP-MS DIRECT	Sr 88 ICP-MS DIRECT	Y 89 ICP-MS DIRECT	Mo 98 ICP-MS DIRECT	Ag 107 ICP-MS DIRECT
	ppb	ppb	ppb	ppb	ppb	ppb
D.L.	0.1	0.05	0.5	0.01	0.05	0.05
95 WDA-100	< 0.1	1.01	1.1	0.04	< 0.05	< 0.05
95 WDA-101	0.3	1.76	2.5	0.03	< 0.05	< 0.05
95 WDA-102	< 0.1	0.45	1.8	0.03	0.27	< 0.05
95 WDA-103	0.2	0.64	1.5	0.01	< 0.05	< 0.05
95 WDA-104	0.3	0.53	1.0	0.05	< 0.05	0.08
95 WDA-105	0.6	1.51	5.4	0.41	0.05	< 0.05
95 WDA-106	0.3	0.74	1.5	< 0.01	< 0.05	< 0.05
95 WDA-107	0.3	1.35	1.5	0.03	< 0.05	< 0.05
95 WDA-108	0.1	0.46	0.7	0.02	< 0.05	< 0.05
95 WDA-109	0.4	0.63	1.3	0.09	< 0.05	< 0.05
95 WDA-110	0.6	0.96	3.5	0.11	< 0.05	< 0.05
95 WDA-111	0.2	1.23	1.0	0.18	< 0.05	< 0.05
95 WDA-112	0.2	0.74	0.6	0.11	< 0.05	< 0.05
95 WDA-113	0.4	0.74	1.6	0.02	< 0.05	< 0.05
95 WDA-115	0.4	0.99	1.3	0.03	< 0.05	< 0.05
95 WDA-116	0.6	0.85	4.0	0.02	< 0.05	< 0.05
95 WDA-117	0.2	0.54	19.7	0.14	< 0.05	< 0.05
95 WDA-118	0.3	0.68	8.1	0.17	< 0.05	< 0.05
95 WDA-119	2.3	0.85	14.1	0.21	< 0.05	< 0.05
95 WDA-120	0.3	1.51	7.3	0.01	< 0.05	< 0.05
95 WDA-121	< 0.1	0.66	1.5	0.02	< 0.05	0.31
95 WDA-122	0.6	1.29	16.8	0.17	0.08	0.17
95 WDA-123	< 0.1	0.54	13.1	0.05	0.19	< 0.05
95 WDA-124	1.5	3.57	36.8	0.44	0.10	0.22
95 WDA-126	0.7	29.11	116.9	0.16	< 0.05	< 0.05
REPEATS						
95 WDA-102	< 0.1	0.45	1.8	0.03	0.27	< 0.05
	< 0.1	0.45	2.2	0.02	0.21	< 0.05
95 WDA-108	0.1	0.46	0.7	0.02	< 0.05	< 0.05
	< 0.1	0.51	0.9	0.02	< 0.05	< 0.05
95 WDA-118	0.3	0.68	8.1	0.17	< 0.05	< 0.05
	0.2	0.73	9.4	0.18	0.07	< 0.05
CONTROLS						
OTT 94	0.5	1.73	43.0	0.14	0.22	< 0.05
	0.6	1.76	46.1	0.13	0.22	< 0.05
	0.9	1.75	45.9	0.14	0.26	< 0.05
	0.5	1.68	44.4	0.14	0.26	< 0.05
	0.6	1.78	51.4	0.13	0.26	< 0.05
	1.3	1.79	45.5	0.15	0.21	< 0.05

Table A3 continued.

Sample	Cd 114 ICP-MS DIRECT	In 115 ICP-MS DIRECT	Sb 121 ICP-MS DIRECT	Cs 133 ICP-MS DIRECT	Ba 138 ICP-MS DIRECT	La 139 ICP-MS DIRECT
	ppb	ppb	ppb	ppb	ppb	ppb
D.L.	0.05	0.01	0.01	0.01	0.2	0.01
95 WDA-100	0.68	< 0.01	0.12	0.03	2.6	0.09
95 WDA-101	1.50	< 0.01	0.30	0.02	9.1	0.04
95 WDA-102	0.26	< 0.01	0.05	< 0.01	2.1	0.06
95 WDA-103	0.63	< 0.01	0.09	< 0.01	3.8	0.04
95 WDA-104	0.61	< 0.01	0.11	0.03	4.4	0.15
95 WDA-105	0.81	< 0.01	0.10	0.06	7.1	0.96
95 WDA-106	0.66	< 0.01	0.15	< 0.01	4.7	0.10
95 WDA-107	0.80	< 0.01	0.20	0.02	8.7	0.10
95 WDA-108	0.74	< 0.01	0.13	< 0.01	3.0	0.07
95 WDA-109	0.39	< 0.01	0.17	0.03	4.7	0.21
95 WDA-110	0.32	< 0.01	0.14	0.07	8.6	0.46
95 WDA-111	0.30	< 0.01	0.08	0.10	5.1	0.43
95 WDA-112	0.12	< 0.01	0.05	0.08	4.2	0.28
95 WDA-113	0.56	< 0.01	0.11	0.02	4.1	0.11
95 WDA-115	0.79	< 0.01	0.11	0.02	5.0	0.16
95 WDA-116	0.18	< 0.01	0.16	0.03	11.5	0.08
95 WDA-117	0.31	< 0.01	0.06	0.02	15.7	0.31
95 WDA-118	0.11	< 0.01	0.07	0.03	7.9	0.40
95 WDA-119	0.39	< 0.01	0.10	0.05	16.0	0.25
95 WDA-120	0.31	< 0.01	0.07	0.02	3.7	0.04
95 WDA-121	1.72	< 0.01	0.06	0.02	6.7	0.05
95 WDA-122	4.20	< 0.01	0.11	0.06	22.0	0.68
95 WDA-123	0.93	< 0.01	0.08	0.02	14.2	0.13
95 WDA-124	2.41	< 0.01	0.04	0.30	44.7	1.61
95 WDA-126	0.24	< 0.01	0.01	2.23	165.0	0.80
REPEATS						
95 WDA-102	0.26	< 0.01	0.05	< 0.01	2.1	0.06
	0.29	< 0.01	0.06	< 0.01	2.0	0.06
95 WDA-108	0.74	< 0.01	0.13	< 0.01	3.0	0.07
	0.79	< 0.01	0.16	0.02	3.0	0.09
95 WDA-118	0.11	< 0.01	0.07	0.03	7.9	0.40
	0.16	< 0.01	0.08	0.04	8.6	0.45
CONTROLS						
OTT 94	< 0.05	< 0.01	0.06	0.01	18.3	0.26
	< 0.05	< 0.01	0.06	< 0.01	16.2	0.25
	< 0.05	< 0.01	0.07	< 0.01	16.7	0.27
	< 0.05	< 0.01	0.06	< 0.01	16.3	0.25
	< 0.05	< 0.01	0.06	< 0.01	16.4	0.27
	< 0.05	< 0.01	0.04	< 0.01	16.6	0.25

Table A3 continued.

Sample	Ce 140 ICP-MS DIRECT ppb	Pr 141 ICP-MS DIRECT ppb	Nd 146 ICP-MS DIRECT ppb	Sm 147 ICP-MS DIRECT ppb	Eu 151 ICP-MS DIRECT ppb	Gd 160 ICP-MS DIRECT ppb
D.L.	0.01	0.005	0.005	0.005	0.005	0.005
95 WDA-100	0.18	0.015	0.073	0.028	< 0.005	0.013
95 WDA-101	0.10	0.014	0.049	0.016	< 0.005	0.012
95 WDA-102	0.12	0.011	0.050	0.008	< 0.005	0.006
95 WDA-103	0.06	0.005	0.024	< 0.005	< 0.005	< 0.005
95 WDA-104	0.27	0.036	0.109	0.019	< 0.005	0.013
95 WDA-105	2.13	0.242	0.918	0.180	0.025	0.118
95 WDA-106	0.05	0.005	0.027	< 0.005	< 0.005	< 0.005
95 WDA-107	0.18	0.018	0.069	0.011	< 0.005	0.007
95 WDA-108	0.14	0.020	0.063	0.022	0.006	0.006
95 WDA-109	0.45	0.050	0.236	0.044	0.007	0.023
95 WDA-110	0.95	0.109	0.398	0.042	0.008	0.039
95 WDA-111	0.88	0.107	0.402	0.080	0.012	0.042
95 WDA-112	0.59	0.078	0.282	0.058	0.006	0.046
95 WDA-113	0.13	0.015	0.048	0.009	< 0.005	0.008
95 WDA-115	0.20	0.024	0.086	0.025	< 0.005	0.013
95 WDA-116	0.14	0.020	0.074	0.010	< 0.005	0.007
95 WDA-117	0.61	0.069	0.296	0.056	0.007	0.041
95 WDA-118	0.93	0.120	0.488	0.093	0.013	0.069
95 WDA-119	0.54	0.069	0.290	0.073	< 0.005	0.054
95 WDA-120	0.06	0.008	0.030	0.010	< 0.005	0.011
95 WDA-121	0.09	0.010	0.036	0.009	< 0.005	0.010
95 WDA-122	1.57	0.186	0.673	0.106	0.012	0.069
95 WDA-123	0.27	0.034	0.159	0.031	0.006	0.020
95 WDA-124	3.31	0.411	1.560	0.268	0.033	0.166
95 WDA-126	0.72	0.073	0.250	0.045	< 0.005	0.023
REPEATS						
95 WDA-102	0.12	0.011	0.050	0.008	< 0.005	0.006
	0.09	0.009	0.040	0.015	< 0.005	< 0.005
95 WDA-108	0.14	0.020	0.063	0.022	0.006	0.006
	0.17	0.012	0.093	< 0.005	< 0.005	0.019
95 WDA-118	0.93	0.120	0.488	0.093	0.013	0.069
	1.00	0.134	0.575	0.125	0.023	0.090
CONTROLS						
OTT 94	0.29	0.065	0.261	0.043	0.007	0.031
	0.29	0.057	0.223	0.037	0.006	0.036
	0.31	0.067	0.246	0.035	< 0.005	0.025
	0.30	0.069	0.217	0.038	0.006	0.040
	0.30	0.053	0.248	0.042	0.005	0.031
	0.32	0.058	0.240	0.046	< 0.005	0.036

Table A3 continued.

Sample	Tb 159 ICP-MS DIRECT	Dy 163 ICP-MS DIRECT	Ho 165 ICP-MS DIRECT	Er 166 ICP-MS DIRECT	Tm 169 ICP-MS DIRECT	Yb 174 ICP-MS DIRECT
	ppb	ppb	ppb	ppb	ppb	ppb
D.L.	0.005	0.005	0.005	0.005	0.005	0.005
95 WDA-100	< 0.005	0.006	< 0.005	< 0.005	< 0.005	< 0.005
95 WDA-101	< 0.005	0.009	< 0.005	< 0.005	< 0.005	< 0.005
95 WDA-102	< 0.005	< 0.005	< 0.005	< 0.005	< 0.005	< 0.005
95 WDA-103	< 0.005	0.006	< 0.005	< 0.005	< 0.005	< 0.005
95 WDA-104	< 0.005	0.012	< 0.005	< 0.005	< 0.005	< 0.005
95 WDA-105	0.016	0.093	0.014	0.031	< 0.005	0.026
95 WDA-106	< 0.005	< 0.005	< 0.005	< 0.005	< 0.005	< 0.005
95 WDA-107	< 0.005	0.017	< 0.005	< 0.005	< 0.005	< 0.005
95 WDA-108	< 0.005	0.007	< 0.005	< 0.005	< 0.005	< 0.005
95 WDA-109	< 0.005	0.023	< 0.005	< 0.005	< 0.005	0.010
95 WDA-110	< 0.005	0.025	< 0.005	0.011	< 0.005	0.007
95 WDA-111	0.005	0.041	< 0.005	0.020	< 0.005	0.011
95 WDA-112	< 0.005	0.021	< 0.005	0.009	< 0.005	0.009
95 WDA-113	< 0.005	< 0.005	< 0.005	< 0.005	< 0.005	< 0.005
95 WDA-115	< 0.005	< 0.005	< 0.005	< 0.005	< 0.005	< 0.005
95 WDA-116	< 0.005	< 0.005	< 0.005	< 0.005	< 0.005	< 0.005
95 WDA-117	< 0.005	0.031	< 0.005	0.015	< 0.005	0.009
95 WDA-118	0.007	0.034	< 0.005	0.017	< 0.005	0.016
95 WDA-119	0.006	0.037	0.008	0.020	< 0.005	0.023
95 WDA-120	< 0.005	< 0.005	< 0.005	0.006	< 0.005	< 0.005
95 WDA-121	< 0.005	< 0.005	< 0.005	< 0.005	< 0.005	0.005
95 WDA-122	0.006	0.030	0.005	0.011	< 0.005	0.015
95 WDA-123	< 0.005	0.008	< 0.005	< 0.005	< 0.005	< 0.005
95 WDA-124	0.017	0.103	0.016	0.040	< 0.005	0.035
95 WDA-126	< 0.005	0.026	< 0.005	0.010	< 0.005	0.013
REPEATS						
95 WDA-102	< 0.005	< 0.005	< 0.005	< 0.005	< 0.005	< 0.005
	< 0.005	< 0.005	< 0.005	< 0.005	< 0.005	< 0.005
95 WDA-108	< 0.005	0.007	< 0.005	< 0.005	< 0.005	< 0.005
	< 0.005	< 0.005	< 0.005	< 0.005	< 0.005	< 0.005
95 WDA-118	0.007	0.034	< 0.005	0.017	< 0.005	0.016
	0.009	0.040	< 0.005	0.020	< 0.005	0.020
CONTROLS						
OTT 94	< 0.005	0.027	< 0.005	0.016	< 0.005	0.014
	< 0.005	0.017	< 0.005	0.013	< 0.005	0.013
	< 0.005	0.019	< 0.005	0.011	< 0.005	0.009
	< 0.005	0.036	< 0.005	0.011	< 0.005	0.012
	< 0.005	0.023	0.006	0.015	< 0.005	0.015
	< 0.005	0.013	< 0.005	0.006	< 0.005	0.015

Table A3 continued.

Sample	Lu 175 ICP-MS DIRECT ppb	Tl 205 ICP-MS DIRECT ppb	Pb 208 ICP-MS DIRECT ppb	U 238 ICP-MS DIRECT ppb	COND DIRECT umhos	pH DIRECT units
D.L.	0.005	0.005	0.1	0.005	1	
95 WDA-100	< 0.005	< 0.005	0.9	0.045	10	6.5
95 WDA-101	< 0.005	< 0.005	0.5	0.075	22	6.7
95 WDA-102	< 0.005	< 0.005	0.6	0.028	7	6.0
95 WDA-103	< 0.005	< 0.005	0.6	0.049	12	6.5
95 WDA-104	< 0.005	< 0.005	6.5	0.088	7	5.7
95 WDA-105	< 0.005	< 0.005	1.3	0.273	31	6.5
95 WDA-106	< 0.005	< 0.005	0.7	0.022	12	6.2
95 WDA-107	< 0.005	< 0.005	1.0	0.087	15	6.3
95 WDA-108	< 0.005	< 0.005	0.6	0.047	9	6.1
95 WDA-109	< 0.005	< 0.005	1.3	0.150	7	6.0
95 WDA-110	< 0.005	0.005	0.8	0.442	11	6.2
95 WDA-111	< 0.005	< 0.005	1.6	0.219	7	6.0
95 WDA-112	< 0.005	< 0.005	2.5	0.153	4	5.7
95 WDA-113	< 0.005	< 0.005	1.7	0.051	11	6.3
95 WDA-115	< 0.005	< 0.005	0.7	0.119	11	6.0
95 WDA-116	< 0.005	0.006	0.3	0.149	11	6.1
95 WDA-117	< 0.005	0.010	3.6	0.649	89	5.6
95 WDA-118	< 0.005	0.009	0.4	1.289	21	6.1
95 WDA-119	< 0.005	< 0.005	1.7	0.443	49	6.2
95 WDA-120	< 0.005	< 0.005	0.6	0.040	19	6.2
95 WDA-121	< 0.005	< 0.005	0.9	0.067	9	6.3
95 WDA-122	< 0.005	0.010	1.7	0.487	71	6.4
95 WDA-123	< 0.005	< 0.005	0.6	0.391	53	6.2
95 WDA-124	0.005	0.042	2.8	1.628	119	6.3
95 WDA-126	< 0.005	0.125	0.3	0.129	359	4.8
REPEATS						
95 WDA-102	< 0.005	< 0.005	0.6	0.028		
	< 0.005	< 0.005	0.6	0.041		
95 WDA-108	< 0.005	< 0.005	0.6	0.047		
	< 0.005	< 0.005	0.7	0.056		
95 WDA-118	< 0.005	0.009	0.4	1.289		
	< 0.005	0.007	0.5	1.474		
CONTROLS						
OTT 94	< 0.005	0.009	0.2	0.074		
	< 0.005	< 0.005	0.2	0.070		
	< 0.005	< 0.005	0.2	0.068		
	< 0.005	0.006	0.2	0.077		
	< 0.005	0.007	0.2	0.076		
	< 0.005	0.005	0.2	0.066		

Analysis notes

There may be supression on the ICP-MS data for some elements on the samples with high conductivity.
(some of the elements had to be determined from dilutions of the sample).The Na values are very high on some of these samples.
Sample 95 WDA-068/069 had very little volume and could only be analysed by ICP-MS on a dilution (therefore higher detection limits.)
The high values for Vanadium and Arsenic may be due to high Cl values that cannot be corrected for (samples 59, 60/61 and 65 especially).
When a 10 or 20x dilution was analysed there was very little Vanadium.

Table A4. Sediment and water analyses from March 1996 boreholes (INAC-01 to INAC-09) and surrounding waters.

Sample	Description	Borehole	Depth(m)	Isotopic Concentrations Oxygen	Deuterium	Grain Size Characteristics (%) Gravel	Sand	Silt	Clay	Moisture Content (%)	Electrical Conductivi (uS/cm)
96WDA-01	snow, Airstrip Lake			-34.06	-268.7						2.82
96WDA-02	surface water, Airstrip Lake			-19.68	-159.0						22.00
96WDA-03	lake ice, Airstrip Lake			-17.80	-145.7						16.80
96WDA-04	surface water, Airstrip Lake			-19.89	-157.4						27.40
96WDA-05	subsurface water, Airstrip Lake			-18.89	-153.8						18.90
96WDA-07	subsurface water, Airstrip Lake			-19.01	-154.2						23.30
96WDA-08	SAND, coarse with GRAVEL, , SP	INAC-01	0.0-0.75			31.67	66.76	1.36	0.21	2.36	
96WDA-09	SAND, med to coarse, SW	INAC-01	0.75-1.50			4.35	93.16	2.11	0.39	2.33	
96WDA-10	SAND, med to coarse, SP	INAC-01	1.50-2.30			30.02	65.53	3.79	0.66	18.84	
96WDA-11	SAND, med, SW	INAC-01	2.30-3.05	-26.82	-206.4	8.40	83.05	7.68	0.88	21.14	
96WDA-12	SAND, med , SP	INAC-01	3.05-3.81	-28.42	-220.4	3.51	86.35	8.63	1.51	26.44	
96WDA-13	SAND, coarse , SW	INAC-01	3.81-4.57	-29.08	-224.7	23.46	71.63	4.15	0.76	12.44	
96WDA-14	SAND, coarse with SILT, SW	INAC-01	4.57-5.33	-29.07	-220.8	4.95	85.20	8.82	1.03	24.50	
96WDA-15	SAND, med. to coarse, SW	INAC-01	5.33-6.10	-29.12	-221.7	22.61	69.73	6.74	0.92	6.57	
96WDA-16	SAND, med to fine, SW	INAC-01	6.10-7.62	-29.78	-227.1	3.39	85.96	9.39	1.26	24.98	
96WDA-17	SAND, coarse and SILT. SP-SM	INAC-01	7.92-8.23	-29.40	-224.2	1.49	84.27	12.11	2.13	20.54	
96WDA-18A	SAND, fine with SILT, SM	INAC-01	8.99-9.07	-28.03	-219.6	0.00	85.07	14.17	0.77	27.25	9.93
96WDA-18B	ICE with fine SAND	INAC-01	9.07-9.14	-28.19	-216.1						
96WDA-19	ICE, some SILT	INAC-01	9.14-9.75	-28.92	-219.5						7.05
96WDA-20	SAND, with SILT, SP-SM	INAC-01	10.05-10.24			0.00	81.44	15.24	3.32	12.07	
96WDA-21	ICE some SILT	INAC-01	10.24	-28.44	-219.1						
96WDA-22	ICE, no sed.	INAC-01	10.31-10.51	-28.22	-216.9	0.00	74.95	22.75	2.30		3.84
96WDA-23A	ICE, some SAND, coarse and SILT	INAC-01	10.61-10.64	-28.74	-220.9						10.38
96WDA-23B	ICE, some SILT	INAC-01	10.64-10.67	-28.70	-217.8						26.50
96WDA-24	SAND, coarse and GRAVEL, SW	INAC-01	10.51-10.61	-26.94	-208.4					13.56	
96WDA-25	ICE, some coarse SAND	INAC-01	10.67-10.82	-28.57	-217.9						9.43
96WDA-26	ICE, some med. to coarse SAND	INAC-01	10.97-11.13	-28.29	-212.7						8.41
96WDA-27	ICE, no sed.	INAC-01	11.17-11.28	-28.82	-223.0						5.43
96WDA-28	ICE, no sed.	INAC-01	11.58	-28.41	-216.8						5.96
96WDA-29	ICE, little or no sed.	INAC-01	11.73	-28.59	-214.2	24.78	63.92	9.48	1.82		5.80
96WDA-30	ICE, no. sed.	INAC-01	11.88	-28.70	-223.0						11.54
96WDA-31	ICE, no. sed.	INAC-01	12.19	-28.68	-218.7						6.12
96WDA-32	ICE, little or no sed.	INAC-01	12.40	-27.66	-214.7						3.27
96WDA-33	ICE, some SILT	INAC-01	12.44	-28.78	-219.6						9.37
96WDA-34	ICE, little or no sed.	INAC-01	12.67	-28.90	-216.3						9.99
96WDA-35	ICE, no sed.	INAC-01	13.03	-28.97	-223.8						7.46
96WDA-36	ICE, some fine SAND or SILT	INAC-01	13.03-13.11	-28.35	-220.9						18.08
96WDA-37	SAND, fine with SILT, SM	INAC-01	13.11-13.26	-27.38	-212.0	0.00	30.33	65.15	4.52	79.14	
96WDA-38A	ICE, some SAND, fine	INAC-01	13.26-13.40	-28.07	-212.9						14.66
96WDA-38B	ICE with SAND, med. to fine, SP	INAC-01	13.40-13.56	-28.16	-214.9	0.00	83.81	14.56	1.63		4.94
96WDA-39	ICE, no sed.	INAC-01	13.71	-28.21	-213.6	11.91	59.79	26.47	1.82		5.25
96WDA-40	ICE, some SILT	INAC-01	13.82	-28.00	-212.3						3.29
96WDA-41	ICE, some SAND, fine and SILT	INAC-01	13.82-14.07	-28.21	-211.3					33.84	3.79
96WDA-42A	ICE, no sed.	INAC-01	14.07-14.15	-27.89	-213.9						8.08
96WDA-42B	SAND, coarse SILTY, SW-SM	INAC-01	14.15-14.22	-27.27	-212.0						67.80
96WDA-43A	ICE, some SAND, fine and SILT	INAC-01	14.22-14.25	-27.72	-211.1						6.58
96WDA-43B	SAND, coarse and fine, SW-SP	INAC-01	14.25-14.33	-27.35	-206.8						

Table A4 continued

Sample	Description	Borehole	Depth(m)	Isotopic Concentrations Oxygen	Deuterium	Grain Size Characteristics (%) Gravel	Sand	Silt	Clay	Moisture Content (%)	Electrical Conductivi (uS/cm)
96WDA-44	ICY, GRAVEL with SAND, coarse, GW	INAC-02	1.52	-30.28	-233.9					60.49	78.10
96WDA-45	SAND, coarse with GRAVEL, SW	INAC-02	2.59	-30.04	-230.6	40.11	52.71	6.34	0.84	53.31	
96WDA-46	SAND, coarse with SILT, SW-SM	INAC-02	4.57	-29.57	-228.1					44.61	
96WDA-47	SAND, coarse and GRAVEL, GW-SW	INAC-02	0.76	-29.86	-226.0	42.07	54.17	3.19	0.57	76.31	
96WDA-48	SAND, coarse SILTY, SM	INAC-02	5.18	-28.46	-221.7	1.12	72.83	21.25	4.79	12.74	
96WDA-49	SAND, coarse SILTY, SM	INAC-02	6.41			5.59	70.89	18.80	4.72	14.21	
96WDA-50	SAND, coarse and GRAVEL, SW	INAC-03	1.14	-26.72	-208.4	25.46	54.47	16.28	3.79	18.07	
96WDA-51	SAND, coarse with silt, SM	INAC-03	1.52-3.65			42.81	52.17	4.14	0.88	12.05	
96WDA-52	SAND, med, SP	INAC-04	0.0-0.75			3.70	94.44	1.60	0.27	4.81	
96WDA-53	GRAVEL, with coarse SAND, GW	INAC-04	3.20-3.96			37.55	55.75	5.57	1.14	7.42	
96WDA-54	SAND, coarse with SILT, SM	INAC-04	5.02			12.74	65.25	17.96	4.05	13.21	
96WDA-55	SAND, coarse with SILT, SM	INAC-04	6.25			13.83	63.89	18.47	3.81	11.61	
96WDA-56	GRAVEL, with SAND, GW	INAC-05	0.0-0.75			31.84	61.70	5.68	0.78	10.33	
96WDA-57	SAND, coarse with SILT, SM	INAC-05	6.71							10.13	
96WDA-58	SAND, coarse with SILT, SM	INAC-05	7.92			6.72	65.55	22.08	5.65	12.77	
96WDA-59	SAND, coarse with SILT, SM	INAC-05	10.43			14.30	62.89	18.39	4.42	11.47	
96WDA-60	GRAVEL, GW	INAC-06	0.46-0.76			85.56	11.67	2.28	0.50	1.77	
96WDA-61	SAND, coarse, SW	INAC-06	0.76-1.68			4.74	92.36	2.37	0.53	2.34	
96WDA-62	SAND, med with SILT, SM	INAC-06	3.96			16.52	61.32	18.74	3.42	14.55	
96WDA-63	SAND, coarse, SW	INAC-06	5.49	-30.55	-236.3	15.84	74.99	7.98	1.19	12.01	
96WDA-64	SAND, med, SW	INAC-07	2.43-2.74			1.15	77.45	17.40	4.00	20.70	
96WDA-65	SAND, med. to fine, SW	INAC-07	3.96	-27.63	-214.7	3.49	69.30	22.69	4.53	16.37	
96WDA-66	SAND, fine, SW	INAC-08	1.52-2.29			1.38	83.65	12.59	2.38	10.62	
96WDA-67	SAND, fine, SM	INAC-08	2.29-3.05			0.00	72.24	23.53	4.23	25.11	
96WDA-68	SAND, fine, SP	INAC-08	3.66-3.81							21.55	
96WDA-69	SAND, fine, SP	INAC-08	3.81-3.96			0.00	93.75	5.74	0.51	21.26	
96WDA-70	SAND, fine, SP	INAC-08	4.11-4.26			0.00	86.53	13.02	0.45	19.76	
96WDA-71	SAND, med to coarse, SP	INAC-08	4.26-4.88	-34.93	-271.6	0.00	96.37	3.00	0.63	26.56	
96WDA-72	SAND, fine, SP	INAC-08	4.88-5.03	-35.19	-274.7	0.17	90.45	8.28	1.10	26.80	
96WDA-73	SAND, fine to very fine, SP	INAC-08	5.03-5.18	-35.05	-273.7	0.00	60.44	37.14	2.42	26.10	
96WDA-74	ICE, some sed.	INAC-08	6.32	-35.69	-278.6						27.80
96WDA-75	SAND, fine with organics, SP-SW	INAC-09	0.0-0.76	-19.54	-152.0	0.00	79.84	17.44	2.72	24.62	
96WDA-76	SAND, med, SW	INAC-09	3.12-3.20	-20.35	-156.1	6.22	81.35	10.26	2.17	24.08	
96WDA-77	SAND,med, SW	INAC-09	3.20-3.81	-19.89	-151.9	0.57	82.37	14.20	2.85	24.08	
96WDA-78	SAND, med. to coarse, SW	INAC-09	4.27-5.03	-27.53	-211.6	1.95	83.48	11.53	3.04	29.49	
96WDA-79	SAND, med, SP-SW	INAC-09	5.64-6.25	-27.84	-212.0	0.00	84.52	12.76	2.71	25.98	
96WDA-80	SAND, med, SP	INAC-09	6.48-6.63	-27.75	-215.8	0.96	98.34	0.59	0.11	27.46	99.20
96WDA-81	SAND, med, SP	INAC-09	6.76-8.23	-27.18	-213.5	0.00	87.93	10.20	1.87	27.64	
96WDA-82	SAND, med. to fine with silt, SP	INAC-09	10.82-11.28	-28.50	-219.2	0.00	84.20	13.32	2.48	30.89	
96WDA-83	SAND, fine to very fine and silt, SM	INAC-09	11.89-12.80	-29.05	-224.3	2.15	42.08	45.98	9.79	28.40	
96WDA-84	ICE, with SILT	INAC-09	12.80-13.87	-25.83	-203.0	1.01	32.01	52.66	14.33	183.25	124.10
96WDA-85	ICE, with SILT	INAC-09	14.02-14.94	-24.48	-191.1	8.36	15.75	56.15	19.75	865.75	35.10
96WDA-86	ICE, with SILT	INAC-09	15.85	-25.42	-199.9	0.00	56.84	36.24	6.92	47.73	117.60
96WDA-87	surface water, Carat Lake			-20.75	-166.0						38.73
96WDA-88	snow sample, Misery Lake			-27.37	-207.7						4.69
96WDA-89	surface water, Misery Lake			-18.34	-152.7						26.90
96WDA-90	ice samples, Misery Lake			-16.00	-138.9						1.61
96WDA-91	interface sample #1, Misery Lake			-17.71	-148.8						23.70
96WDA-92	subsurface water,core 3,Misery Lake			-18.96	-152.7						21.30

Table A5. Oxygen and deuterium isotopic analysis from various water sources in the Slave Geological Province.

Sample	Description	Values Relative to Standard Mean Ocean Water	
		Deuterium Isotopes	Oxygen Isotopes
9	surface water	-158.1	-19.41
11	ice wedge	-157.0	-20.74
12	snow	-192.6	-25.59
13	aufeis	-151.0	-19.33
14	aufeis	-141.2	-17.55
16	ice wedge	-188.8	-24.75
17	ice wedge	-184.0	-24.38
20	ice wedge	-188.7	-24.83
21	ice wedge	-184.6	-24.08
22	ice wedge	-187.8	-24.06
29	surface water	-161.1	-21.16
30	surface water	-156.9	-19.43
33	ice wedge	-170.6	-21.93
34	ice wedge	-191.7	-24.75
40	ice wedge	-180.2	-23.13